PhD degree in Molecular Medicine (curriculum in Molecular Oncology)

European School of Molecular Medicine (SEMM),

University of Milan and University of Naples "Federico II"

Settore disciplinare: MED/04

GM-CSF and MMP9 are key regulators of the effect of adipose progenitors over breast cancer onset and metastatic progression

FRANCESCA REGGIANI

European Institute of Oncology (IEO), Milan

Matricola n. R10318

Supervisor: Dr. FRANCESCO BERTOLINI

European Institute of Oncology (IEO), Milan

Added Supervisor: Prof. GIUSEPPE VIALE

European Institute of Oncology (IEO), Milan

Anno accademico 2015-2016

Table of Contents

List of abbreviations

AIOM = Italian Association for Medical Oncology

αSMA = Alpha smooth muscle actin

AMPK = 5’ AMP-activated protein kinase

ASC = Adipose-derived stem cell

ATCC = American Type Culture Collection

BAT = Brown adipose tissue

BC = Breast cancer

BCA = Bicinchoninic acid

BCL-2 = B-cell lymphoma 2

bFGF = Basic fibroblast growth factor

BM = Bone marrow

BMI = Body mass index

BSA = Bovine serum albumin

CAA = Cancer-associated adipocyte

CAF = Cancer-associated fibroblast

CCD = Charge-coupled device

CL = Claudin-low

CLS = Crown-like structures

COX-2 = Cyclooxygenase-2

CXCL = C-X-C Motif chemokine ligand

DAPI = 4′,6-diamino-2phenylindole

DIO = Diet-induced obesity

DMEM = Dulbecco’s modified eagle medium

DMSO = Dimethyl sulfoxide

EBM = Endothelial basal medium

ECM = Extracellular matrix

EDTA = Ethylenediamine tetra acetic acid

ELISA = Enzyme-linked immunosorbent assay

EGF = Epidermal growth factor

EGFR = Epidermal growth factor

EMT = Epithelial to mesenchymal transition

EPC = Endothelial progenitor cell

ER = Estrogen receptor

FBS = Fetal bovine serum

FDA = Food and drug administration

G = Gram

GEM = Genetically engineered mouse

GM-CSF = Granulocyte-macrophage colony-stimulating factor

GM-CSFR = Granulocyte-macrophage colony-stimulating factor receptor

G-MDSC = Granulocytic myeloid derived suppressor cell

H&E = Hematoxylin and eosin

HER2 = Human epidermal growth factor receptor 2

HFD = High-fat diet

HGF = Hepatocyte growth factor

IDC = Invasive ductal carcinoma

IEO = European Institute of Oncology

IF = Immunofluorescence

IGF-1 = Insulin-like growth factor 1

IHC = Immunohistochemistry

IL = Interleukin

ILC = Invasive lobular carcinoma

IP = Intraperitoneal

JAK/STAT = Janus kinase/signal transducer and activator of transcription

KO = Knock out

LDS = Lithium dodecyl sulphate

LFD = Low-fat diet

LKB1 = Liver kinase B1

MCP-1 = Monocytes chemoattractant protein 1

MDSC = Myeloid derived suppressor cell

MHC = Major histocompatibility complex

MMP = Matrix metallopeptidase

MMTV = Mouse mammary tumor virus

MoAb = Monoclonal antibody

Mo-MDSC = Monocytic myeloid derived suppressor cell

MVD = Microvessels density

mTOR = Mammalian target of rapamycin

NaCl = Sodium chloride

NF-kB = Nuclear factor-kappa B

NK = Natural killer

NO = Nitric oxide

NS = Not significant

NSAIDs = Nonsteroidal anti-inflammatory drugs

NSG = NOD SCID IL2Rϒ null

OS = Overall survival

PAI-1 = Plasminogen activator inhibitor-1

PBS = Phosphate-buffered saline

PDGF = Platelet-derived growth factor

PI3K/AKT = Phosphatidylinositol 3-kinase/protein-kinase B

PMSF = Phenylmethylsulfonyl fluoride

PPARϒ = peroxisome proliferator-activated receptor gamma

PR = Progesteron receptor

qRT-PCR = Quantitative Reverse Transcriptase– Polymerase Chain Reaction

RIPA = Radio immuno precipitation assay

ROS = Reactive oxygen species

RPM = Rotations per minute

RPMI = Roswell Park Memorial Institute

RT = Room temperature

SAT = Subcutaneous adipose tissue

SDF-1 = Stromal cell-derived factor 1

SDS = Sodium dodecyl sulphate

SEM = Standard error of the mean

SVF = Stromal vascular fraction

TAM = Tumor associated macrophage

TBS = Tris buffered saline

TGF = Transforming growth factor

TIMP = Tissue inhibitor of MMPs

TNBC = Triple negative breast cancer

TNF = Tumor necrosis factor

T-reg = T-regulatory

uPA = Urokinase plasminogen activator

VAT = Visceral adipose tissue

VEGF = Vascular endothelial growth factor

WAT = White adipose tissue

WB = Western blotting

WHO = World Health Organization

List Figures and Tables Index

FIGURES

TABLES

Abstract

Recent epidemiological and clinical data underlined the critical role of obesity in breast cancer (BC) progression. Among several white adipose tissue (WAT) cells, which may promote a permissive tumor microenvironment, a population with progenitor-like phenotype ($CD45^{-}CD34^{+}$) was reported to support local and metastatic BC. This population is composed by distinct WAT progenitors: adipose-derived stem cells (ASCs) and endothelial progenitor cells (EPCs), displaying complementary role in BC progression in preclinical models. However, molecular mechanisms involved in this interaction have been so far elusive and need to be clarified.

An extensive screening of candidate molecules revealed two proteins being significantly up-regulated in WAT-derived progenitors after being co-cultured with several BC cells: Granulocyte-macrophage colony-stimulating factor (GM-CSF) and Matrix metallopeptidase 9 (MMP9). Both factors were detected over-expressed in orthotopic xenograft models, when co-injected with BC and human WAT progenitors. ASC and EPCs displayed similar ability to induce GM-CSF/MMP9, suggesting a complementary role in their release. GM-CSF neutralization in WAT progenitors inhibited MMP9 secretion, which was also reduced by IL-1β neutralization. GM-CSF displayed an additional positive feedback regulation on its own release.

The inhibition of GM-CSF in diet-induced obese (DIO) syngeneic mice led to reduced intratumor vascularization and strong impairment of immunosuppressive microenvironment, targeting mainly tumor-associated macrophages (TAMs), myeloid derived suppressor cells (MDSCs) and T-regulatory (T-regs) cells. This resulted in a significant impairment of local BC growth and a slower metastatic progression.

Conversely, MMP9 inhibition reduced neoplastic angiogenesis and significantly decreased local and metastatic tumor growth. The combined GM-CSF/MMP9 inhibition synergically impaired tumor angiogenesis, local and metastatic BC growth.

Metformin was reported to significantly affect tumor progression and neoplastic angiogenesis, targeting both BC and WAT cells. In the present study, Metformin inhibited GM-CSF and MMP9 release from WAT progenitors *in vitro* and in xenograft models. Metformin had similar effects of GM-CSF/MMP9 specific inhibitions in DIO syngeneic mice, but was more effective in reducing tumor angiogenesis and targeted different immune cells.

Collectively, these results indicate GM-CSF and MMP9 as new potential targets to prevent the pro-tumorigenic effect of WAT progenitors on BC.

Furthermore, Metformin ability to reduce GM-CSF and MMP9 supports Metformin administration in clinical studies on BC, especially in a setting of obesity and/or insulin resistance.

1. Introduction

1.1 Breast cancer

Mammary carcinoma is one of the world-wide leading causes in women. It is characterized by high heterogeneity with different histo-pathological features, treatment sensitivity profiling and clinical outcomes.

1.1.1 Epidemiology and risk factors

Breast cancer (BC) is the most diffuse tumor in women, approximately 29% of newly diagnosed cancers in United States (American Cancer Society, 2015). The mortality has been decreased in recent years, but still 40.000 women die every year for BC, which is the second leading cause of cancer death in United States. According to the AIOM (Italian Association for Medical Oncology), 48.000 new cases are diagnosed every year in Italy and 12.000 people died of BC last year (AIOM, 2015).

Breast cancer incidence rates increase with age, especially in premenopausal years, reaching a plateau at 50-55 years old and increasing again after 60 years old (American Cancer Society, 2015). The age correlation could be explained by the progressive exposure of mammary endothelium to endocrine signaling and/or to the accumulated DNA and epigenetic alterations.

From a geographical point of view, the incidence of BC in western countries is ten-fold higher in United States and Europe, directly correlating that to the modern western lifestyle (AIOM, 2015). Indeed, the consumption of alcohol and fatty acids-enriched food is associated with an increase risk. In particular, obesity is a recognized risk factor predisposing to post-menopausal BC (van den Brandt *et al.*, 2000). The alterations occurring in the adipose tissue surrounding the mammary gland and the increased estrogen synthesis, which actively hyper-stimulates mammary epithelium, might predispose to BC

(Cleary P and Grossmann, 2009). Obesity has also been associated with a higher tumor size at diagnosis, higher tumor grade and, in general, to a poorer prognosis and increased mortality in both pre- and post-menopausal women (Cleary and Grossmann, 2009).

Triple negative breast cancers (TNBC) were significantly associated with overweight in pre-menopausal women, whereas Luminal B ($HER2^-$) tumors were significantly more frequent in post-menopausal overweight women (Agresti *et al*., 2016, Table 1).

		Breast cancer subtype				
BMI (Kg/m^2)	*Total*	**Luminal A**	**Luminal B (HER2-)**	**Luminal B HER2+**	**Triple negative**	**HER2+ (not luminal)**
		%	%	%	%	%
Pre-menopausal women						
< 25	465	25.4	51.2	11.2	6.7	5.6
≥ 25	131	19.8	47.3	13.0	13.0	6.9
Post-menopausal women						
< 25	512	31.3	48.4	9.0	6.6	4.7
≥ 25	588	24.3	57.0	8.2	5.6	4.2

Table 1. Epidemiological data correlating obesity/overweight to BC incidence. Principal subtypes are included (adapted from Agresti *et al*., Breast Cancer Res. Treat. 2016).

1.1.2 Histopathological classification

The current histological classification was proposed by the World Health Organization (WHO) in their guidelines (Lakhani *et al*., 2012). BC could arise from different breast anatomical structures, affecting milk ducts (ductal carcinoma or not otherwise specified) or mammary glands (lobular carcinoma). These two types may display invasive properties (invasive carcinoma) or not (*in situ* carcinoma). Invasive carcinomas are composed by malignant epithelial tumors, characterized by infiltration in surrounding tissues with irregular borders and metastatic spread. Noninvasive tumors display aberrant proliferation, without crossing basal membrane or invading surrounding tissues.

Invasive carcinomas are routinely graded based on the assessment of tubule/gland formation, nuclear pleomorphism and mitotic counts. The histology of the tumor is associated with the clinical outcome and prognosis: grade 1 is associated with a well differentiated tumor with a good prognosis, grade 2 with a moderately differentiated tumor and grade 3 with a poorly differentiated carcinoma with a worse prognosis.

According to the American Cancer Society (2015), the most diffuse (80%) invasive carcinoma is the invasive ductal carcinoma (IDC), which is characterized by an initial hyperplasia of ductal epithelium, followed by the formation of aggregates of malignant cells invading the surrounding stroma, constituted by adipose tissue. Atypical tumor cells originate ribbons, tubules or nest and frequently are associated with necrotic areas. In the stroma, IDC induces desmoplastic reaction with abundant fibrosis and collagen deposit.

Invasive lobular carcinoma (ILC) constitutes approximately 10% of all invasive carcinoma (American Cancer Society, 2015). ILC typically grows as single cells, single lines or sheets. ILC is usually larger than IDC, but better differentiated and with a later metastatic spread. ILC might be characterized by bilateral and multifocal growth.

However, this histological classification was unable to reflect the high heterogeneity of BC, because, within each group, tumors displayed different biological and clinical features. Therefore, the histological classification showed poor prognostic and predictive impact.

1.1.3 Molecular Classification

Due to the limited prognostic and predictive power of the histological classification, the molecular profiling of different breast carcinoma has been done to better characterize tumor heterogeneity (Sorlie *et al.*, 2001). The presence or absence of estrogen receptor (ER), progesteron receptor (PR) and human epidermal growth factor receptor 2 (HER2/neu) protein over-expression is commonly used for this classification (Fig.1). It seems to display more prognostic value and to better predict the response to chemotherapy (Viale, 2012). Different molecular signatures correspond to distinct tumor severity and

prognosis, together with clinic-pathological parameters, such as tumor grade, size and lymph nodes involvement.

Luminal tumors are the most diffuse type of breast carcinoma, displaying hormone receptors expression (ER^+PR^+) and several genes normally expressed by luminal epithelium, including cytokeratines. Two distinct subtypes are differentially characterized: Luminal A, which is negative for HER2 expression, and Luminal B, which may express or not HER2. Luminal B tumors usually have a higher grade compared to Luminal A, with a poorer prognosis.

Tumors, characterized by over-expression of HER2, are considered as specific group and lack of other hormone receptors. These tumors are associated with a poor prognosis and are usually characterized by deep genomic alterations: the over-expression of several genes in HER2 amplicon and p53 mutations.

Basal tumors are mainly composed by TNBC, which are characterized by the absence of expression of all hormone receptors and HER2. Higher expression of proliferation-related genes and basal markers, such as keratins or EGF (Epidermal growth factor) receptor, completes the tumor profile, which is very aggressive with a poor prognosis. TNBCs are clinically relevant due to their lack of responsiveness to standard chemotherapies.

Another BC subtype was recently identified and defined as claudin-low (CL) subtype (Sabatier *et al*., 2014). These tumors are characterized by the absence of luminal markers, high genomic instability, expression of epithelial to mesenchymal transition (EMT)-related genes and stem cell-like characteristics. Claudin-low tumors displayed a poor disease-free survival similar to luminal B or TNBC tumors (Sabatier *et al.*, 2014).

Tumor proliferation is another important prognostic parameter to be evaluated in molecular classification. In clinical practice, the evaluation is done by Ki67 staining. However, its use as a prognostic marker is still debatable, due to the lacking in standardization and reproducibility (Viale, 2012).

A certain grade of heterogeneity can be also found within a single tumor, with differential expression of hormone receptors and HER2 in different tumor areas. This discordance has also been reported between primary tumors and the matched metastatic lesions.

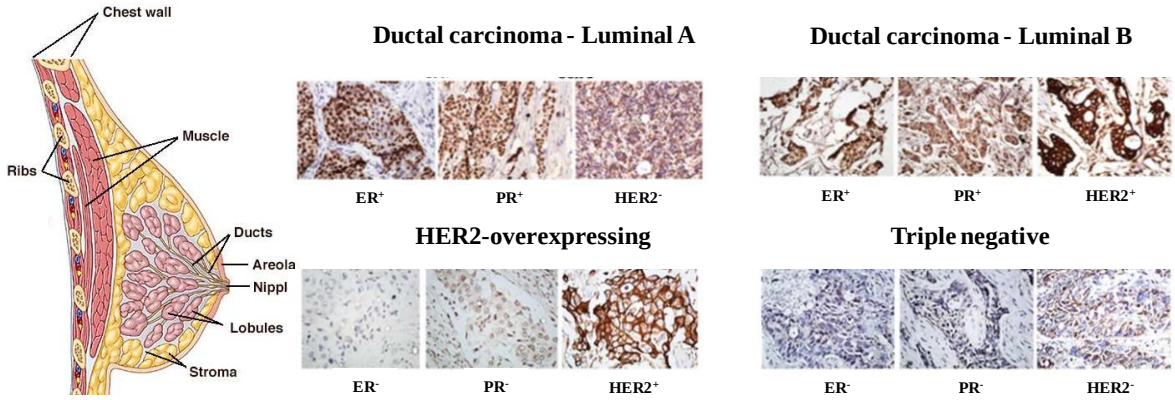

Fig.1 Representative images of BC subtypes according to histological and molecular classifications. Tumors are classified according to their anatomical localization in the mammary glands, in ducts or lobules (left). From a molecular classification, staining of ER, PR and HER2 identifies different subtypes (right) (adapted from Thorat *et al.*, Oncol. Lett. 2013).

1.1.4 Preclinical models of breast cancer

Animal models are useful in studying BC development and progression, and in testing novel therapeutic approaches. These models ideally possess genetic and abnormalities similar to human counterparts. The most suitable available model is the xenograft, in which human cells or tissue are implanted either heterotopically (subcutaneously) or orthotopically (into mammary fad pad). Many models are also available to analyze the role of immune system on tumor progression, like the syngeneic models or genetically engineered mouse (GEM) models. Each preclinical model presents advantages and limitations, which need to be carefully considered in the choice of the appropriate one.

1.1.4.1 Syngeneic models

Syngeneic models are immunocompetent mice bearing tumors derived from the strain of origin. These models are extensively used to analyze the impact of a functional immune system on tumor biology. Recently, they are widely used to develop immunotherapy protocols, able to stimulate immune system against tumor cells.

The principal limitations of these models include the intrinsic differences between the biology of tumors in rodents and humans (Kim *et al*., 2004): i) in the mammary gland of rodents, unlike humans, a full glandular maturation is contingent on pregnancy, generating important differences regarding multipotent stem cells and their role in carcinogenesis; ii) the shorter lifespan of rodents leads to a rapid tumor progression, which may develop very aggressive tumors with multiple genetic alterations; iii) many human BC are hormone responsive, while the vast majority of mouse tumors are hormone independent; iv) BC in humans usually spreads through lymphatic system and the principal sites of distant metastasis are bones, brain, adrenal gland, liver and lungs. In contrast, murine BC metastasizes almost exclusively to lungs through blood vessels; v) profound differences in metabolism between rodents and humans affect tumor behavior and microenvironment.

1.1.4.2 Genetically engineered mouse (GEM) models

These models are characterized by genetic profile alterations in one or several genes, likely involved in transformation or malignancy of tumor cells. These genes could be deleted, over-expressed or defective, leading to spontaneous tumor development. GEM models are useful to study the impact of specific alterations in tumor biology and to evaluate *in vivo* novel therapeutic responses to these tumors. The molecular events triggering human BC can be reproduced in GEM models. For example, mouse mammary tumor virus (MMTV)/c-neu transgenic mice express an activated rat *c-neu* oncogene (*Erbb2*). This alteration mimics the aberrant activation of ErbB2 receptors in human tumors, leading to

multifocal mammary tumors development with metastatic spread to lungs in mice, starting from 5-10 months of age (Muller WJ *et al.*, 1988). However, many oncogene-bearing or tumor suppressor-knock out (KO) transgenic mice have a whole-body phenotype, in which all tissues and cells are affected. Thus, these tumors do not mimic sporadic forms arising from a single cell transformation in a normal microenvironment. To overcome this limitation, tissue-specific promoters are commonly used to generate the alteration only in targeted tissues. Hormone-sensitive promoters are usually used in BC preclinical models, such as the MMTV long terminal repeat, which are not the natural promoters of human BC, leading to inappropriate tumorigenesis.

1.1.4.3 Xenograft models

The ability of human tumors to grow in immunodeficient mice characterizes xenograft models, able to recapitulate the growth of human tumors in a whole organism.

Several genetically induced immunodeficient mice are available (Kim *et al.*, 2004): nude mice, characterized by T-deficiency induced by chromosomic autosomal recessive mutation; severe combined immunodeficiency (SCID) mice, with a single mutation that inactivates a DNA protein kinase, leading to a defective T- and B-cells mediated immune response. Many human xenograft models are available for BC research, principally derived from established human BC cell lines or genetically engineered immortalized breast epithelial cells (Kim *et al.*, 2004). However, the use of established cancer lines is questioned as source for xenograft models, due to alterations arising in cancer cells during the *in vitro* culture passages. Primary BC cells would be the optimal choice for xenograft, reflecting tumor original phenotype. However, the difficulty in obtaining reproducible xenografts and the purity of primary samples from stromal cells might limit the use of these models. The principal limitation of xenograft mice is the absence of a functional immune system, which exclude their use in immunological studies.

1.2 White Adipose Tissue (WAT)

White adipose tissue (WAT) is found subcutaneously, mostly in abdomen and in the lower body (gluteal-femoral), and in visceral regions of mammals (Fig.2).

Main functions of WAT involve the regulation of metabolic body homeostasis, including triglycerides storage, in presence of energy consumption, and fatty acid release, when energy expenditure exceeds energy intake. This regulation affects endocrine, paracrine and autocrine signaling pathways and is important for the functionality of organs, such as brain, liver, muscles and pancreas**.** Additional functions include the mechanical protection and support of organs and the prevention of heat loss through the skin.

Accordingly to its anatomical depots, WAT displays unique features: visceral adipose tissue (VAT), located in the abdominal cavity and mediastinum, significantly differs in metabolic and hormonal profiles from the subcutaneous adipose tissue (SAT), mainly located in hypodermis.

Metabolic differences between VAT and SAT are due to different storage and mobilization capacities (Muller C *et al*., 2013). SAT has a role in thermo insulation and displays lower metabolic activity than VAT, with higher short- and long-term storage capability of triglycerides. Insulin and cathecolamines, the principal hormones regulating lipids storage and mobilization, exert different effects on the adipose depots, leading to higher lipolysis rate in VAT compared to SAT.

SAT and VAT display also a distinct secretion profile, with differential expression of adipokines, inflammatory mediators and angiogenesis-related factors. VAT is characterized by higher pro-inflammatory activity compared to SAT, higher vascular endothelial growth factor (VEGF) release and higher accumulation of macrophages and immune cells (Muller C *et al*., 2013). Regional heterogeneity characterized both VAT and SAT, showing different histological and metabolic characteristics, according their specific

location. For instance, SAT in mammary gland displays physiological specialization and special biochemical properties.

WAT is morphologically and physiologically different from its neonatal counterpart, the brown adipose tissue (BAT), which is mainly located in the supraclavicular area and almost lost with aging. WAT is characterized by adipocytes with a single lipid droplet, whereas BAT contains adipocytes with multiple lipid droplets. BAT presents a larger number of mitochondria and is specialized in heat production during thermogenesis. The typical brown color of BAT reflects the increased mitochondria content and the density of vasculature.

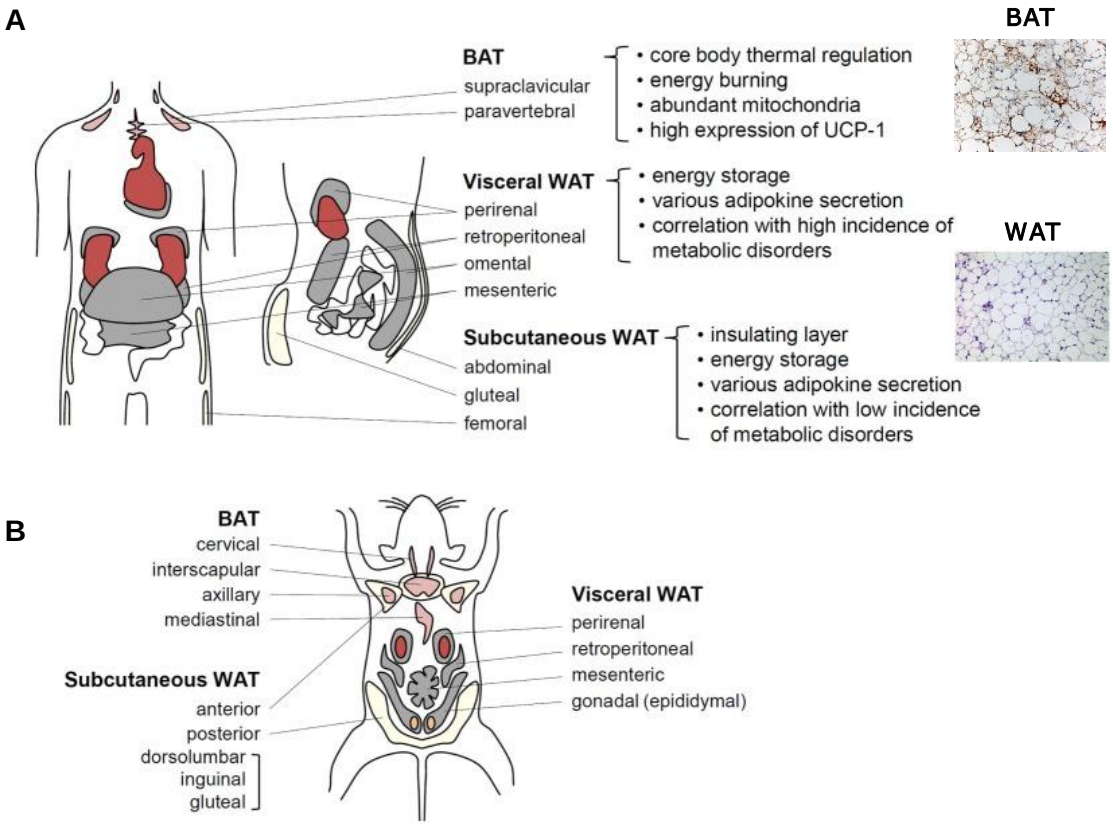

Fig.2 Differential distribution of body fat depots. WAT and BAT localization in humans **(A)** and mice **(B)**, with their principal functions (adapted from Choe *et al.*, Front. Endocrinol. 2016).

1.2.1 Cellular composition of WAT

WAT composition varies among different individuals according to age, metabolic status and presence of pathological conditions, such as obesity, diabetes mellitus and cancer. In physiological conditions, approximately one third of the tissue is constituted by mature adipocytes, whereas the remaining part is a combination of blood vessels, nerve tissue, fibroblasts and pre-adipocytes at various stages of development (Armani *et al.*, 2010). Beside adipocytes, the fraction of WAT that contains several cell populations, namely the stromal vascular fraction (SVF), can be easily isolated after digestion with collagenase and centrifugation (Martin-Padura *et al*., 2012).

1.2.1.1 Adipocytes

Adipocytes are characterized by large cellular size (30-70μm diameter), due to the presence of a massive lipid droplet, which usually occupies 90% of the cytoplasm. These cells are characterized by narrowed nucleus, displayed on one side. The histological appearance of WAT shows spherical or oval cells with irregular profile, due to lipid extraction during tissue processing (Fig.3). Adipocytes are organized in lobules surrounded by a connective stroma, which supports the network of cells and neurovascular elements.

Mature adipocytes derive from pre-adipocytes, originated from a specific line of connective tissue. Pre-adipocytes are characterized by a spindle shape, a fully developed endothelium reticulum and an active Golgi. The production and accumulation of lipid droplets start in pre-adipocytes during pre-natal period. The number and size of lipid droplets increase with time and the shape of the adipocyte changes from a spindle to a sphere, characterizing the mature differentiated form.

Adipocytes have a primary role in WAT energetic metabolism, being the principal source of fatty acids. Adipocytes uptake fatty acids, glucose and amino acids, storing them under the form of triglycerides. These molecules are mostly accumulated in intracellular lipid

droplets. Specific signals are able to stimulate the hydrolysis and release of free fatty acids into circulation. All these processes are under the control of the neuroendocrine system (Muller C *et al*., 2013).

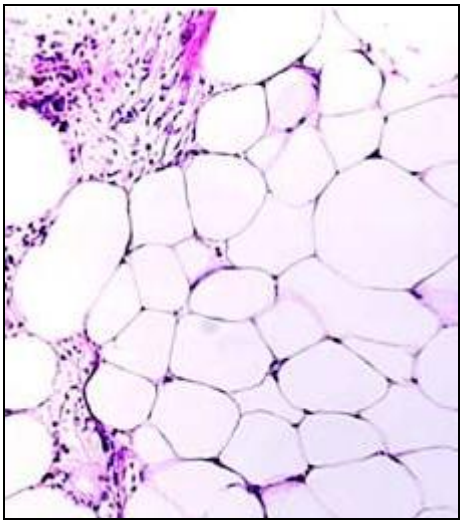

Fig.3 Representative image of WAT histology. Hematoxylin & Eosin (H&E) staining (adapted from Ledoux *et al*., Diabetes 2008).

1.2.1.2 Adipose stem cells and progenitors

Bone marrow (BM)-derived progenitors appear to be less responsive to stimuli with age, displaying a decreased capacity to face injury repairs in peripheral tissues. Therefore, other organs are likely to be the source of mobilized progenitor cells.

The plasticity of WAT throughout life is often associated with the presence of a resident population of stem/progenitor-like cells, which was detected in the $CD45^{-}CD34^{+}$ fraction, contained in the SVF (Martin-Padura *et al*., 2012). This population of progenitors is composed by two distinct cell sub-populations: adipose-derived stem cells (ASCs) and endothelial progenitor cells (EPCs) (Orecchioni *et al*., 2013).

ASCs represent the major cell population of the SVF ($CD45^{-}CD34^{+}$ fraction) and display proliferative potential similar to BM-derived mesenchymal progenitors, but with unique

features (Martin-Padura *et al.*, 2012): freshly isolated ASCs from lipotransfer material display higher expression of perivascular genes, such as Endosialin, Adam12, Platelet-derived growth factor (PDGF) receptors and Transforming growth factor (TGF)-β. ASCs immunophenotype is characterized by brilliant expression of CD34 progenitor marker, CD13, CD90 and CD44 expression and the absence of CD45 and CD31 markers (Fig.4).

ASCs were reported to be involved in adipogenesis, osteogenesis, myogenesis, cardiomyogenesis and neurogenesis**,** if exposed to appropriate stimuli *ex vivo* (Freese *et al*., 2015). In their work, Rodeheffer and colleagues (2008) demonstrated that ASCs, transplanted into fat pads of A-Zyp lipodystrophic mice, were able to regenerate functional WAT depots, confirming the multipotency of these cells. Of note, ASCs isolated from VAT showed higher self-renewal ability than progenitors isolated from SAT (Zhang Y *et al*., 2010). ASCs contributed also to endothelial cells proliferation and new blood vessels formation, through the release of VEGF, Hepatocytes growth factor (HGF) and other pro-angiogenic mediators (Rodeheffer *et al*., 2008). Therefore, these WAT-derived cells might be a powerful tool in regenerative medicine approaches.

In addition to ASCs, EPCs can be isolated from the $CD45^{-}CD34^{+}$ fraction. These cells are able to generate *in vitro* and *in vivo* mature endothelial cells (Fig.4) (Orecchioni *et al*., 2013). EPCs are usually identified as BM-derived progenitors, being released into circulation after certain stimuli, such as the increase of tissue hypoxia or mediators involved in wound healing. The recruitment of EPCs into new blood vessels (vasculogenesis) occurs also in adult subjects. However, EPCs are found to be resident not only in BM, but also in extramedullary organs, as in WAT. EPCs detected in WAT are small and undifferentiated cells, over-expressing endothelial-related genes, such as VE-Cadherin, Claudin 5 and Tie-2 (Martin-Padura *et al.*, 2012). Resident WAT-derived EPCs are positive for CD34, CD31 and CD105 markers, whereas are negative for CD45 expression (Fig.4). WAT-EPCs share with BM-EPCs similar levels of stemness- and

pluripotency- related genes, such as NANOG, SOX2 and Lin28 (Martin-Padura *et al.*, 2012). However, WAT-derived EPCs displayed significantly higher expression of angiogenesis-related genes compared to BM-derived EPCs, including CD144, VEGFR2 and ALK-1 (Martin-Padura *et al.*, 2012). EPCs were also detected to be about 263-fold more abundant in WAT than in BM (Martin-Padura *et al.*, 2012).

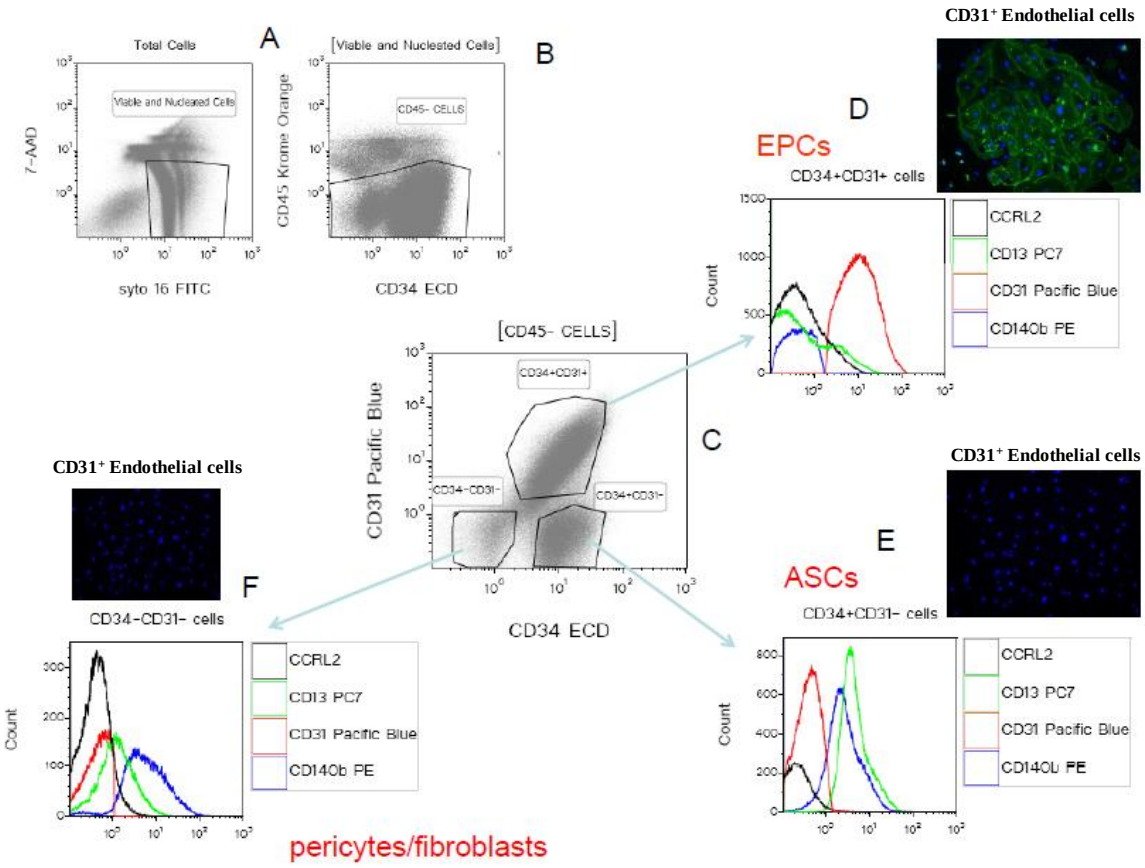

Fig.4 Multiparametric flow cytometry analysis of SVF isolated from WAT and depleted for CD45$^+$ hematopoietic cells. A-B) Gating strategy. **C)** Differential expression of CD34 and CD31 markers on ASCs, EPCs and other stromal cells. **D)** EPCs immunophenotype; these cells can differentiate into CD31$^+$ mature endothelial cells (*green*) *in vitro*. **E)** ASCs immunophenotype; ASCs were unable to generate *in vitro* endothelial cells. **F)** Pericytes/fibroblasts immunophenotype; these cells were not able to differentiate into endothelial cells *in vitro* (adapted from Orecchioni *et al*., Cancer Res. 2013).

1.2.1.3 Resident immune cells

CD45 expressing cells are included in the SVF of WAT and represent the hematopoietic derived population. These cells are mainly involved in the regulation of immunity and inflammation. They are expanded from a WAT resident pool or, alternatively, a rapid turnover of immune cells occurs with a constant recruitment from circulation.

The principal population is constituted by resident macrophages, which display a specific polarization accordingly WAT physiological or pathological status (Lumeng *et al*., 2007). Signals from microenvironment drive macrophages toward a classic (M1) or alternative (M2) activation state (Lumeng *et al.*, 2007). M1 macrophages display higher expression of pro-inflammatory cytokines and MHC (Major Histocompatibility complex) class II molecules. Conversely, M2 macrophages show increased expression of different genes, involved in wound healing and in inflammation balance, such as pro-angiogenic mediators and immunosuppressive factors. Lymphocytes also enrich the SVF, mainly with T lymphocytes and T-regulatory (T-reg) cells.

1.2.2 Obesity

The increased average weight of human population, due to the modern lifestyle, has been associated with a dramatic raise of the pathological condition defined obesity. Overweight, with body mass index (BMI) between 25 and 30 kg/m^2, and obesity, with BMI higher than 30 kg/m^2, are rising worldwide to epidemic proportions. The WHO estimated that more than 1.9 billion adults were affected in 2014 (WHO, 2016).

The abnormal and excessive amount of body fat is commonly linked to an increased risk of cardiovascular diseases, diabetes mellitus, metabolic syndromes and the incidence of different types of cancers, with a decreased overall survival (OS) and increased relapse (Renehan *et al*., 2008).

The first relevant epidemiological study, investigating the correlation between adiposity and cancer incidence, has been published in 1979 (Lew and Garfinkel, 1979). The cancer mortality was increased by a third among men, due to colorectal cancers, and by 55% among women, due to gallbladder, breast, cervical, endometrial and ovarian cancers.

A meta-analysis, published in 2001, suggested that the majority of new cases of cancers in Europe were related to obesity and overweight (Bergstrom *et al*., 2001). Cancers most significantly associated with obesity were tumors affecting endometrium, kidney, gallbladder, colon and breast (Bergstrom *et al*., 2001).

The cellular composition and functionality of WAT are completely altered in obese subjects (Santander *et al.*, 2015): adipocytes display hypertrophy (increased number of adipocytes) and hyperplasia (increased size and intracellular lipids storage) (Fig.5). The excessive and rapid adipocytes expansion leads to un-appropriated ECM remodeling and angiogenesis, with a consequent cellular hypoxia, oxidative stress and low-grade inflammation.

The establishment of a chronic inflammation is widely detected in obese individuals and might play a central role in the WAT pro-tumorigenic effects, acting both locally and systemically (Iyengar *et al.*, 2016). The inflammation is usually characterized by the presence of crown-like structures (CLS), which are formed by apoptotic adipocytes surrounded by a crown of activated macrophages (Santander *et al*., 2015). In turn, recruited macrophages secreted C-X-C Motif Chemokine Ligand (CXCL)-12, which further promoted angiogenesis and chronic inflammation (Arendt *et al.*, 2013).

Macrophages are enhanced in obese subjects with a positive correlation with BMI and adipocyte size, reaching up to 40-50% of cells found in WAT, compared to the physiological level of 10% (Weisberg *et al.*, 2003). Resident WAT macrophages displayed a preferential M1-polarization in obesity, whereas in lean mice the M2-phenotype was detected to be predominant (Lumeng *et al.*, 2007).

The adipose concentration of myofibroblasts was also increased, changing the stiffness of ECM: the fibrosis, generated by excessive ECM deposition, is commonly found in WAT from obese subjects (Seo *et al.*, 2015).

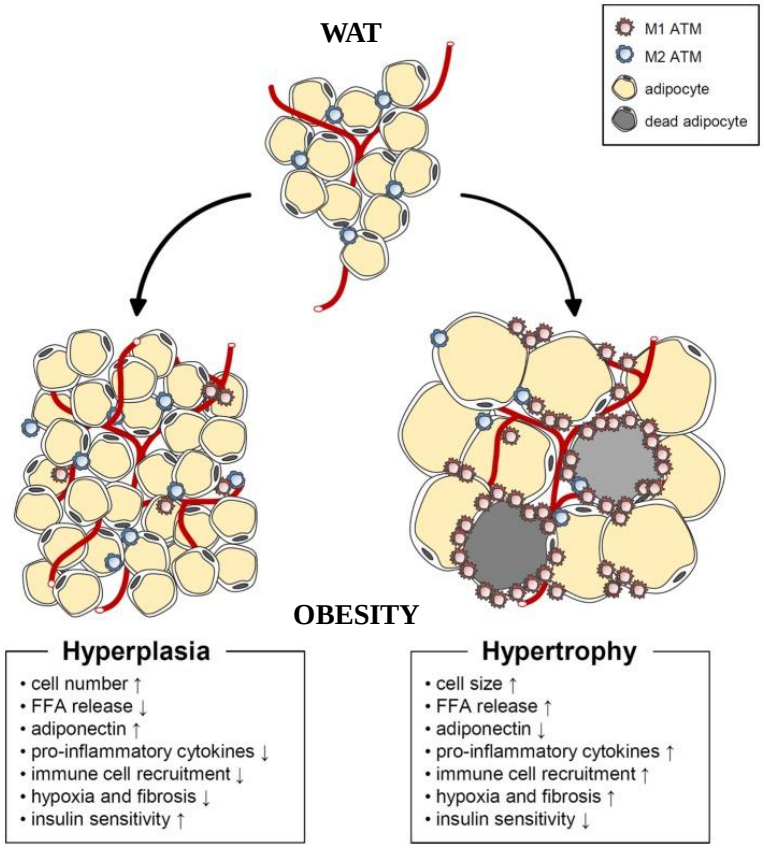

Fig.5 Two mechanisms mediating WAT expansion in obesity: hyperplasia and hypertrophy. Both mechanisms are regulated by environmental and genetic factors (adapted from Choe *et al.*, Front. Endocrinol. 2016).

Metabolic and secretory differences between SAT and VAT are exacerbated in obesity, leading to deregulation in adipokines, pro-inflammatory mediators and angiogenic factors. Adipokines are molecules produced by both adipocytes and SVF cells, composed by a heterogeneous class of more than 50 soluble factors involved in metabolism, inflammation, immune system, angiogenesis and ECM regulation (Paz-Filho *et al.*, 2013).

Leptin is the main adipocyte-derived hormone, able to regulate food intake and body energy homeostasis. Leptin levels are associated with BMI, with a tremendous increase in obese individuals (Al-Hamodi *et al*., 2014). Leptin controls different pathways, regulating cell proliferation and survival, such as JAK/STAT (Janus Kinase/Signal Transducer and Activator of Transcription), PI3K/AKT (phoshatidylinositol 3-kinase/protein-kinase B) and AMPK (5' AMP-activated protein kinase). Therefore, leptin may act as mitogen, pro-inflammatory mediator, pro-angiogenic and anti-apoptotic factor.

In contrast, adiponectin levels are markedly reduced in obesity, with a negative correlation with BMI (Al-Hamodi *et al*., 2014), deeply affecting the physiology of glucose and lipid metabolism. Adiponectin acts as insulin sensitizer, anti-inflammatory and anti-angiogenic factor able to regulate the balance of vasculature and inflammation in WAT.

The obesity-related low-grade inflammation is associated with high release of pro-inflammatory mediators, such as interleukin (IL)-6, IL-1β, tumor necrosis factor (TNF)-α and monocytes chemoattractant protein-1 (MCP-1 or CCL2) produced by adipocytes and activated immune cells. These factors deeply alter the activities of other WAT cells, influencing cellular proliferation, ECM properties and angiogenesis.

Circulating levels of VEGF are higher in obese subjects, both humans and animals, being associated with a poor prognosis in many obesity-related cancers (Liu Y *et al*., 2011). VEGF can be produced by adipocytes to stimulate endothelial cells proliferation, promoting new blood vessels formation.

Visfatin is also up-regulated in obesity, since it is mainly produced by VAT macrophages, rather than adipocytes. This adipokine has a role in regulating vascular inflammation and angiogenesis, up-regulating the expression of different metalloproteinases (MMPs), including MMP2 and MMP9, able to remodel ECM. Similarly, the plasminogen activator inhibitor-1 (PAI-1) is higher released by VAT (in particular by endothelial cells and adipocytes) in obesity, mainly affecting ECM properties.

Resistin is a specific adipose tissue secreted factor, which is highly produced by macrophages and increased in obese subjects. Resistin highly release is frequently associated with insulin resistance through AMPK inhibition. Insulin resistance is frequently associated with obesity and the raising of metabolic disorders. Several other mechanisms might be responsible, including the reduction of insulin sensitizers levels (such as adiponectin) or the increased inflammation (pro-inflammatory mediators promote insulin resistance, such as IL-6, TNF-α).

1.2.3 Preclinical models of human obesity

The choice of the appropriate model for obesity studies is essential to unveil its complexity. Among rodent preclinical models, different types can be distinguished (Nilsson *et al.*, 2012): monogenic or polygenic, which are usually diet-induced obesity (DIO) models. Although these models are useful, they display many limitations: animals suffer of immune deficiency, hormones imbalances and dysfunctional bone homeostasis, altering the effects of obesity over concomitant pathologies, such as cardiovascular disorders or neoplastic disease **(**Khandekar *et al.*, 2011).

1.2.3.1 Monogenic models

Monogenic models are characterized by a distinct phenotype, usually obtained altering a single gene expression.

Since leptin has been extensively analyzed as the principal cytokine linked to obesity, monogenic mice with genetic deficiency of leptin (*ob*/*ob*) or leptin receptor (*db*/*db*) are very common models in obesity studies. In *ob*/*ob* mice the excessive body weight is early displayed, whereas insulin resistance and hyperglycemia arise later. Leptin deficiency is associated with an increased food intake, defects in thermogenesis and enhanced liver lipogenesis. The C57 background strain of *ob*/*ob* mice is essential to define the severity of

the observed phenotype and variations were still observed according to the type of *ob* mutation (Nilsson *et al*., 2012). Treatment of *ob*/*ob* mice with recombinant leptin was able to reverse the pathological phenotype, restoring glucose turnover and improving insulin sensitivity (Burcelin *et al.*, 1999). *Db*/*db* mice display a more severe phenotype with hyperglycemia and diabetes, compared to *ob*/*ob* mice (Nilsson *et al*., 2012). However, in humans most of obese individuals display leptin resistance, rather than deficiency. Therefore monogenic models do not fully reflect the actual complexity detected in obesity and could be not the best option to evaluate pharmaceutical treatments or concomitant pathologies.

1.2.3.2 Polygenic models – DIO models

Polygenic mice models are usually preferred compared to monogenic, due to the more achievable complexity and because they better recapitulate human-like condition. Human obesity is caused by the interplay of several genes and the environment, making the polygenic dietary-induced models the most suitable. DIO models are characterized by excess of calories intake through the diet. Interestingly, not all mice strains are susceptible to DIO, indicating that the genetic background is essential in defining body weight response (West *et al.*, 1992).

Commercially available research diets, able to induce obesity in rodent preclinical models, are within a range of 30-78% of total energy intake. The fat sources prevalently derive from soybean oil and lard, which are in different amounts according to the percentage of energy intake. Conversely, the use of high-carbohydrate-low-fat diets is not efficient in inducing obesity in preclinical models. Mice administered with high-fat diet (HFD) displayed similar effects on body weight, adiposity and hyperglycemia compared to obese humans with a diet rich of lipids and carbohydrates (Nilsson *et al*., 2012). C57BL/6J mice administered with HFD or low-fat diet (LFD) starting from 8 weeks of age, significantly

increased body weight according to the type of diet and sex, already 4 weeks after starting the diet (Yang *et al*., 2014). BALB/c mice appeared to be more resistant to a significant body weight increase under HFD regimen, but displayed increased adiposity, hepatic oxidative stress and high WAT inflammation compared to LFD mice, similarly to other strains analyzed, including C57BL/6J and FVB/N mice (Montgomery *et al.*, 2013).

1.3 Molecular mechanisms of breast cancer progression in obesity

Epidemiological studies suggested an association between BC and obesity. Furthermore, preclinical GEM models (MMTV-TGFα) administered with HFD developed mammary tumors at earlier age compared to their lean counterparts (Cleary MP *et al*., 2004).

Different mechanisms were reported to cause the increased incidence and severity of BC in obese individuals, including the involvement of soluble and cellular players (Bertolini *et al.,* 2014; Orecchioni *et al.,* 2015). Multiple signals and pathways are involved in the cross-talk among different WAT microenvironment components, revealing a complex regulatory network. WAT produces a large number of fatty acids, growth factors, cytokines and hormones, many of which are reported to stimulate tumor growth and progression, through paracrine or endocrine signaling.

Inflammation is probably one of the principal mechanisms involved in the pro-tumorigenic effect mediated by WAT-derived cells. The higher release of pro-inflammatory mediators by dysfunctional adipocytes and infiltrated macrophages, such as MCP-1, TNF-α, IL-6, was found significantly increased in patients with BC (Iyengar *et al.*, 2016). This might be due to the higher activation of nuclear factor-kappa B (NF-κB) pathways (Morris *et al.*, 2011). All hallmarks of inflammation were associated with a worse prognosis in BC patients.

1.3.1 Soluble factors

Different pathways have been considered when analyzing soluble factors involved in the pro-tumorigenic effect of WAT (Paz-Filho *et al*., 2013) (Fig.6): i) Insulin-like growth factor 1 (IGF-1), which is systemically enhanced in obesity and associated with increased activation of mammalian target of rapamycin (mTOR) pathway; ii) Aromatase activity, with alterations of estrogen metabolism or estrogen receptor signaling and the consequent

increased estradiol production; iii) Increased leptin and/or reduced adiponectin; iv) Pro-inflammatory mediators altered release.

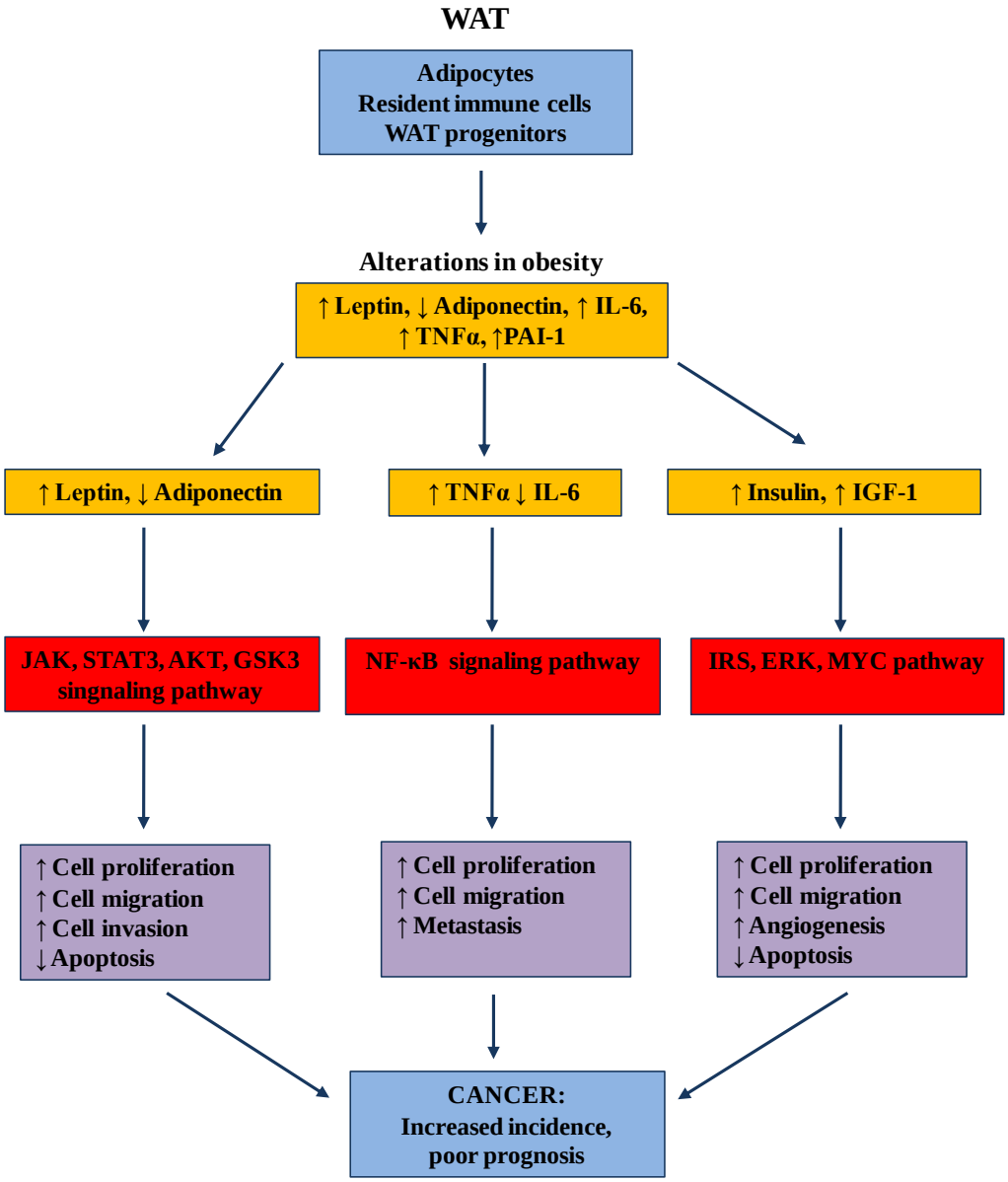

Fig.6 Schematic view of adipokines and soluble factors altered in obesity. Potential mechanisms involved in promoting BC onset and progression (adapted from Paz-Filho *et al.*, Springer Ed. 2013).

A recent work from Subbaramaiah and colleagues (2011) proposed the higher release of pro-inflammatory mediators as the key mechanism. In details, TNF-α, IL-1β and cyclooxygenase-2 (COX-2) were found tremendously up-regulated in WAT of both DIO and *ob*/*ob* mice. Of interest, the increase of these pro-inflammatory mediators was detected

in the SVF after the exposure to saturated fatty acids, released from adipocytes, and directly linked to the up-regulation of aromatase expression. Other adipokines, including leptin, failed to be effective in contributing to this regulatory axis, suggesting a primary role of pro-inflammatory mediators in triggering BC premalignant lesions.

However, leptin release by adipocytes in obesity was reported to promote BC progression, acting as growth factor and activator of several downstream signaling pathways, such as ERK, STAT3 or MAPK in tumor cells. This promoted BC migration and invasion, trans-activating ErbB2 and EGF receptor (Paz-Filho *et al*., 2013). In addition, leptin stimulated aromatase expression, with consequent increased estrogens synthesis and stimulation of ER^+ BC cells (Paz-Filho *et al*., 2013). Leptin could also mediate angiogenesis through VEGF release (Rene Gonzalez *et al.*, 2009). Of note, *ob/ob* leptin deficient mice did not develop transgene-induced mammary tumors compared to wild type mice (Cleary MP *et al*., 2003), suggesting an important role in BC growth.

In contrast, a prospective analysis revealed that adiponectin was inversely correlated to BC incidence in post-menopausal women, but not in pre-menopausal women (Tworoger *et al*., 2007). The mechanism by which adiponectin might inhibit BC progression is still under investigation. Possible molecular targets might be TNF-α and the consequent NF-κB pathway, which is involved in tissue inflammation and angiogenesis, or AMPK and PI3K/AKT signaling, which are involved in BC invasion and proliferation (Paz-Filho *et al*., 2013).

The increased IGF levels are still controversial in obesity: some studies reported higher IGF serum levels in obese diabetic patients and in rodent models (Khandekar *et al*., 2011). However, the regulation of IGF secretion usually depends on hormones which are reduced in obesity, leading to a more complex network of regulations (Khandekar *et al*., 2011). Obesity-induced insulin resistance might lead to a prolonged hyper-insulinemia, enhancing the expression of the active form of IGF1, which act as mitogen, pro-angiogenic mediator

and promoter of tumor migration (Paz-Filho *et al.*, 2013). IGF interacts with its receptor, triggering the activation of oncogenic pathways such as RAS-MAPK and PI3K-AKT. IGF activity seemed essential in BC development, as suggested by transgenic mice over-expressing *Igf1* or its receptor (Carboni *et al.*, 2005).

1.3.2 Cellular players

Different cells in WAT contribute to BC progression, revealing a bidirectional dynamic cross-talk between cellular microenvironment and tumor cells. BC induces a permissive microenvironment and, in turn, stroma cells support tumor progression, mainly through the release of growth factors, chemokines and ECM-modifying enzymes. Both resident WAT cells and systemically mobilized cells are recruited in tumor microenvironment, contributing to tumor inflammation, ECM remodeling, angiogenesis, immune suppression and energy supply (Fig.7).

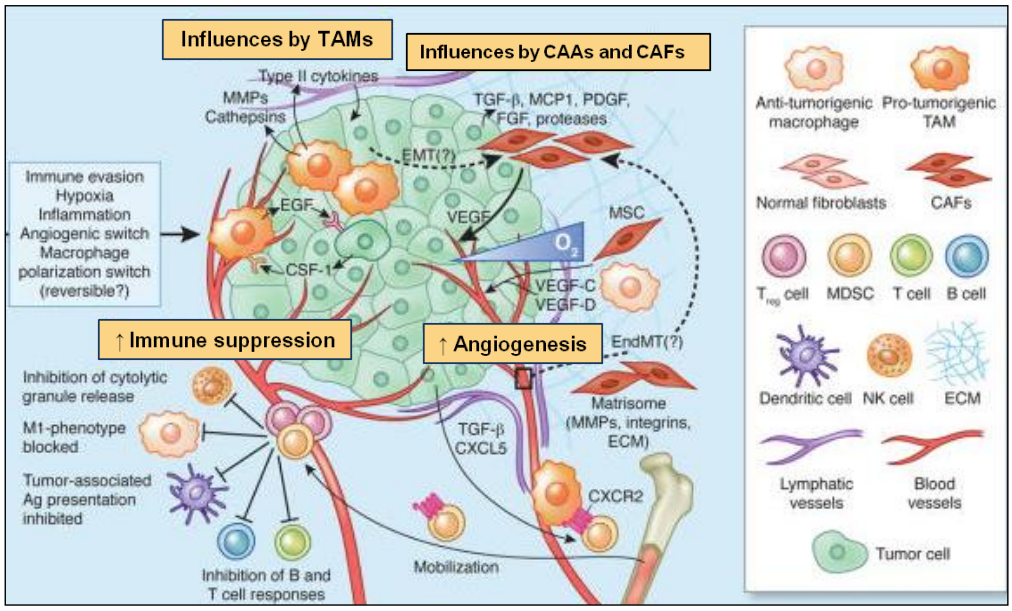

Fig.7 Tumor microenvironment alterations. A permissive microenvironment is detected in obesity-related tumors, with increased angiogenesis, immune suppression and stimulation of BC growth and invasion (adapted from Quail and Joyce, Nat. Med. 2013).

1.3.2.1 Cancer-associated adipocytes (CAAs)

In the work of Dirat and colleagues (2011) cancer-associated adipocytes (CAAs) were morphologically and functionally compared to normal adipocytes. CAAs were detected at the tumor invasive front in BC patients and displayed delipidation, smaller size and a fibroblast-like phenotype. Loss of expression of adipogenesis-related markers and increased secretion of pro-inflammatory cytokines, MMPs and ECM components were associated with this aberrant phenotype. The consequent permissive microenvironment increased BC invasiveness and metastasis *in vitro* and *in vivo*. Of note, adipocytes surrounding diffuse BC, with lymph nodes involvement, displayed the highest IL-6 expression (Dirat *et al*., 2011). CAAs and dysfunctional obesity-related adipocytes share common features, such as the altered secretion profile of pro-inflammatory mediators and ECM-related enzymes. This suggests that the deleterious cross-talk between adipocytes and BC cells might be amplified in obesity, partially justifying the associated poor prognosis.

1.3.2.2 Tumor associated macrophages (TAMs)

Increased macrophages accumulation in obesity might be essential to BC onset and metastatic progression. As previously described, in obese subjects WAT is enriched by M1-polarized macrophages, mainly involved in the establishment of a low-grade chronic inflammation and, likely, contributing to cancerogenesis (Iyengar *et al.*, 2016). Macrophages infiltration in BC was strongly associated with a reduced relapse-free survival and a general worse OS (Zhang Y *et al*., 2013). Direct interactions with tumor cells induce macrophages to acquire a particular phenotype, which characterizes tumor-associated macrophages (TAMs).

Frequently, TAMs are characterized by M2-associated genes expression, important for physiological wound healing and balance of inflammation: TAMs are able to promote

angiogenesis, ECM remodeling and suppress adaptive immunity. The presence of TAMs actively contributes to a permissive microenvironment, enhancing tumor growth, angiogenesis, metastasis and invasion into surrounding tissues (Arendt *et al*., 2013; Su *et al.*, 2014). However, different subsets of TAMs were detected in tumor microenvironment: Movahedi and collaborators (2010) analyzed macrophages isolated from mouse mammary tumors and suggested that TAMs were composed by a mixed population of M1 and M2 polarized macrophages. Tumor hypoxic regions were associated with a prevalence of M2-like TAMs. Hypoxia is a well known inducer of M2 polarization and frequently associated with cancer growth and progression. M2-like TAMs rapidly increased in number during tumor growth, becoming the prevalent form of macrophages detectable in tumor microenvironment.

TAMs were recruited mainly by MCP-1 (CCL2), which was found highly released by dysfunctional adipocytes in obesity (Arendt *et al*., 2013) and its expression was associated with a poor prognosis in BC patients (Ueno *et al*., 2000). TAMs almost exclusively originated from circulating inflammatory monocytes being chemoattracted by MCP-1 (Movahedi *et al.*, 2010).

1.3.2.3 Myeloid derived suppressor cells (MDSCs)

In addition to macrophage accumulation and dysfunctional activation, other immune cells were altered in obesity, with a potential role in promoting BC. Accumulation of myeloid derived suppressor cells (MDSCs) in WAT inhibits T-specific cells response and induces M2 polarized macrophages, further triggering an immunosuppressive microenvironment, essential to BC progression and immune escape. The MDSCs population is heterogeneously composed by different myeloid precursor cells, displaying several stages of differentiation and being able to generate macrophages, granulocytes and dendritic cells. Two main sub-populations were described: Monocytic (Mo)-MDSCs and Granulocytic (G)-MDSCs, differing for surface markers expression and reactive oxygen species (ROS)

and nitric oxide (NO) production, but displaying similar immunosuppressive activity (Youn *et al*., 2008). MDSCs are characterized by a rapid turnover and expansion in tissues and in circulation. In several preclinical models of cancer, MDSCs rapidly increased with a prevalent expansion of the G-MDSCs population (Youn *et al*., 2008).

1.3.3 WAT-derived progenitor cells

The $CD45^{-}CD34^{+}$ fraction, isolated from the SVF of WAT, contains two populations of resident progenitor-like cells, ASCs and EPCs (Orecchioni *et al*., 2013). To investigate the potential role of these progenitors in BC onset and metastatic progression, the whole fraction or purified sub-populations were co-injected with human BC cells in immunodeficient mice (Fig.8). WAT-derived progenitors significantly enhanced tumor growth and metastatic progression in a complementary manner, suggesting an important pro-tumorigenic activity mediated by these cells (Martin-Padura *et al.*, 2012; Orecchioni *et al.*, 2013).

1.3.3.1 Adipose derived stem cells (ASCs)

Xenograft models of human BC were obtained through the co-injection with human ASCs: the presence of ASCs in BC tumors was associated with an increased local growth, metastatic spread to lungs and axillary lymph nodes (Zhang Y *et al.*, 2009; Orecchioni *et al.*, 2013). ASCs, resident in endogenous WAT, were systemically mobilized and recruited by tumors, engrafting into microenvironment and contributing to tumor progression (Zhang Y *et al.*, 2009; Zhang Y *et al.*, 2012; Orecchioni *et al*., 2013). Recruited ASCs were able to differentiate into CAAs and pericytes, actively contributing to tumor vasculature in tumor microenvironment (Zhang Y *et al*., 2012; Orecchioni *et al*., 2013). In their recent study, Zhang T and collaborators (2016) demonstrated that ASCs migration was driven by a gradient of CXCL1 and CXCL8 chemokines, produced by pancreatic

tumor. The release of these chemokines was indeed obesity-dependent. In another study, using murine models of BC, ASCs migrated towards PDGF, which was produced by tumor cells (Gehmert *et al*., 2010).

ASCs proliferation was associated with WAT expansion in obesity: the number of progenitors per gram of tissue was significantly increased in obese subjects, both in patients and preclinical models (Martin-Padura *et al*., 2012; Zhang Y *et al*., 2012; Dallaglio *et al*., 2014). Accordingly, the level of ASCs was found significantly enhanced in systemic circulation of obese patients (Zhang T *et al*., 2016) and circulating ASCs were 6-fold increased in tumor-bearing obese mice (Zhang Y *et al*., 2012). Moreover, ASCs isolated from lean subjects contributed less significantly to BC growth (Strong *et al.*, 2013). Recruitment of endogenous ASCs in obesity was associated with increased vascularization, adipogenesis and enhanced proliferation of neighboring malignant cells (Zhang Y *et al.*, 2012).

Culture experiments revealed the ability of tumor conditioned media to differentiate ASCs progenitors into cancer-associated fibroblasts (CAFs), expressing α-SMA and fibronectin (Chandler *et al*., 2012). Of note, ASCs isolated from *ob/ob* mice displayed enhanced pro-fibrotic phenotype compared to ASCs isolated from lean mice (Seo *et al.*, 2015). Therefore, these cells might contribute to fibrosis and desmoplastic reactions, frequently associated with BC and obesity. These results were confirmed by the observation that ASCs, collected from obese mice, enhanced tissue stiffness and fibrosis, altering the mechanical properties of the stroma and promoting tumor growth (Seo *et al*., 2015).

1.3.3.2 Endothelial progenitor cells (EPCs) resident in WAT

The role of WAT-derived EPCs was investigated in xenograft models of BC (Orecchioni *et al.*, 2013): EPCs were able to differentiate into mature endothelial cells *in vitro* and to be recruited to tumor blood vessels *in vivo*. EPCs promoted tumor migration and metastatic spread to lungs and axillary lymph nodes in these preclinical models. Of note, ASCs were

more effective in promoting local tumor growth, whereas EPCs increased more efficiently tumor invasion and metastasis (Fig.8). Complementary to ASCs, EPCs promoted EMT in ductal carcinoma, inducing the over-expression of EMT-related genes, such as ZEB1 and SNAIL2 (Orecchioni *et al*., 2013).

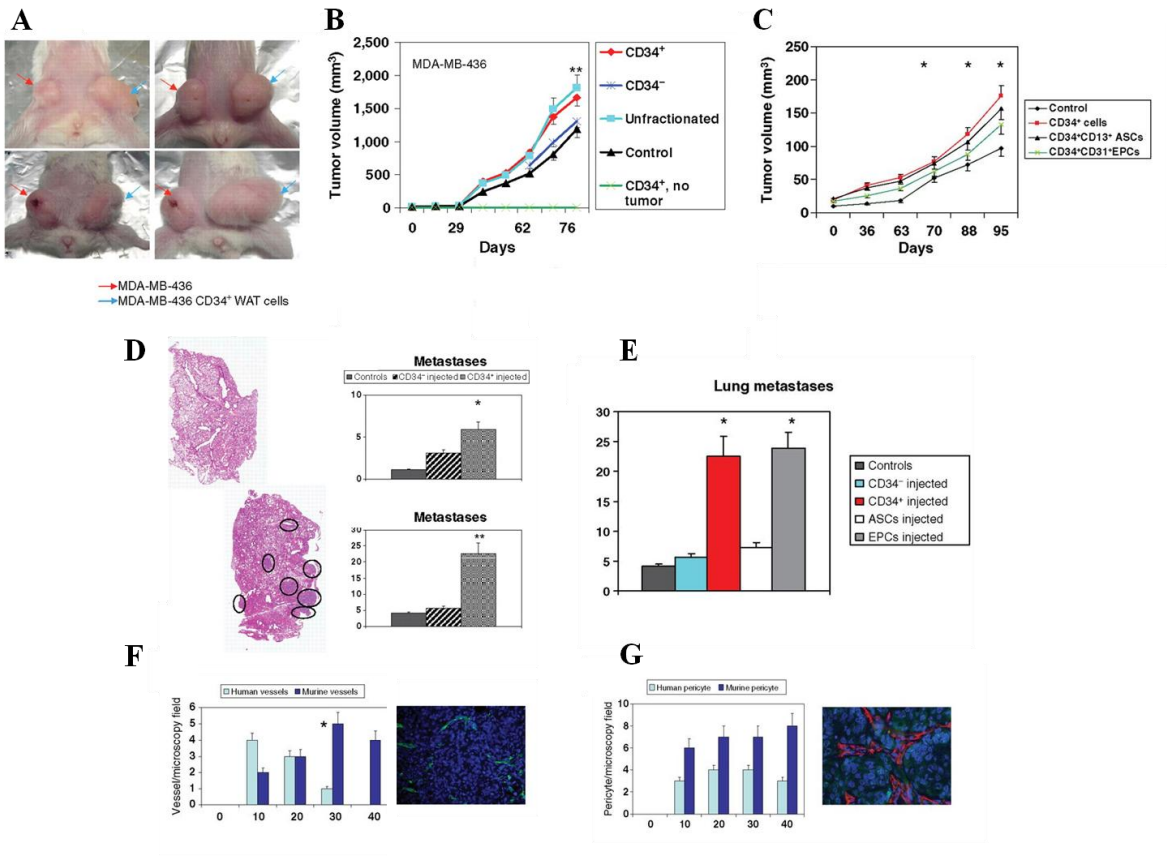

Fig.8 Effects on BC progression in orthotopic models of WAT CD34^{+}CD45^{-} progenitors, EPCs and ASCs. A-B) Tumor growth was enhanced in NSG mice injected with BC and CD34^{+} WAT progenitors compared to other fractions in the SVF; **C)** Effects of purified ASCs and EPCs on tumor growth; **D-E)** Lungs metastasis detection; **F)** Contribution to vascular endothelial cells generation of EPCs; **G)** Relative contribution of ASCs differentiating into perivascular pericytes (adapted from Martin-Padura *et al.*, Cancer Res. 2012 and Orecchioni *et al.*, Cancer Res. 2013).

1.4 Interaction between BC cells and WAT-derived progenitors

The molecular interaction between BC and resident WAT progenitors has not been elucidated yet. The aim of the present work was to identify some factors possibly involved in this bidirectional interaction.

Several works suggested that distinct factors might be relevant in this interplay, such as IL-6, IL-10, TGFβ and MMPs. Two factors were investigated for the first time in the present work as possible key interactors: Granulocyte-macrophage colony-stimulating factor (GM-CSF) and MMP9.

1.4.1 Background

Several paracrine and cell-to-cell mechanisms were investigated to clarify the interaction between ASCs and BC cells. ASCs conditioned medium was reported to be able alone to increase *in vitro* BC cells proliferation, due to the release of IL-6, IL-8, IL-10 and MCP-1 (Kucerova *et al*., 2013). Conditioned medium was reported to be more efficient than direct co-culture in promoting BC proliferation, EMT and motility. This suggested a prevalent paracrine interaction. However, some authors claimed that an exosome-mediated cell-to-cell contact was necessary for the increased tumor cell proliferation induced by ASCs, followed by the activation of Wnt pathway (Lin *et al*., 2013).

ASCs isolated from VAT of obese subjects displayed altered gene expression profile, including leptin and aromatase higher production, probably due to excessive estrogens exposure (Strong *et al.*, 2013). ASCs were found able to secrete high levels of CCL5 in co-cultures with BC cells, with a consequent increased migratory potential of tumor cells, due to elevated MMPs secretion by BC cells (Pinilla *et al*., 2009). In another study, IL-6 produced by ASCs was instead reported to promote migration and invasiveness of BC cells in xenograft models (Walter *et al.*, 2009).

Stromal cell-derived factor 1 (SDF-1) was also identified to be important in BC spread, suggesting that ASCs promoted human (MDA-MB-231) and murine (4T1) BC migration through its release (Muehlberg *et al*., 2009). The production of several MMPs by ASCs suggested that interplay of MMPs, rather than a single type, promoted ECM remodeling, facilitating tumor invasion and promoting angiogenesis (Hattori and Ishihara, 2015).

ASCs ability to establish a permissive tumor microenvironment included the enhancement of angiogenesis, through the production of VEGF and HGF, which directly stimulated endothelial cells proliferation (Rodeheffer *et al*., 2008). Immunomodulatory effects of ASCs were investigated in the work of Razmkhah and colleagues (2011): IL-4, IL-10 and TGFβ were highly released by ASCs, with consequent T-regs expansion and anti-inflammatory response, leading to induce immune suppression.

To date, fewer efforts were addressed to identify specific factors involved in WAT-derived EPCs/BC interaction. Nevertheless, several studies investigated possible factors involved in BM-derived EPCs and BC cells. EPCs were mobilized from BM and recruited to hypoxic tumor site, where contributed to tumor neo-angiogenesis in a paracrine manner, by release of pro-angiogenic mediators (VEGF, basic fibroblast growth factor (bFGF), Arginine1, Arginine2) and MMPs (MMP2, MMP9) (Suriano *et al*., 2008).

1.4.2 Granulocyte-macrophage colony-stimulating factor (GM-CSF)

GM-CSF is a cytokine able to induce myeloid cells differentiation and expansion of hematopoietic BM-derived progenitor cells (Fig.9). The factor is produced by several cells, including immune cells (monocytes, macrophages, granulocytes, and T lymphocytes), endothelial cells and fibroblasts. GM-CSF expression is finely regulated in a cellular-specific manner, by the presence of a specific enhancer detected only in the promoter of expressing cells.

GM-CSF has a pleiotropic activity, acting as growth factor for myeloid cells (mainly monocytes/macrophages, neutrophils and dendritic cells), pro-angiogenic mediator able to stimulate the proliferation and migration of endothelial cells, and inducer of wound healing processes. GM-CSF is a potent chemotactic factor for immune cells, which are recruited to inflammation sites, including both myeloid and lymphoid populations. It is also associated with increased expression of pro-inflammatory mediators, such as IL-1β and TNF-α, which, in turn, up-regulated GM-CSF itself (Kim *et al.*, 2008). GM-CSF was deeply involved in the low-grade chronic inflammation detected in WAT from DIO mice and in the observed macrophages accumulation (Kim *et al.*, 2008). The involvement of the factor in immune-modulation, tolerance and autoimmune diseases was also investigated (Bhattacharya *et al.*, 2015). GM-CSF seemed to be more involved in myeloid regulation in presence of inflammation than in the steady state: the factor was a potent inducer of tolerogenic dendritic cells, which, in turn, promoted T-regs expansion (Bhattacharya *et al.*, 2015).

GM-CSF acts on target cells through the binding of its receptor GM-CSFR (GM-CSF receptor), activating four distinct signaling pathways: PI3K-Akt, ERK1/2, JAK2/STAT5 and NF-κB (Bhattacharya *et al.*, 2015). GM-CSF promotes cell survival and differentiation through PI3K and JAK/STAT5 signaling, whereas cell proliferation and inflammatory response are induced through activation of ERK1/2 and NF-κB pathways.

GM-CSF receptor is expressed on myeloid lineage cells (including monocytes, macrophages, neutrophils, granulocytes, basophiles, and dendritic cells), $CD34^+$ progenitors, fibroblasts and vascular endothelial cells. It is not detected on the majority of lymphoid cells. GM-CSF production is enhanced by pro-inflammatory mediators such as IL-1 and TNF-α, microbial products and the lipopolysaccharide protein.

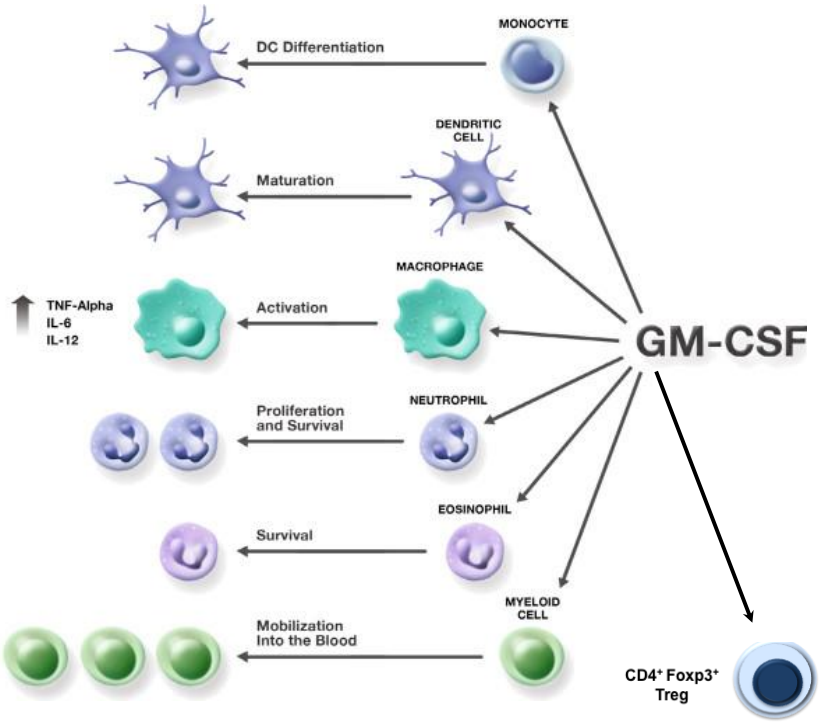

Fig.9 Pleiotropic effects of GM-CSF on myeloid and other immune cells. (adapted from Kaufman *et al*., J. Immunother. Cancer 2014).

The role of the factor in tumor biology remains controversial.

On one hand, it is used to mobilize hematopoietic progenitors for autologous or allogeneic transplantation and to ameliorate chemotherapy-induced neutropenia (Arellano *et al*., 2008). Recently, GM-CSF administration as adjuvant in immunotherapy protocols was addressed to achieve a proficient anti-tumor immune response: GM-CSF may enhance tumor-specific antigens presentation by dendritic cells (Arellano *et al*., 2008). However, the lymphocytic and inflammatory infiltrate at the site of cytokine injection not always correlated with improved clinical outcomes, calling into question the real efficacy of the treatment.

On the other hand, GM-CSF has been described as tumor promoting factor in different types of cancer (Gutschalk *et al*., 2013; Su *et al*., 2014; Wang *et al*., 2014; Ghirelli *et al*., 2015). GM-CSF was able to enhance tumor cells proliferation and migration *in vitro* and *in vivo* in squamous cell carcinoma (Gutschalk *et al*., 2013). GM-CSF targeted not only

tumor cells, but also the stromal cells in tumor microenvironment. GM-CSF was shown to induce the release of VEGF and to enhance tumor angiogenesis in colorectal carcinoma (Wang *et al*., 2014). Furthermore, high levels of the factor, produced by BC, were associated with suppression of immune response and a poor prognosis (Ghirelli *et al*., 2015).

1.4.3 Matrix metallopeptidase 9 (MMP9)

MMPs are heterogeneous class of 25 enzymes able to remodel ECM and involved in the pathogenesis of several diseases. Physiologically, MMPs play a role in tissue remodeling in embryonic development, angiogenesis, ovulation, mammary gland involution and wound healing. These proteases can be divided into sub-groups, according to the domain structure and substrate specificity: interstitial collagenases, gelatinases, stromelysins and membrane MMPs. The substrate specificity of MMPs is not limited to ECM components, but includes different target molecules, such as growth factors, receptors and other MMPs. The consequent effect is a tight regulation of microenvironment, not only limited to ECM plasticity. A family of tissue inhibitors of MMPs (TIMPs) is physiologically present to balance the activity of MMPs, binding them with 1:1 ratio and repressing their activity.

MMP9 is a 92kDa zinc-dependent endopeptidase belonging to the class of gelatinases, together with MMP2. The two gelatinases degrade gelatin (denatured collagen) and different types of collagen, sharing mostly substrate specificity, differing only for some growth factor receptors. Many MMPs, including MMP9 and MMP2, are secreted as inactive pro-forms (pro-MMP9; pro-MMP2), which are extracellular activated by cleavage mediated by other proteases. MMP9 interacts with its specific inhibitor TIMP1. Altered secretion or regulation of MMPs leads to dysfunctional ECM, basal membrane degradation and increased angiogenesis, which were frequently detected in invasive and metastatic BC (Duffy *et al*., 2000).

MMP9 higher expression was investigated in invasive carcinoma and involved in tumor initiation, regulating the expression of several oncogenes and tumor-suppressor genes (Duffy *et al.*, 2000)**.** MMP9 was detected to be produced both by BC and other cells in tumor microenvironment, including vascular endothelial cells, TAMs, neutrophils and fibroblasts (Pellikainen *et al.*, 2004).

La Rocca and colleagues (2004) demonstrated for the first time that MMP9 levels were significantly higher in sera collected from BC patients compared to healthy subjects, with a positive correlation with ErbB2 over-expression. This suggested a regulatory axis involved in the establishment of metastasis and invasion mediated by tumor cells. MMP9 was included in the list of genes of Rosetta signature for poor prognosis in BC (van't Veer *et al*., 2002) and was found highly expressed by several human BC. TNBC were reported to express higher levels of MMP9, compared to other BC subtypes (Mehner *et al*., 2014).

In the GEM model, MMTV-PyMT, MMP9 release by neutrophils was associated with increase lungs metastasis (Martin *et al.*, 2008). In xenograft model of TNBC the injection of human cell line (MDA-MB-231), silenced for MMP9 expression, was characterized by the absence of lung metastasis compared to scramble controls (Mehner *et al*., 2014). Furthermore, the presence of $CD31^+$ endothelial cells was significantly reduced in MMP9 KO mice compared to scramble, confirming the active role of MMP9 in promoting angiogenesis. MMP9 silencing in TNBC cells resulted in dramatic transcriptional alterations, with impairment of the invasive phenotype (Mehner *et al*., 2014).

MMP9 was also proposed to bind CD44, a hyaluronan receptor expressed on BC cells or WAT-derived progenitors, actively participating to invadopodia formation, invasion and angiogenesis through its proteolytic activity or other mechanisms (Yu and Stamenkovich, 2000).

1.5 Therapeutic strategies targeting BC-WAT interplay

Targeting factors involved in the cross-talk between BC and stroma cells in tumor microenvironment, represents a promising strategy for pharmacologic intervention, to prevent or control cancer in obese patients.

The clinical implication of the deleterious cross-talk between BC and WAT cells might also have impact on the oncological safety of lipotransfer procedures. In plastic and reconstructive surgery, autologous fat grating (lipofilling) allows soft tissue augmentation and is increasingly used for breast reconstruction after mastectomy. Injected adipose tissue might promote relapse of BC, due to several mechanisms: activation of tumor cells during the procedure (for hypoxia or mechanical stress) or release of paracrine factors interacting with quiescent tumor cells. Recently, Petit and colleagues (2013) found increased local BC recurrence in a case-control study: a specific subgroup of patients undergoing surgery for *in situ* carcinoma and lipofilling for breast reconstruction, displayed higher incidence of relapsed tumors within 5 years of the follow-up.

Lipotransfer material may also be enriched by autologous ASCs or freshly isolated SVF cells, to promote the retention of graft volume. This procedure should be considered even more carefully, considering the reported pro-tumorigenic activity of cells isolated in the SVF.

1.5.1 Targeted molecular therapy

As alternative to overall weight reduction, which may be not beneficial in oncological patients, targeting individual pathways or cells involved in the tumor promoting role of WAT might be the right strategy.

Since obesity is associated with an altered level of hormones, the use of estrogen antagonists, such as tamoxifen, has been one of the main strategies for the treatment of hormone-dependent BC (Dignam *et al*., 2003). Tamoxifen binds in a competitive manner

ERs, inhibiting estrogens-associated signaling, which stimulates BC growth. Alternatively, aromatase inhibitors were used to impair aromatase activity and reduce estrogens synthesis, which are dramatically enhanced in obesity (Morris *et al*., 2011). However, third generation aromatase inhibitors were less effective in obese compared to lean post-menopausal women (Sestak *et al*., 2010). These inhibitors failed to completely block estrogens production, or even enhanced leptin levels, which, in turn, might activate AMPK-dependent ER pathway.

Leptin has been suggested as suitable target for therapeutic intervention. Pegylated leptin peptide receptor antagonist (PEG-LPrA2) was used in several preclinical models, both syngeneic and xenograft (Rene Gonzalez *et al*., 2009). The inhibitor significantly reduced the growth of both ER^+ and ER^- BC.

A recent approach suggested that the leptin:adiponectin ratio was more influent over BC progression than the single adipokines absolute quantitation, since the ratio was particularly altered in obesity and needed to be balanced (Al-Hamodi *et al.*, 2014).

Inhibition of angiogenesis was another possible strategy to reduce BC progression in obesity. Bevacizumab was the main targeted anti-angiogenic therapy, approved by the Food and Drug administration (FDA) in 2008 for metastatic BC, to be used in combination with chemotherapy (paclitaxel). This monoclonal antibody (MoAb) targets VEGF, but displayed disappointing results in clinical trials, with poor benefits in patients OS and an high rate of cases of resistance (Montero *et al*., 2012). For these reasons, FDA withdraws the approval for BC treatment in 2011. The failure of bevacizumab in obtaining clinical benefits might be explained by the ability of BC and microenvironment to bypass VEGF-dependent pathways, stimulating angiogenesis through alternative ways, such as a novel CCL2/IL-1β/CXCL12 axis promoted by WAT macrophages (Arendt *et al*., 2013). This effect was exacerbated in obesity and, accordingly, the efficacy of bevacizumab was found impaired in obese colorectal cancer patients, compared to lean patients (Faruk Aykan *et al*., 2013).

1.5.2 Antidiabetic drugs - Metformin

Metformin (dimethylbiguanide) is a widely used oral drug for diabetes type II treatment. It is characterized by the absence of toxicity, with limited and transient side effects, even after prolonged administration. The drug has been recently investigated due to some epidemiological observations in diabetic patients treated with Metformin: the incidence of several types of cancer was significantly reduced, including colorectal, liver, pancreatic and breast tumors (Zhang P *et al*., 2013). Of note, subjects who received the highest doses or the longest administration of the therapy displayed the lower cancer rates.

The drug is active on both BC cells and tumor microenvironment, including endothelial cells and WAT-derived progenitors (Dallaglio *et al*., 2014; Orecchioni *et al.,* 2015). Metformin has been reported to inhibit the growth of several BC subtypes, regardless their ER expression or p53 status (Goodwin *et al*., 2011).

Metformin lowers liver gluconeogenesis and reduces the overall levels of insulin, contributing to improve insulin resistance, very common in obese patients. Metformin effect is mainly mediated by activation of AMPK pathway, through two distinct mechanisms: the inhibition of complex I of the mitochondria respiratory chain and the activation of an up-stream regulator, liver kinase B1 (LKB1). AMPK activation leads to down-stream mTOR inhibition, which reduces protein synthesis and cell proliferation (Fig.10). mTOR is frequently altered both in BC and obesity. Other mechanisms may not be mediated by AMPK, as the regulation of cell cycle: in TNBC the levels of cyclins D1 and E were reduced, with a consequent impaired tumor proliferation and cell cycle arrest (Liu B *et al.*, 2009). In these cells, Metformin was also able to increase apoptosis, through activation of both intrinsic and extrinsic signaling pathways. Additional studies revealed that Metformin was able to balance aromatase activity in adipose breast stromal cells, reducing the overall levels of estrogens synthesis in obese subjects (Brown *et al*., 2010).

The anti-tumor activity of the drug was associated with its anti-proliferative and pro-apoptotic effects on both BC and WAT progenitors (Orecchioni *et al*., 2015). *In vivo*

preclinical models, Metformin administration significantly reduced BC growth and metastatic spread in syngeneic, GEM and xenograft models, including both ER^+ BC and TNBC (Orecchioni *et al*., 2015).

Metformin affected also angiogenesis, mainly through the suppression of VEGF-dependent activation of ERK1/2, leading to a decreased microvessel density in matrigel assay *in vitro* and *in vivo* (Dallaglio *et al*., 2014) and reducing blood vessels formation in syngeneic models of BC (Orecchioni *et al*., 2015). Moreover, Metformin reduced resident EPCs in WAT from obese mice, further impairing their angiogenic potential (Dallaglio *et al*., 2014). Metformin targeted more efficiently WAT EPCs than ASCs, justifying the observed imbalanced pericytes/endothelial cells ratio (Orecchioni *et al*., 2015). This imbalance was possibly one of the causes of branching and dysplastic cancer vessels phenotype observed in Metformin-treated tumors.

Therefore, Metformin might be an ideal supplemental antitumor drug able to neutralize obesity-induced effects and targeting both tumor and microenvironment cells, including WAT-derived progenitors.

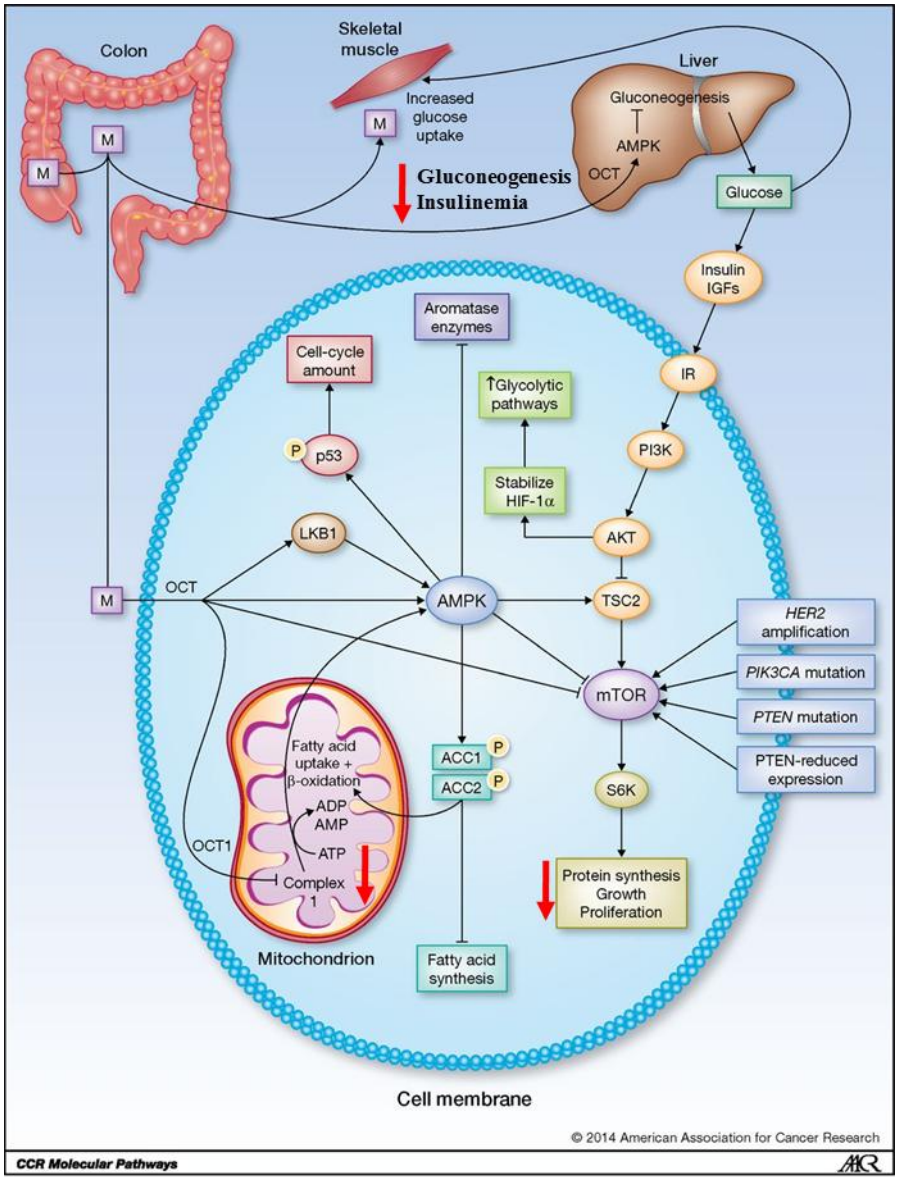

Fig.10 Metformin's mechanisms of action. The drug impairs liver gluconeogenesis and circulating insulin. In BC and microenvironment cells, Metformin activates AMPK through LKB1 or by complex I inhibition in mitochondria. Activated AMPK inhibits mTOR signaling with reduction of protein synthesis and cell proliferation (adapted from Thomson, Clin. Cancer Res. 2014).

1.5.3 Anti-inflammatory drugs - NSAIDs

Anti-inflammatory drugs, such as Aspirin and other nonsteroidal anti-inflammatory drugs (NSAIDs), were a promising strategy to reduce obesity- and tumor- associated low-grade chronic inflammation. Low-dose aspirin administration reduced incidence of several tumors, including BC in obese and overweight women (Bowers *et al.*, 2014). The mechanism was associated with COX2 inhibition and the consequent block of prostaglandins release, which affected aromatase and pro-inflammatory mediators release by adipocytes and macrophages. Additional studies suggested that aspirin might induce apoptosis in tumor cells in a COX2-independent mechanism, which involved Bcl-2 (B-cell lymphoma 2) nuclear translocation and phosphorylation in BC cells (Choi *et al.*, 2013).

In preclinical models of both ER^+ BC and TNBC, low-dose aspirin was not effective alone in reducing tumor growth or metastases, whereas in combination with Metformin displayed a synergistic effect over BC inhibition (Talarico *et al.*, 2016).

Aspirin might have a protective role over BC development, through reduction of WAT inflammation and angiogenesis, or might be used as adjuvant to other therapies.

2. Materials and Methods

2.1 WAT cells collection and processing

Lipotransfer material was collected from women undergoing breast reconstruction at the European Institute of Oncology (IEO, Milan), after the signature of an informed consent. Patients sample included women from 40 to 65 years-old, that were previously operated for primary BC at IEO and did not show a tumor recurrence before lipofilling intervention. Adipose tissue was collected through Lipokit technique by the breast surgery unit and syringes transported in aseptic conditions. The received material was transferred to sterile falcon tubes and stored at 4°C. All the procedures were performed under laminal flow hood to avoid contamination and to protect operators from biological risks. Adipose tissue was centrifuged 3500rpm (rotation per minute) for 5 minutes at room temperature (RT) to separate the tissue from water, blood and lipocaine, which may contaminate the material. The oil accumulated at the top of the gradient and should be removed. The adipose tissue phase was then collected with sterile pipettes and transfer to sterile bottles. 50 ml of collagenase solution must be used for each 10ml of tissue, to maximize digestion efficiency. The collagenase solution was composed by 1mg/ml collagenase type IV (Sigma Aldrich, Italy), 3.5% bovine serum albumin (BSA) dissolved in PBS (Phosphate-buffered saline, Euroclone, Italy). Digestion occurred under agitation at 37°C for at least 1 hour, until the complete digestion of the tissue. The chosen temperature is optimal for collagenase enzymatic activation. After digestion, the material was collected in falcon tubes and centrifuged at 2000rpm for 5 minutes at RT. The undigested tissue and residual oil were then separated from the pellet, constituting the SVF, which was further re-suspended in a Buffer composed by PBS added with 2mM EDTA (ethylenediamine tetra acetic acid, Sigma-Aldrich) and 0.5% BSA. Cells were counted in Trypan Blue (Sigma-Aldrich) with a Burker chamber, to count only viable cells. Cells were then magnetically labeled with anti-human CD45 micro-beads (Miltenyi Biotec, Germany): 20µl of

microbeads should be used every $10x10^6$ of cells, accordingly manufacturer's instructions. After 15 minutes of incubation at 4°C, cell suspension was washed with PBS to remove unbounded beads. After a centrifugation at 1300rpm for 5 minutes at 4°C, cell pellet was re-suspended in 1ml of Buffer and loaded into a magnetic column (LD columns, Miltenyi Biotec). Labelled cells, which are $CD45^+$, were captured by the column, whereas the $CD45^-$ fraction was collected as unbounded fraction. Columns were washed twice with 1ml Buffer, before being discarded. Cell suspension was again centrifuged (1300rpm for 5 minutes) in order to concentrate collected cells. Cells were counted in Trypan Blue and purity/viability assessed by flow cytometry, as described below. Only populations with purity higher than 95% and with a good viability (higher than 80%) were further used for subsequent experiments.

In some experiments the $CD45^-CD34^+$ fraction was further separated into two sub-populations, which differ for CD31 expression: ASCs ($CD31^-$) and EPCs ($CD31^+$). Cells were labeled with anti-human CD31 micro-beads (Miltenyi Biotec): 20µl of FcR Blocking Reagent and 20µl of microbeads were added to $10x10^6$ cells, following manufacturer's instructions. After an incubation of 15 minutes at 4°C, cells were washed with Buffer to remove unbound beads. WAT progenitors were magnetically separated through LS column (Miltenyi Biotec). The column was washed three times with 3ml Buffer: $CD31^-$ fraction (ASCs) was collected as unbounded population, whereas the labeled $CD31^+$ fraction (EPCs) was kept into the column. To recover the positive fraction, the column was removed from the separator, placed into a new collection tube and flushed with 5ml Buffer. Purity and cell viability was checked with flow cytometry, as described below.

Murine adipose tissue was obtained from 8-12 weeks old female mice (FVB/Hsd) housed in our animal facilities at the IEO campus (Milan). Subcutaneous and intra-peritoneal WAT was collected in aseptic conditions, transported in PBS and finely cut in small pieces. The tissue was then processed as human samples, using instead anti-mouse CD45

micro-beads (Miltenyi Biotec). All murine studies were approved, as requested, by the Italian Ministry of Health.

2.2 Cell line culture

Human cell lines (MDA-MB-436, MDA-MB-231, HCC1937, ZR-75-1) and a murine cell line (4T1) were bought from American Type Culture Collection (ATCC, Manassas, VA), amplified and stored accordingly manufacturer's instructions. MDA-MB-436 and MDA-MB-231 were cultured in 1:1 DMEM (Dulbecco's modified Eagle medium, Euroclone)/Ham's F12 (Euroclone) medium, added with 10% FBS (Fetal bovine serum, Euroclone), antibiotics (100U/ml penicillin/streptomycin, Euroclone) and 2mM L-Glutamine (Euroclone); HCC1937 in RPMI (Roswell Park Memorial Institute) 1640 medium (Euroclone) added with 15% FBS, antibiotics and L-Glutamine; ZR-75-1 in RPMI 1640 added with 10% FBS, antibiotics, L-Glutamine and 1mM Sodium Pyruvate (Sigma Aldrich); 4T1 cells in RPMI 1640 added with 10% FBS, antibiotics and L-Glutamine. Glutamine is usually present in commercial mediums, but due to its instability at 4°C, was freshly added. All these cell lines grow in adhesion without a feeding layer. Cultures were kept in incubators at 37°C and 5% CO_2. All manipulations were done under laminal flow hood to avoid cell contaminations. When reached confluence, cells were detached with 2.5% Trypsin (Euroclone), centrifuged (1300rpm for 5 minutes) and seeded 1:3 into new culture flasks. For long term storage, cells (preferably with lower passage) were frozen in FBS added with 10% DMSO (dimethyl sulfoxide, Alchimia, Italy) in frozen nitrogen tanks. Cells were periodically tested and authenticated by Stem cell Elite ID (Promega, Fitchburg, WI).

2.3 Primary breast tumor cells isolation from GEM

Murine HER2 MMTV-ErbB2$^+$ BC cells were obtained from genetically engineered mouse (GEM) FVB-NK1Mul/J (Envigo, UK) as previously described (Cicalese *et al.*, 2009).

These models develop spontaneous breast tumors and lymph nodes swelling, starting from 6-8 weeks of age. Mice were euthanized with CO_2 and all the masses were collected in aseptic conditions and transported in sterile PBS. Tumors were dissected and added to a solution composed by 300U/ml collagenase, 100U/ml hyaluronydase (Sigma-Alidrich) dissolved in 1:1 DMEM/Ham's F12 medium. To maximize the digestion process, the solution was transferred to MACs tubes (Miltenyi Biotec) dissected into MACs dissociator (Miltenyi Biotec), followed by a 2.5 hours digestion at 37°C. The solution was collected and centrifuged (600rpm for 5 minutes). Tumor pellet was washed with Buffer EL (Qiagen, Germany) to remove erythrocytes contamination. A second digestion was performed with 2.5% Trypsin at RT for 3 minutes. After neutralizing Trypsin by adding FBS and by centrifugation, the pellet was incubated with a DNAse (100µg/ml, Qiagen)/Dispase (5mg/ml, Stemcell, Canada) solution for 3 minutes at RT to complete the digestion. After washing with PBS, the solution was filtered (100µm) to remove undigested material and viable cells were counted in Trypan Blue through Burker chamber. Cells were frozen in FBS+10% DMSO in liquid nitrogen tanks.

Cells were cultured in 1:1 DMEM/Ham's F12 medium, added with 10% FBS, antibiotics, L-Glutamine, human insulin (5µg/ml, Sigma-Aldrich), hydrocortisone (0.5µg/ml, Euroclone) and 25mM HEPES (Euroclone) to adjust pH. EGF (Epidermal growth factor, 10ng/ml, Sigma-Aldrich) and cholera toxin (50ng/ml, Euroclone) were freshly added to, respectively, stimulate tumor cell proliferation and inhibiting fibroblasts growth.

2.4 *In vitro* co-cultures

In vitro co-cultures were performed in 6-wells plates using BC cells and primary WAT $CD45^{-}CD34^{+}$ cells. WAT-derived cells requested collagen coating (Corning, NY) and Endothelial Basal Medium (EBM)-2 medium (Lonza, Switzerland) to properly grow *in vitro* (Martin-Padura *et al*., 2012). Medium was supplemented with 0.5% Gentamycin (Thermo Fisher Scientific) to avoid contamination: no growth factors, cytokines or serum

were added to avoid interference within cellular interaction. Two types of co-cultures were obtained: a) Transwell co-cultures using 0.4µm transwell permeable inserts (Corning), with BC cells seeded on the top of the insert and WAT cells on the bottom collagen. The two cell populations can interact only through soluble factors. b) Cells seeded together on collagen coating, to evaluate adhesion molecules involvement.

Single cell cultures were used as controls. In all conditions, cells were plated ($0.8x10^6$ each cell type) in 4.2ml medium and incubated for 72 hours in humidified conditions (37°C, 5% CO_2), without changing the medium. This timing was chosen to be suitable to analyze soluble factors release into culture media. Moreover, cells retained a good viability after 72 hours (60-70% of viable cells). Media were collected, briefly centrifuged to remove cell debris and stored at -20°C. Cells were detached with Accutase (Sigma-Aldrich), used instead of Trypsin due to the higher sensibility of the primary adipose cells. Cells were re-suspended in RLT Buffer (Qiagen) to preserve the RNA.

Some drugs or specific inhibitors were tested in the co-culture system, to assess their ability to interfere within the analyzed cell interaction. Preliminary experiments were done to assess the suitable concentrations unaffecting cell viability. Drugs or monoclonal antibodies (MoAb) were directly added to the medium and, in details, Metformin Hydrochloride (Sigma-Aldrich) was used from 2mM to 10mM; Bortezomib (Sigma-Aldrich) from 3nM to 50nM; Anti-human IL-1β MoAb (#MAB201, R&D systems, MN) from 0.2µg/ml to 0.5µg/ml; Anti-human GM-CSF MoAb (#sc-377039, Santa Cruz Biotechnology, TX) from 0.5µg/ml to 1µg/ml; SB-3CT (#S1326, Sigma-Aldrich) from 0.5µM to 1µM.

2.5 *In vivo* **experiments**

All experiments were carried out in accordance with the Italian laws (D.L.vo 26/14 and following additions) and the institutional guidelines. All *in vivo* studies were approved by

the Italian Ministry of Health. Mice were bred and housed under pathogen-free conditions in IEO animal facility.

2.5.1 Xenograft models of human BC

Six- to eight-week old females NOD SCID IL2RɣŸ null (NSG) were injected into mammary fat pad with $1x10^6$ human BC cells (MDA-MB-436, MDA-MB-231, HCC1937) alone or in combination with $0.2x10^6$ human WAT (hWAT) $CD45^-CD34^+$ cells (n=12 per study arm). Some mice were injected with hWAT $CD45^-$ cells alone as negative controls (n=5). All surgical procedures were performed in aseptic conditions, under laminar flow hood. The generation and optimization of this xenograft model has already been described (Martin-Padura *et al*., 2012). Briefly, mice were anesthetized with 25mg/Kg of Avertin (2-2-2-Tribromoethanol and 2-methylbutanol-2, Sigma-Aldrich), the injection was performed in the right fourth mammary gland through the nipple, using a Hamilton syringe (Hamilton, NV). Cells to be injected were re-suspended in a sterile PBS solution (20µl/mouse) added with 25% Matrigel™ (BD, NJ) and 10% Trypan Blue. Matrigel™ is a solubilized matrix, enriched of several growth factors and ECM proteins, providing an anchorage for the effective attachment and differentiation of cells. A minimum amount of Trypan Blue was used to track the site of injection.

In a separate setting of experiments, half of mice were administered with Metformin (2mg/ml in drinking water) starting 3 days post injection until sacrifice (n=12 per study arm). The chosen dose was already used in preclinical models of BC (Liu B *et al*., 2009; Orecchioni *et al.*, 2013) and was associated with a reduced tumor growth, without impairing mice health, such as weight changes or hypoglycemia. Tumor growth was weekly monitored with digital caliper and tumor volume was calculated according to the formula: $L \times W^2/2 = mm^3$, where W represents the width and L the length of the tumor mass. Every two weeks, peripheral blood (PB) was collected from tail vein or, alternatively, serum or plasma were obtained. For plasma, PB was mixed with EDTA to

avoid coagulation (30µl EDTA for 1ml of whole blood) and, within 30 minutes, centrifuged at 2000rpm for 20 minutes at RT. After centrifugation, the upper yellow phase was carefully collected and stored at -80°C. For serum collection, PB was centrifuged twice at 4000rpm for 15 minutes to separate the clot. The quantitation of seric levels of glucose, cholesterol and triglycerides was performed with Architect c8000 (Abbott, IL).

When the volume of the tumor reached the maximum diameter of 1.2cm, in at least one mouse, all mice were sacrificed through CO_2 inhalation. Tumors were collected and processed, as described below.

2.5.2 DIO orthotopic models

Six-week old FVB/Hsd female mice (Envigo) or BALB/cOlaHsd (Envigo) were administered with *ad libitum* High Fat Diet (HFD) (60% kcal from fat, D12492, Brogaarden, Sweden). This research diet is commonly used to generate DIO preclinical models (Yang *et al*., 2014; Nilsson *et al.*, 2012). Mice weight was weekly monitored. The difference in weight with chow-diet mice became evident one month after the beginning of the diet. A that timing, mice were orthotopically injected into mammary fat pad with either $0.5x10^6$ MMTV-ErbB2$^+$ primary tumor cells (FVB/Hsd) or $0.03x10^6$ 4T1 cells (BALB/c) (n=10 per study arm). The amount of injected cells was chosen within each model, to be suitable with a gradual tumor growth and progression, with a relatively short latency.

Three days (FVB/Hsd) or one day (BALB/c) after injection, inhibition therapy was started every other day until the end of experiments.

For GM-CSF inhibition intraperitoneal (ip) administration of 50µg neutralizing anti-mouse GM-CSF MoAb (clone 22E9, #BE0259, BioXcells, NH) was performed, accordingly the schedule applied by Kowanetz *et al*. (2010) in preclinical model of BC.

For anti-MMP9 inhibition, 25mg/Kg SB-3CT (#S1326, Sigma-Aldrich) was ip administered. SB-3CT was dissolved in a vehicle constituted by PBS-0.1% Tween20 (Sigma-Aldrich)-10% DMSO. SB-3CT is hydrophobic, liposoluble compound which

requires, to avoid precipitation, a vehicle with DMSO concentration higher than 20mg/ml. The used vehicle has already been tested in mice, without showing any signs of toxicity. The chosen administration dose of SB-3CT was already used in preclinical metastatic tumor models (Kruger *et al.,* 2005) and in several ischemia models (Cui *et al.,* 2012; Hadass *et al.,* 2013). The repeated ip administration of SB-3CT did not alter physiological parameters, such as blood pressure or glucose levels, being well tolerated by mice (Cui *et al*., 2012). The selected dose was able to significantly inhibit tissue MMP9 levels, both active and pro-forms, already 7 days after treatment (Hadass *et al.,* 2013).

As controls, respectively 50µg Rat IgG2a MoAb (#BE0089, BioXcell) and/or vehicle were administered to mice.

Some mice (n=5) were administered with Metformin in drinking water (2mg/ml).

Tumor growth was monitored weekly, as previously described. Every 30 days for FVB/Hsd or every 15 days for BALB/c mice, PB was collected from tail vein, mixed with EDTA and analyzed for circulating immune cells through a multiparametric flow cytometry analysis, as described below. When the volume of the tumor reached 1.2cm diameter, mice were sacrificed through CO_2 inhalation or, alternatively, tumor resection (mastectomy) was performed, as already described (Martin-Padura *et al*., 2012). Briefly, mice were anesthetized with 25mg/Kg Avertin and immobilized on their back. In correspondence of the tumor, the skin was carefully cut with aseptic instruments and tumor removed, cauterizing surrounding blood vessels to minimize bleeding. Mammary gland around the tumor was also removed, to prevent the incomplete removal of tumor cells. Skin was stitched with surgical clips and 2-iodiopovidone (Farmec, Italy) was applied to disinfect the wound.

In case of mastectomy, mice were sacrificed 30 days later, to evaluate the metastatic spread to lungs and axillary lymph nodes. Tumor tissue, subcutaneous WAT surrounding tumor and lungs/axillary lymph nodes were collected from all mice to be further analyzed.

2.5.3 Tissue collection and storage

All collected tissues were overnight fixed in 4% phosphate-buffered formalin (Bio-Optica, Italy), followed by paraffin embedding. Five-micron sections of paraffin embedded-lungs and lymph nodes were cut by microtome and stained with standard Hematoxylin and Eosin (H&E, Bio-Optica) for metastases evaluation. Images were acquired with Scan Scope XT device (Leica, Germany) and analyzed with Aperio Digital pathology system software.

Additional samples of tumors and WAT were collected and stored at -20°C for RNA extraction (small pieces in 1ml of RNA later, Qiagen) or at -80°C for protein analysis (small pieces frozen in liquid nitrogen).

2.6 Protein analysis

2.6.1 Screening with Proteomic Array

In vitro co-cultures supernatant was screened for 55 soluble factors involved in human angiogenesis, through the Proteome Profiler antibody array (#ARY007, R&D, MN) following manufacturer's instructions. The use of a multiplex antibody array, based on a membrane-sandwich immunoassay, allowed the detection of different proteins in a single sample, minimizing the sample amount needed. Analyzed analytes included growth and differentiation factors, ECM components, proteases, membrane-bound receptors and intracellular signaling molecules. The screening allowed a preliminary selection of soluble factors possibly involved in the interaction between BC and WAT progenitor cells, comparing co-cultures with single cell cultures media.

2.6.2 ELISA

Selected factors were further validated with Quantikine enzyme-linked immunosorbent assay (ELISA, #DGM00 and #DMP900, R&D), following manufacturer's instructions. ELISA provided higher level of specificity, accuracy and sensitivity in analyte

quantification, compared to proteomic array. Each sample of cultures supernatant was tested in duplicate. The absolute quantitation was obtained.

Plasmatic levels of human GM-CSF (CSF-2) in xenograft NSG mice were measured with Quantikine High Sensitive (HS) ELISA (#HSGM0, R&D), following manufacturer's instructions. The assay does not cross-react with GM-CSF from different species, including murine GM-CSF, according to manufacturer's indications. Quantikine HS ELISA kits were suitable for quantitation of low levels proteins, providing an amplification of the signal, which detected femtogram levels of target protein.

The optical density was measured with Epoch Microplate Spectrophotometer (BioTek, VT) set at 450nm, with wavelength correction at 540nm, to correct optical imperfections in the plates.

2.6.3 Western Blotting

Western Blot (WB) analysis was used to compare different samples for MMP9 expression in a semi-quantitative way. Cellular media were already suitable for WB, whereas cells collected from frozen tissues needed to be digested to obtain whole tumor lysates. Briefly, samples were digested for 30 minutes under constant rotation at 4°C in RIPA (Radio Immunoprecipitation Assay) Buffer (150mM Sodium Chloride (NaCl, Sigma-Aldrich), 1% Triton X-100 (Sigma-Aldrich), 0.5% Sodium deoxycholate (Sigma-Aldrich), 0.1% SDS (Sodium Dodecyl Sulphate, Sigma-Aldrich), 50mM Tris pH 8 (Thermo Scientific, MA), Proteases Inhibitor Cocktail Set III (1:200, Calbiochem, Germany), 1mM PMSF (Phenylmethylsulfonyl Fluoride, Sigma-Aldrich), 7.5mM Sodium Fluoride (Sigma-Aldrich), 5mM EDTA). Samples were additionally sonified, to further break cell membranes and share DNA, for 2-3 minutes (cycles of 10 seconds impulse/10 seconds rest, power of 180W) with Sonifier® Ultrasonic cell disruptor (Branson, CT). Samples were then centrifuged 10000g for 20 minutes at 4°C, to separate cellular debris.

Supernatants were collected and separately stored at -80°C, to avoid repeated freeze-thaw cycles that might affect protein loss and degradation.

Before gel loading, protein concentrations were always measured with the bicinchoninic acid (BCA) assay (Thermo Scientific) and normalized to 1mg/ml.

Samples (10-15µg) were added with ¼ NuPage® LDS (Lithium Dodecyl Sulfate) Sample Buffer (Thermo Scientific) and 5% of beta-mercaptoethanol (Sigma-Aldrich). This passage is necessary to the following polyacrylamide gel electrophoresis, which requires denaturating condition and protein disulfide bonds reduction. Samples were boiled for 5 minutes at 97°C, for complete proteins denaturation.

Proteins were resolved on 7.5% Mini Protean® precast gels (Bio-Rad, CA). This percentage was suitable for the optimum resolution of MMP9 proteins. Precision Plus Protein™ Prestained Standards Dual color (Bio-Rad) was used as marker for molecular weight. The running was performed in denaturing conditions with Tris/Glycine/SDS Running Buffer 1x (Bio-Rad) at low voltage, 100V constant for 1.5 hours, in Mini-Protean Tetra cells (Bio-Rad). The low voltage was convenient for large proteins and to prevent excessive heating.

Proteins were transferred through a Semi-dry blotting to a nitrocellulose membrane (Amersham, GE Healthcare, Italy) with Trans-Blot Turbo™ Transfer System (Bio-Rad) at standard conditions (25V for 25 minutes). Transfer Buffer contained 20% Methanol (Applichem, Germany) and NuPage® Transfer Buffer 1x (Thermo Scientific). Staining with Ponceau S (Sigma-Aldrich) was used to confirm the efficiency of transfer. Membranes were destained with 0.1M NaOH and rinsed in distilled water.

Membranes were blocked with 5% skimmed milk in PBS-0.1% Tween20 for 1 hour at RT. The immunostaining was performed overnight at 4°C with rabbit anti-human MMP9 (1:2000 #ab76003, Abcam, UK or 1:200 #10375-2-AP, Proteintech, IL) and anti-human beta actin 1:5000 (#A5441, Sigma-Aldrich) to normalize protein concentration. After the incubation, washing steps were required to remove excess or unspecific bonds of primary

antibodies and, in general, to minimize signal background (Tris Buffered Saline (TBS)-0.5% Tween20 for 5 times, 10 minutes each). An incubation of 1 hour at RT was done with secondary antibodies horseradish peroxidase (HRP)-conjugated (1:5000, Donkey anti-Rabbit IgG and Goat anti-Mouse IgG, Thermo Scientific). The detection was accomplished with SuperSignal West Dura substrate (Thermo Scientific). This substrate was chosen to be suitable in case of relatively low expressed proteins, due to its enhanced sensitivity and providing detection of mid-femtogram levels of target proteins. The generated signals were detected with CCD (Charge-coupled device) imaging system, ChemiDOC MP System (Bio-Rad). Bands quantitation was obtained with the aid of ImageJ software.

2.6.4 Zymography

Zymogram was used to detect proteases activity within a gel, composed by the substrate of the target enzyme, as gelatin for MMP9/MMP2 (Hu and Breeton, 2010). Proteins were separated according specific molecular weight under nonreducing conditions, but in a denaturating SDS gel electrophoresis. After the running, a renaturation step was necessary to reactivate enzymatic activity.

To assess MMP9 proteolytic activity, co-culture supernatants or whole tumor lysates (15-20µg) were added 1:2 to Zymogram sample Buffer (Bio-Rad). No heating step was required. Proteins were resolved on a 10% Ready Zymogram precast gel (Bio-Rad). The running was performed in denaturing conditions with Tris/Glycine/SDS Running Buffer 1x (Bio-Rad) at 100V constant for 1 hour in Mini-Protean Tetra cells (Bio-Rad). Precision Plus Protein™ Prestained Standards Dual color was used as control for molecular weight.

Gels were then incubated 0.5 hours in Zymogram Renaturation Buffer 1x (Bio-Rad), which removes SDS from the gel, allowing proteins renaturation. A second incubation was required with Zymogram Development Buffer 1x (Bio-Rad), which contained the divalent metal cation (calcium), necessary for enzymatic activity. The incubation was done overnight at 37°C. Gels were then stained with PageBlue™ (Thermo Scientific) for 4-5

hours at RT and images were acquired with ChemiDOC MP System. The gelatin in the gel appeared stained (blue), whereas areas around active proteases were lighter due to the proteolytic activity.

2.7 Real-time PCR

RNA extraction from cells or tissues was performed with Qiamp Mini Blood kit (Qiagen), following manufacturer's instructions. RNA amount and quality was checked with NanoDrop 2000 (Thermo Scientific). RNA (0.5-1µg) was retro-transcribed with Ipsogen RT kit (Qiagen), following manufacturer's instructions.

Quantitative reverse transcriptase-polymerase chain reaction (qRT-PCR) was carried out with ABI Prism 7000 platform (Applied Biosytems, Thermo Scientific), using primers and probes from TaqMan® Gene Expression Assays (Thermo Scientific) listed in Table 2. The housekeeping human gene ABL1 was used as internal control, with primers, probe and plasmids from Ipsogen BCR-ABL1 kit (#670013, Qiagen). Each reaction was performed in duplicate using TaqMan® Universal Master Mix (Thermo Scientific).

The threshold of the reaction was set to 0.1 and the results were calculated as:

ΔCt = Ct of the target gene – Ct housekeeping gene

ΔΔCt = ΔCt – number of cycles (50)

Final value = 2^ (-ΔΔCt)

The up- or down-regulation of target genes among different samples was expressed as times-fold expression compared to controls.

RT^2 Profiler PCR array for mouse inflammation and immunity cross-talk (#PAMM-181Z, Qiagen) was performed according manufacturer's instruction on ABI 7000 platform. The analysis of collected data was done with web-based software RT^2 Profiler PCR Array Data Analysis (SABiosciences, Qiagen). The array allowed the simultaneous analysis of the expression of 84 genes, including the principal mediators and effectors in the cross-talk between tumor cells and immune system. A set of controls were inside each array, enabling

data analysis through the ΔΔCT method of relative quantification, the evaluation of RT and PCR performances, and the presence of genomic DNA contamination.

2.8 Flow cytometry

Cells were counted through Burker chamber in Trypan Blue or, in case of blood samples, in Turk's solution (Bio Optica, Italy) to remove red blood cells. Cells ($1x10^6$) were seeded in tubes containing a mix of different fluorochrome-conjugated antibodies, listed in Table 3. To allow antibodies binding, an incubation of 20 minutes at 4°C was performed in a Buffer composed by PBS added with 2mM EDTA (to avoid cell aggregation) and 0.5% BSA (to preserve cell viability). Cells were washed to remove unbound antibodies and re-suspended in the same Buffer. An additional step was required to remove red blood cells contamination from blood samples, which may interfere with the acquisition, by incubating cells in Buffer EL (Qiagen) at 4°C for 15 minutes. For intracellular markers (Annexin V) the incubation was performed in Annexin V Buffer 1x (BD Biosciences, CA).

At least 500.000 total cells per sample were acquired on a flow cytometer equipped with 3 lasers (Navios, Beckman Coulter, Italy). Analysis was performed with KALUZA software (Beckman Coulter), after selection of DNA-containing ($Syto16^+$, Invitrogen) and viable (7-aminoactinomycin; $7\text{-}AAD^-$, Beckman Coulter) cells. Analysis gates were set with the aid of "fluorescence minus outcomes" isotype controls. Cells were labeled with a panel of antibodies (Beckman Coulter; BD Biosciences; eBioscience, UK; Bio-Legend, CA; Bio-Rad) to analyze immune cell populations and WAT-derived progenitors, as illustrated in Table 4.

The characterization of lymphocytes, macrophages, granulocytes and dendritic cells was done accordingly standard markers expression (Lai *et al*., 1998), whereas a specific marker, CD335, was used to identify Natural Killer (NK) cells (Walzer *et al*., 2007). MDSCs were analyzed accordingly a recent classification, including main subtypes Mo-MDSCs and G-MDSCs (Gabrilovich *et al*., 2012); TAMs accordingly the findings of Su *et*

al. (2014). A complete surface markers characterization was previously described for WAT-derived progenitors, including both ASCs and EPCs (Martin-Padura *et al.*, 2012; Orecchioni *et al.*, 2013).

2.9 Immunofluorescence (IF) and confocal microscopy

Formalin-fixed paraffin-embedded samples were sectioned 5µm thick on poli-L-lysine slides (Thermo Scientific). After deparaffination and hydratation, antigen retrieval was heat-mediated (95°C for 30 minutes) in 10mM Sodium Citrate Buffer added with 0.05% Tween20 (Sigma-Aldrich; pH adjusted to 6.06). Samples were then permeabilized with 0.1% Triton X-100 in PBS for 30 minutes at RT. Before staining, slides were incubated for 1 hour in a 10% BSA solution, to avoid unspecific signals and reduce background. All washing steps between incubations were performed in PBS 1x (3 times, 5 minutes each). Overnight incubation at 4°C was performed with primary antibodies diluted in 10% BSA solution: rabbit polyclonal antibody anti-mouse CD31 (1:20, #ab28364, Abcam) and mouse monoclonal antibody anti-Alpha Smooth Muscle Actin (αSMA) (1:3000, #A2547, Sigma-Aldrich). Secondary antibodies were incubated for 1 hour at RT: Alexa Fluor 555 Goat anti-mouse IgG2A (1:200, Thermo Scientific) and Alexa Fluor 488 Donkey anti-rabbit IgG (1:200, Thermo Scientific). Slides were stained with 4′,6-diamino-2phenylindole (DAPI, Sigma-Aldrich) and mounted with Vectashield (Vector Laboratories, CA) to preserve fluorescence. Negative controls, without primary antibodies, were conducted for each staining to exclude unspecific signals.

For confocal imaging, all the z-stacks were collected on a Lieca SP5 II confocal microscope (Leica) using a 20x oil immersion objective with a numerical aperture of 1.3 at zoom 1.7. Fluorochromes were excited using a 405nm diode laser for DAPI, an argon 488 laser for Alexa Fluor 488 and a 561 diode laser for Alexa Fluor 555. Detector slits were configured to minimize the cross-talk between channels and to maximize the signal arising from the sample: PMT1, 407 to 485 nm (DAPI); PMT2, 492 to 556 nm (Alexa Fluor 488);

PMT3, 579 to 684 nm (Alexa Fluor 555). The cross-talk was also limited by the fact that the stacks were collected in "between frame mode": the blue and red fluorescence (spectrally well separated) were collected simultaneously, while the green one by itself. Every single image of the collected z-stacks was 1.024×1.024 pixel^2 (about 228×228 μm^2), whereas the z-step between 2 images within a stack was 0.8μm, resulting in a voxel size of 0.223×0.223×0.8 μm^3. The acquisition parameters, the microscope, and all the detectors were controlled by means of the software LAS-AF (Leica).

2.10 Immunohistochemistry (IHC)

Formalin-fixed paraffin-embedded tumors were sectioned 5μm thick on poli-L-lysine slides, deparaffinized and hydrated. Heat-mediated antigen retrieval through Sodium Citrate Buffer, permeabilization and blocking steps were done, as previously described for IF staining. Immunostaining was performed with rabbit anti-human MMP9 MoAb (1:100, #ab76003, Abcam) and donkey anti-rabbit IgG-HRP (1:1000, Thermo Scientific). The incubation with primary antibody was done overnight at 4°C, whereas slides were incubated with the secondary antibody for 1 hour at RT. Gill's Hematoxylin (Bio-Optica, Italy) was used as counterstain. Slides were mounted with Eukitt® mounting medium (Bio-Optica). Images were acquired with Scan Scope XT device (Leica).

2.11 Statistical analysis

The Shapiro-Wilk test was used to assess normality. The very large majority of data were not normally distributed. Therefore, statistical comparisons were carried out using the nonparametric U test of Mann–Whitney. All reported p values were two sided (significance from $p<0.05$). All displayed values are mean ± standard error of the mean (SEM).

Table 2
List of primers and probes TaqMan® Gene Expression Assay (Thermo Scientific).

Cat.n.	Target gene	Species
Hs00929873_m1	**CSF-2 (GM-CSF)**	**Human**
Hs00234579_m1	**MMP9**	**Human**
Hs00174097_m1	**IL1β**	**Human**
Mm01290062_m1	**CSF-2 (GM-CSF)**	**Mouse**
Mm00442991_m1	**MMP9**	**Mouse**
Mm00437762_m1	**B2m (β2 microglobuline)**	**Mouse**

Table 3

List of antibodies used for multiparametric flow cytometry analysis.

Anti-human CD13 PE-Cy7 (#A46528, Beckman Coulter)
Anti-human CD31 PE-Cy7 (#IM995128, Beckman Coulter)
Anti-human CD34 APC (#IM2472, Beckman Coulter)
Anti-human CD45 Alexa Fluor 750(#A79392, Beckman Coulter)
Anti-human Ki67 PE (#51-36525X, BD)
Anti-mouse CD3 FITC (#555274, BD)
Anti-mouse CD4 PE (#553730, BD)
Anti-mouse Ly6C PE-Cy7 (#560593, BD)
Anti-mouse Ly6G FITC (#551460, BD)
Anti-mouse CD8a APC (#553035, BD)
Anti-mouse CD11b Alexa Fluor 700 (#101222, BioLegend)
Anti-mouse CD11c FITC (#557400, BD)
Anti-mouse CD19 PE-Cy7 (#552854, BD)
Anti-mouse CD25 APC (#557192, BD)
Anti-mouse CD31 PE-Cy7 (#25-0311-82, eBioscience)

Anti-mouse CD34 PE (#551387, BD)
Anti-mouse CD45 APC-Cy7 (#557659, BD)
Anti-mouse CD127 PE-Cy7 (#560733, BD)
Anti-mouse CD206 Brilliant Violet 421 (#141717, BioLegend)
Anti-mouse CD335 Alexa Fluor 700 (#561169, BD)
Anti-mouse F4/80 APC (#MCA497APC, Bio-Rad)
Anti-mouse Gr1 PE-Cy7 (#25-5931-81, eBioscience)
Anti-mouse MHC-II PE-Cy7 (#107630, BioLegend)
APC Annexin V (#550474, BD)
APC-conjugated anti-rat IgG2b isotype (#553991, BD)
APC-conjugated anti-mouse IgG1 isotype (#IM2475, Beckman Coulter)
Alexa Fluor 750-conjugated IgG1 isotype (#A79393, Beckman Coulter)
FITC-conjugated anti-rat IgG isotype (#11-4811-85, eBioscience)
PE-conjugated anti-mouse IgG1 isotype (#550083, BD)
PE-conjugated anti-rat IgG1 isotype (#12-4301-73, eBioscience)
PE-Cy7-conjugated anti-mouse IgG1 isotype (#737662, Beckman Coulter)

Table 4

Flow cytometry markers for the analysis of human and murine samples.

Murine cells

Lymphocytes	T-helper	T-cytotoxic	B-cells	NK	T-regs
$CD45^{+}$ **low SSC**	$CD3^{+}$ $CD4^{+}$	$CD3^{+}$ $CD8^{+}$	$CD19^{+}$	$CD335^{+}$	$CD4^{+}$ $CD25^{++}$ $CD127^{low}$

Myeloid cells	Macrophages	Monocytes	TAMs	Inflammatory monocytes	Granulocytes	Dendritic cells
$CD45^{+}$ **high SSC**	$F4/80^{+}$ $Gr1^{-}$ $CD11b^{+}$	$F4/80^{+}$ $Gr1^{-}$ $CD11b^{-}$	$F4/80^{+}$ $Gr1^{-}$ $CD11b^{+}$ $CD206^{+}$ $MHC\text{-}II^{low}$	$F4/80^{+}$ **bright** $GR1^{+}$ **bright** $CD11b^{+}$	$F4/80^{-}$ $GR1^{+}$	$CD11c^{+}$

MDSCs	Mo-MDSCs	G-MDSCs
$CD45^{+}$ **high SSC**	$CD11b^{+}$ $Gr1^{mid}$ $Ly6G^{-}$ $Ly6C^{+}$ $F4/80^{+/-}$	$CD11b^{+}$ $Gr1^{bright}$ $Ly6G^{+}$ $Ly6C^{low}$ $F4/80^{+/-}$

Human and murine cells

WAT progenitors	EPCs	ASCs
$CD45^{-}$ $CD34^{+}$	$CD31^{+}$	$CD31^{-}$ $CD13^{+}$

3. Results

3.1 Identification of factors involved in BC-WAT progenitors interplay

3.1.1 Screening of soluble factors with proteomic array

BC (MDA-MB-436) cells were cultured with WAT-derived progenitors ($CD45^{-}CD34^{+}$), which were isolated from the SVF of a lipofilling sample. Co-cultures were performed for 72 hours through two distinct systems: in one case only paracrine interaction among cells was allowed (transwell co-culture), in the other, also the physical interaction was permitted (direct co-culture). The presence of soluble factors involved in human angiogenesis, inflammation and ECM remodeling was investigated in cellular media with a proteomic antibody array (Fig.11). The expression of proteins in co-cultures was compared to baseline expression in single cell cultures (WAT or BC cells seeded alone). All values were normalized for internal standard controls included in the array.

Notably, WAT cells produced a limited number of soluble factors, whereas BC cells expressed several molecules involved in angiogenesis and inflammation, according to the aggressive and high tumorigenic potential of this TNBC cell line.

The highest released molecules by BC cells were SerpineE1, IL-8, urokinase plasminogen activator (uPA), TIMP-1, VEGF, Pentraxin3 and Angiogenin. However, the overall level of these molecules did not change when BC cells were cultured alone or in presence of WAT progenitors (Fig.11). Molecules mainly expressed by WAT progenitors were IL-8 and SerpinE1.

The quantitation of dots intensity identified two molecules, which were differentially expressed between co-cultures and single cultures: GM-CSF and MMP9 (Fig.11B).

GM-CSF release was doubled in transwell and direct co-cultures compared to BC cells alone, whereas it was almost not expressed by WAT progenitors, when seeded alone. ,

MMP9 was up-regulated about 4-fold higher than BC alone in direct co-cultures, only 2.5-fold more in transwell system.

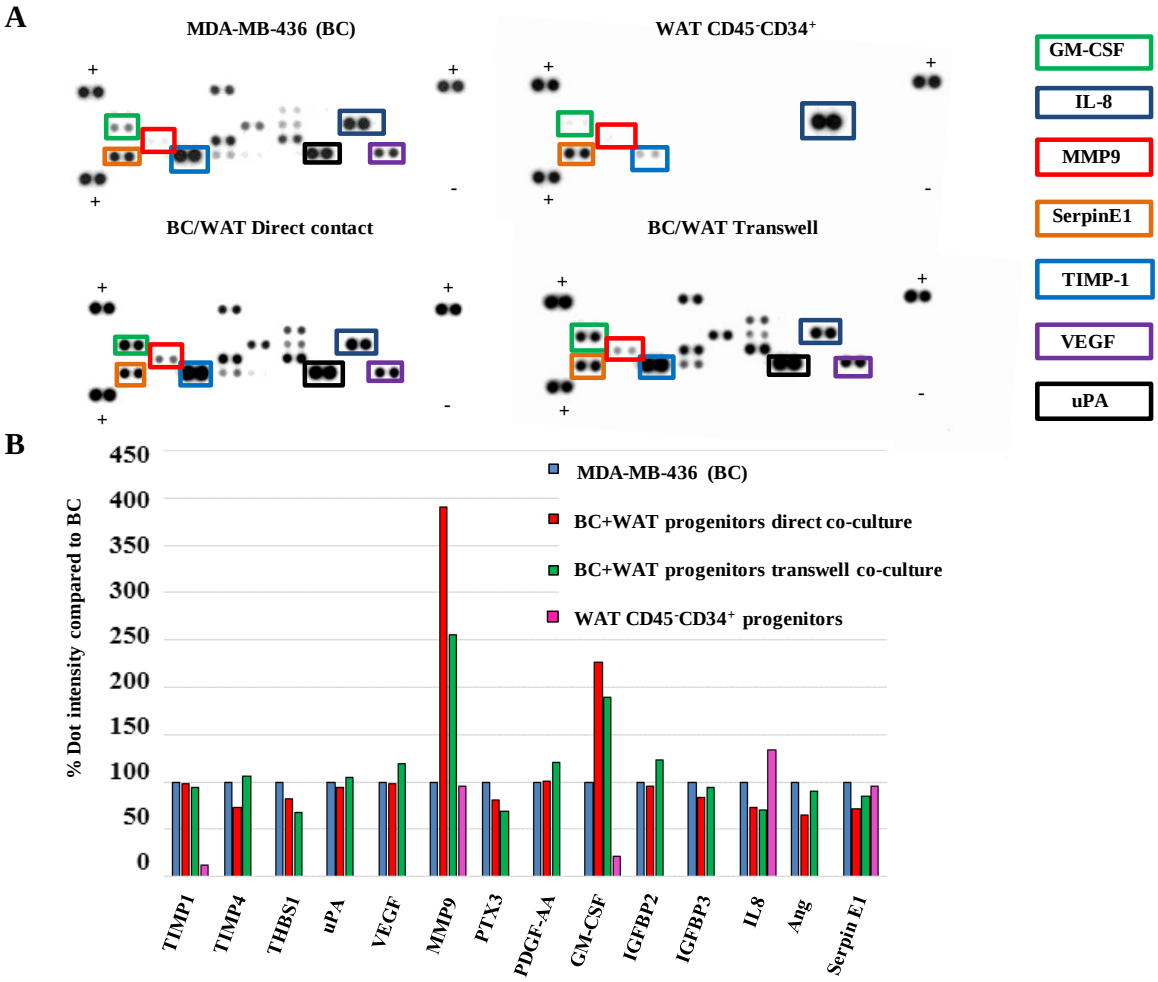

Fig.11 Screening with antibody array on cellular supernatant. Human angiogenesis Proteome Profiler (#ARY007, R&D) screened soluble factors in BC-WAT progenitors co-cultures. **A)** Representative images acquired with ChemiDoc MP System: dots represent released factors (each in duplicate); **B)** Quantitation of mean dot intensity using ImageJ software. GM-CSF and MMP9 were the most up-regulated factors in co-cultures compared to single cell cultures.

3.1.2 Validation of GM-CSF highly release *in vitro*

The up-regulation of human GM-CSF (hGM-CSF) in co-culture supernatant was confirmed with ELISA. WAT-derived progenitors were isolated from lipofilling samples, collected from 20 different subjects. Several human TNBC cell lines were used, including MDA-MB-436, MDA-MB-231 and HCC1937. ZR-75-1 ductal carcinoma ER^+ cell line was also analyzed.

WAT cells alone did not express any detectable GM-CSF, whereas BC cells displayed variable baseline expression, cell line-dependent: MDA-MB-231 and MDA-MB-436 secreted high levels of GM-CSF; HCC1937 produced minimal amount of the protein; ZR-75-1 production was below the sensitivity of the assay (7.8pg/ml) (Fig.12A).

Culture conditions affected GM-CSF production as well, since BC cells seeded on collagen coating released more protein compared to the amount released by cells seeded on transwell insert. Therefore, for each cell line, two distinct controls for BC cells were used.

The release of GM-CSF was significantly enhanced in co-cultures with all TNBC cell lines (Fig.12B). In particular, the release of the cytokine was enhanced, independently from the type of co-culture (transwell or direct), suggesting the evidence of a paracrine interaction between BC and WAT progenitors.

The observed up-regulation was significant for MDA-MB-436 and HCC1937, whereas the higher release was less detectable in MDA-MB-231 co-cultures.

In co-cultures between ZR-75-1 and WAT progenitors, GM-CSF levels remained under the detection limit of the assay.

These results suggested that the up-regulation occurred mostly in co-cultures with TNBC cells, characterizing a more aggressive tumor phenotype.

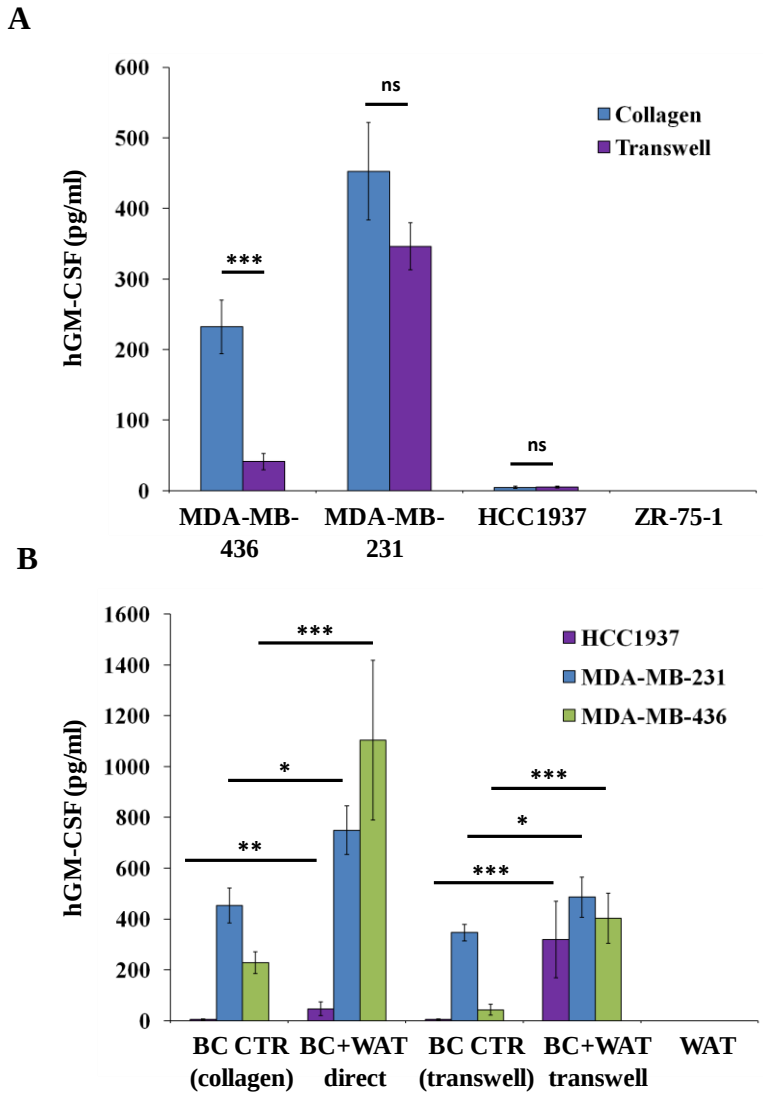

Fig.12 GM-CSF absolute quantitation through ELISA. Human GM-CSF was quantified in media of cultures with Quantikine ELISA kit (#DGM00, R&D). **A)** BC cell lines displayed differential release of the factor, according to cell line and culture conditions (n=5, ***p<0.001, ns: not significant, transwell vs. collagen); **B)** Absolute quantitation in cellular supernatants of co-cultures, direct or transwell, and single cultures used as controls (n = 5, * p<0.05, ** p<0.01, *** p<0.001, vs. BC control).

3.1.3 Validation of MMP9 highly release *in vitro*

Cellular supernatants were analyzed for human MMP9 (hMMP9) through ELISA. However, the target protein was below the detection limit of the assay in all samples (data not shown).

WB was used for a semi-quantitative evaluation of MMP9 protein. MMP9 appeared as a single band at 92kDa, corresponding to the secreted inactive form, called pro-MMP9 (Fig.13).

A dramatic increase of MMP9 release was detected in direct co-cultures, whereas only a slight up-regulation was displayed in transwell system. A certain variability was observed among replicated co-cultures, using WAT-derived progenitors isolated from different subjects (Fig.13A).

MMP9 release *in vitro* was minimal in WAT-derived progenitors cultured alone. MMP9 baseline secretion was detected in all TNBC cell lines (Fig.13B), but was poorly expressed by ZR-75-1 (data not shown).

Band intensity quantitation allowed the comparison of different samples (Fig.13C). MMP9 was released about 6-fold more in direct co-cultures compared to WAT control: an average of 6.2 (± 1.2) times increased for MDA-MB-436, 7.0 (± 2.8) times for MDA-MB-231 and 6.5 (± 1.3) times for HCC1937.

Zymography detected MMP9 enzymatic activity in cellular supernatants: lighter bands were proportional to gelatin digestion, catalyzed by the enzyme (Fig.14). Gelatin digestion was significantly increased in co-cultures compared to single cell cultures, in particular with MDA-MB-436 and HCC1937. According to WB results, supernatant collected from direct co-cultures showed higher MMP9 activity compared to supernatant collected from transwell system.

All together, these data suggested that MMP9 was enhanced mostly in direct co-cultures, rather than transwell system. That might depend on adhesion-related mechanisms or, alternatively, might require higher concentration or stability of paracrine inducer(s).

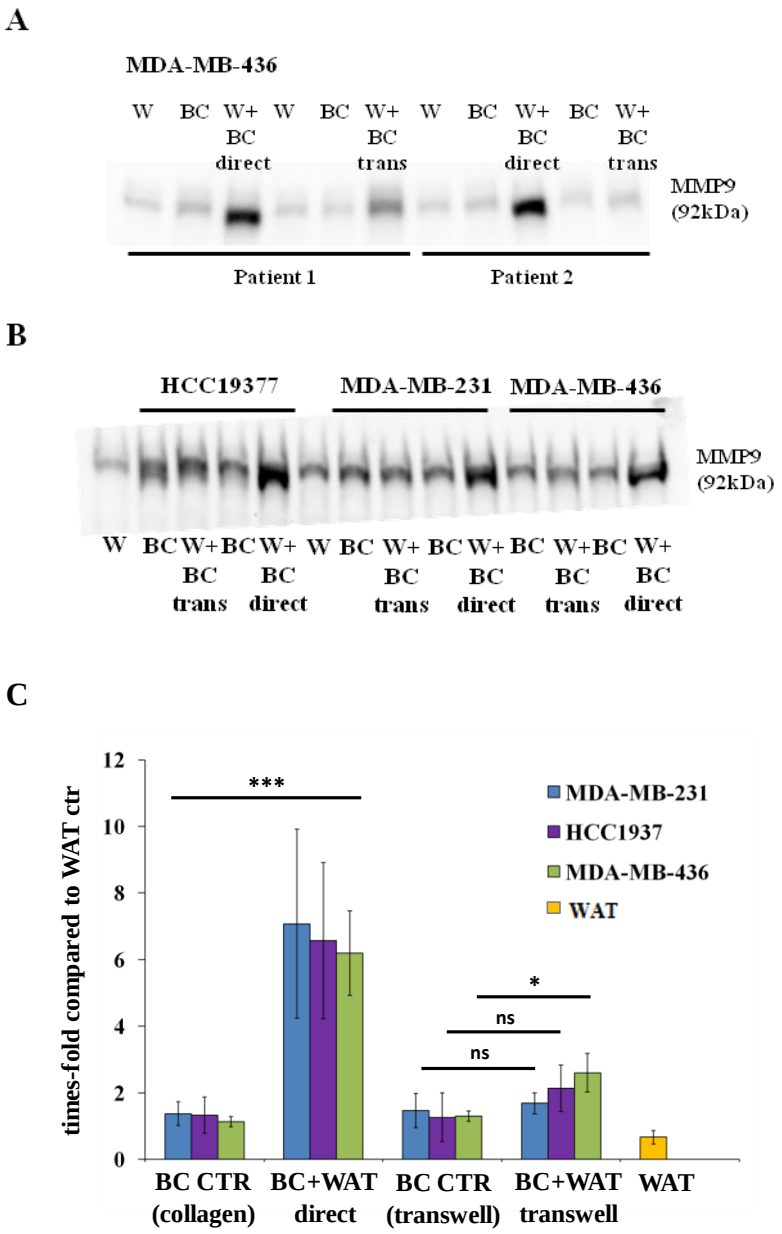

Fig.13 WB for MMP9 evaluation in co-cultures. Cellular media of co-cultures and single cultures analyzed for MMP9, using 1:2000 rabbit monoclonal anti-human MMP9 (#ab76003, Abcam). **A)** Representative images of secreted pro-MMP9 (92kDa) using MDA-MB-436 (BC) and WAT $CD45^{-}CD34^{+}$ progenitors (W) isolated from different patients. Images were acquired with ChemiDOC MP System; **B)** Comparison of several TNBC cell lines ability to highly release MMP9, using WAT-progenitors from a single patient; **C)** Average bands quantitation using ImageJ software. Values are expressed as times-fold compared to WAT cells seeded alone (n=5, * $p<0.01$, *** $p<0.001$, ns: not significant, vs. BC control).

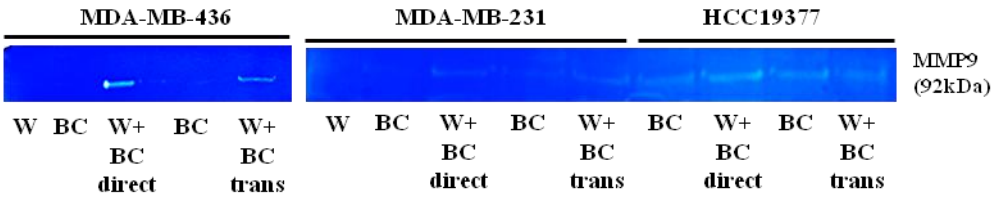

Fig.14 Zymography on cellular supernatants from co-cultures. Representative images acquired with ChemiDOC MP System. Samples analyzed were TNBC cell lines (BC) alone or in co-cultures with WAT-derived progenitors $CD45^{-}CD34^{+}$ (W). The activity of the pro-form MMP9 (92kDa) was detected to be increased in direct co-cultures, only slightly in transwell system. The effect was minimal for MDA-MB-231, more significant in MDA-MB-436 and HCC1937.

3.1.4 qRT-PCR

To assess which population up-regulated GM-CSF and MMP9 in co-cultures, qRT-PCR was performed in WAT and BC cell (MDA-MB-436) co-cultured in transwell system, separately collected and analyzed. The expression level of each factor was normalized for housekeeping gene expression and compared to BC baseline expression (Fig.15A).

BC cells after transwell co-cultures with WAT progenitors did not change the expression, compared to BC cells cultured alone. Conversely, WAT progenitors dramatically up-regulated transcripts for GM-CSF and MMP9 in co-cultures, compared to WAT single cultures: about 250-fold increase for GM-CSF and 75-fold for MMP9.

To confirm that WAT-derived progenitors were the only source of GM-CSF and MMP9 transcriptional up-regulation, co-cultures between murine WAT $CD45^{-}CD34^{+}$ progenitors and human BC (MDA-MB-436) were analyzed. qRT-PCR revealed that murine transcripts were up-regulated in both transwell and direct co-cultures, whereas human transcripts did not change their levels (Fig.15B).

The up-regulation occurring in WAT progenitors was detected after being co-cultured with all TNBC analyzed (Fig.16). Notably, WAT progenitors co-cultured with ZR-75-1 displayed a weak up-regulation, not significant as in TNBC (Fig.16).

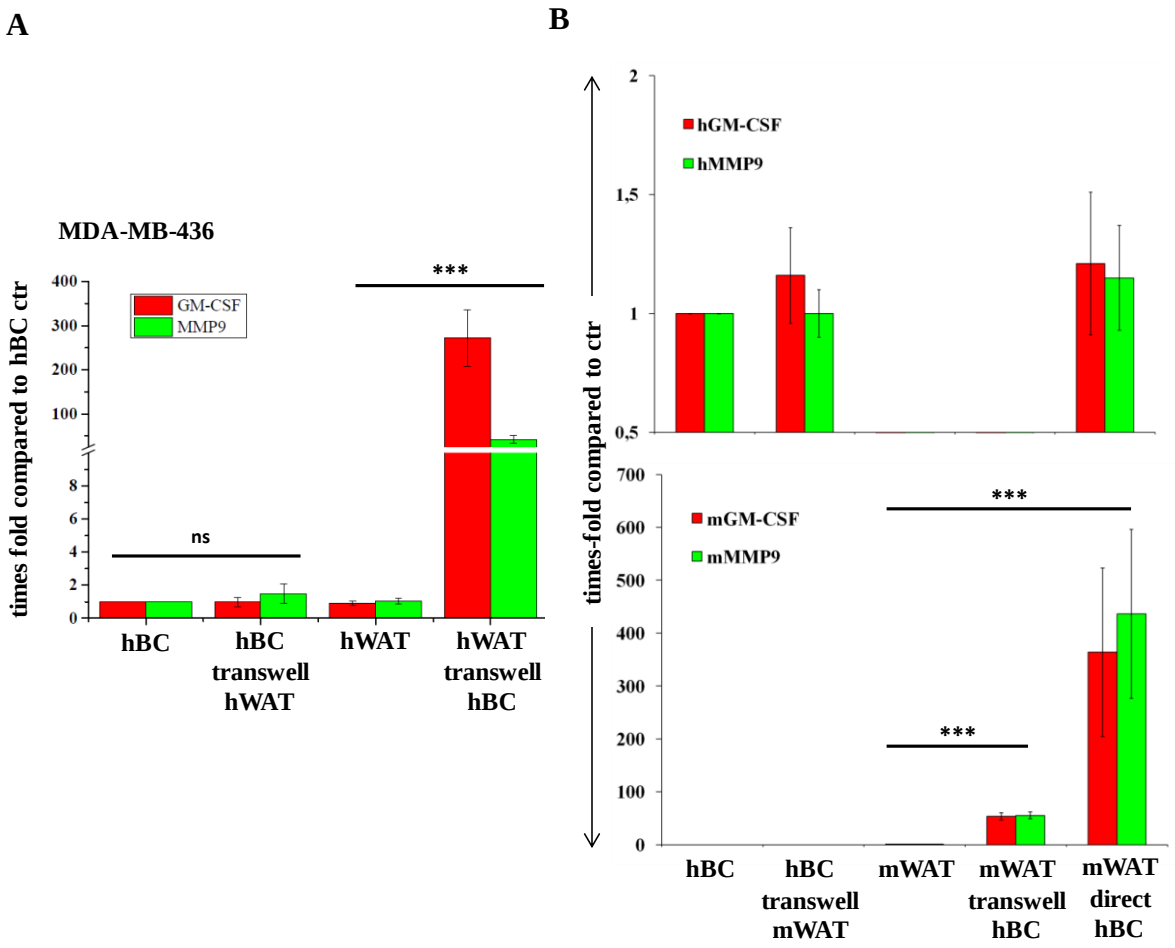

Fig.15 qRT-PCR analysis on cells from co-cultures. MDA-MB-436 (BC) were cultured alone or in co-cultures with human or murine WAT $CD45^{-}CD34^{+}$ cells. Expression of GM-CSF (CSF-2) and MMP9 transcripts were normalized for housekeeping genes (ABL for human transcripts, β2-microglobulin for murine ones). Values are expressed as times-fold to respective controls (BC control for humans, mWAT control for murines). **A)** hWAT progenitors up-regulated both transcripts in co-cultures with hBC compared to single cultures, whereas hBC did not change the expression (n=10, *** $p<0.001$, ns: not significant, vs. single culture); **B)** hBC were cultured with mWAT progenitors and analyzed for human and murine transcripts. Only murine transcripts were detected up-regulated in transwell and direct co-cultures (n=3, *** $p<0.001$, vs. mWAT control).

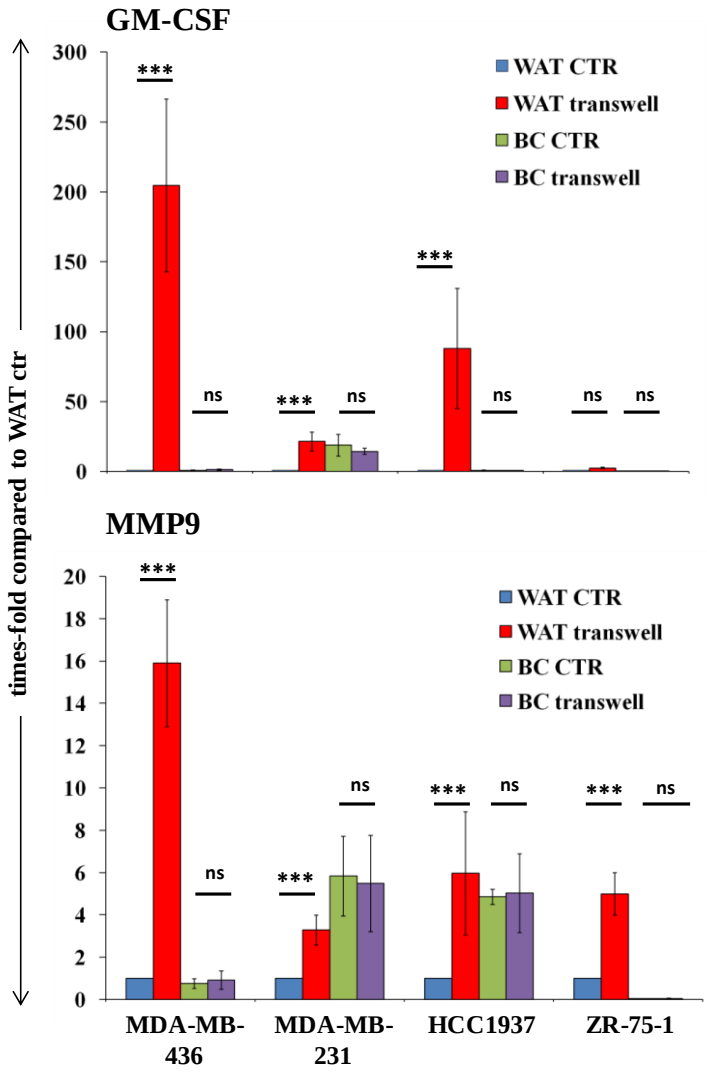

Fig.16 Analysis of GM-CSF and MMP9 transcripts from co-cultures using different BC cell lines. Primary WAT-derived progenitors $CD45^{-}CD34^{+}$ were co-cultured in transwell with TNBC (MDA-MB-426, MDA-MB-231, and HCC1937) and ductal carcinoma ER^{+} (ZR-75-1) cell lines. Single cells cultures were used as controls. All values were normalized for ABL housekeeping gene expression and displayed as times-fold to WAT control (n=3 for each BC cell line using WAT progenitors from different subjects, *** $p<0.001$, ns: not significant). GM-CSF (top panel) and MMP9 (bottom panel) were up-regulated in WAT progenitors after being co-cultured with TNBC cells.

3.2 GM-CSF and MMP9 up-regulation in xenograft models

Xenograft BC models were generated injecting human TNBC cells alone or in combination with primary hWAT $CD45^{-}CD34^{+}$ progenitors, isolated from different subjects. As negative controls, mice were injected with hWAT progenitors alone, which did not develop tumors.

Tumor growth was weekly monitored and confirmed the previously reported pro-tumorigenic effect of WAT progenitors on BC local growth (Fig.17).

Mice were periodically checked to assess circulating levels of hGM-CSF and hMMP9.

Plasmatic hGM-CSF was quantified through HS ELISA. Results confirmed the existence of an *in vivo* up-regulation of the human cytokine, when hWAT progenitors were co-injected with MDA-MB-436 (Fig.18A) or MDA-MB231 (Fig.18B). Mice injected with hWAT cells alone did not have any detectable circulating hGM-CSF. This suggested that GM-CSF release in WAT progenitors was tumor-dependent. In mice injected with HCC1937, the level of circulating hGM-CSF was lower than other TNBC cell lines, mostly under the detection limit of the assay (data not shown).

No circulating hMMP9 was detected in PB through WB (data not shown). Tumor microenvironment was then investigated for the expression of hMMP9: the protein was higher detected in tumors co-injected with hWAT cells, compared to tumor injected alone (Fig.19).

Distinct forms of MMP9 were detected through WB in whole tumor lysate: full-length precursor (pro-MMP9, 92kDa) and cleaved MMP9 active forms, 82kDa or the prevalent 67kDa (Fig.20). All MMP9 proteins were found up-regulated in MDA-MB-436/WAT co-injected mice, with a predominant expression of the 67kDa biologically active form (Fig.20A). In HCC1937 xenograft model, the over-expression of the 67kDa cleaved active form was confirmed in co-injected mice (Fig.20B). Conversely, hMMP9 was poorly expressed in MDA-MB-231 xenograft model, with no evident bands detected through WB (data not shown).

Accordingly, MMP9 displayed increased enzymatic activity in tumors co-injected with hWAT compared to controls, as detected by zymography (Fig.21).

According to the *in vitro* results, the qRT-PCR analysis on BC did not detect any up-regulation of the transcripts for both factors, confirming WAT $CD45^{-}CD34^{+}$ as the putative secreting cells (Fig.22).

A

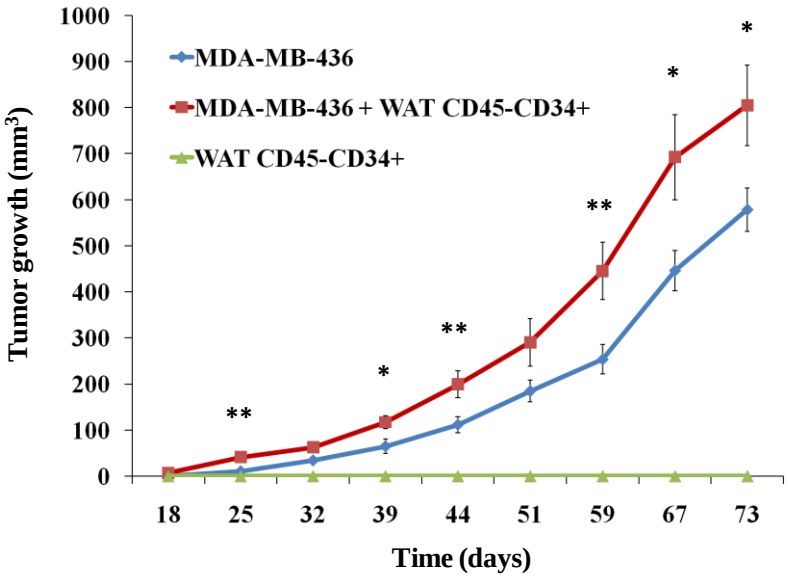

B

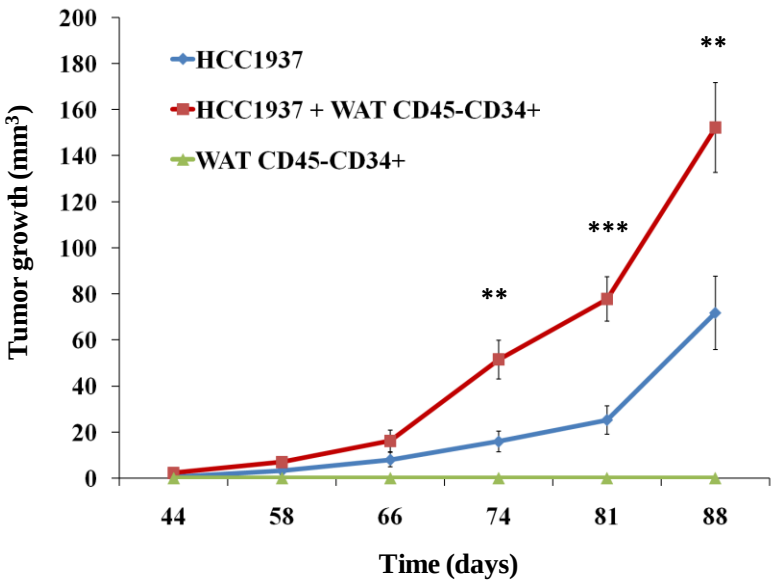

C

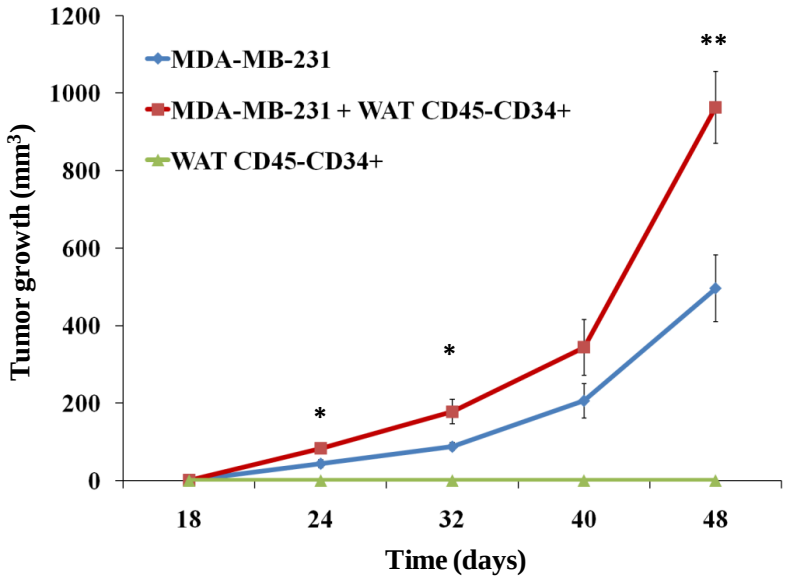

Fig.17 Tumor growth in xenograft with human TNBC. Tumor growth was significantly increased in co-injected NSG mice ($1x10^6$ hBC cells + $0.05x10^6$ hWAT progenitors $CD45^-CD34^+$) compared to mice injected with hBC alone (n=10, * $p<0.05$, ** $p<0.01$, *** $p<0.001$). NSG injected with hWAT cells alone were used as negative controls (n=5). **A)** MDA-MB-436; **B)** HCC1937; **C)** MDA-MB-231.

A

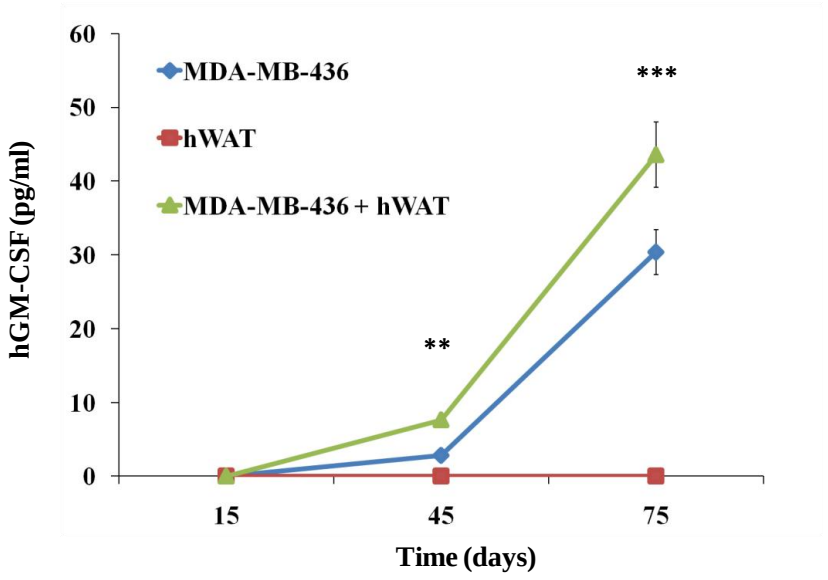

B

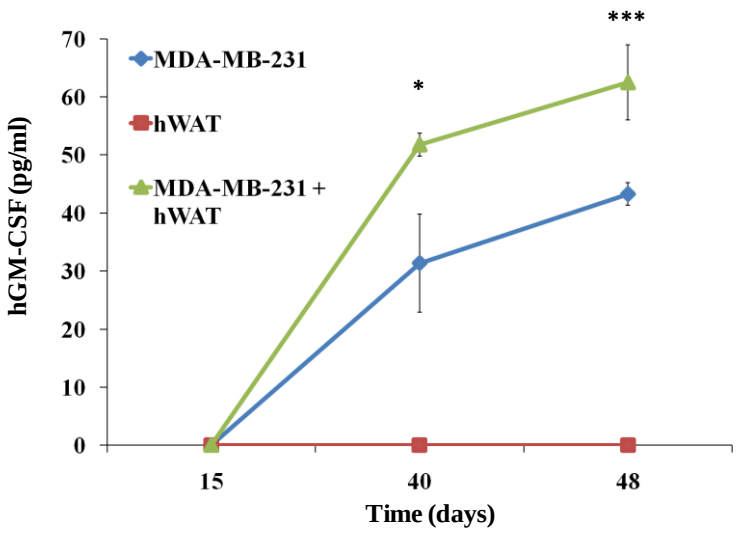

Fig.18 Circulating hGM-CSF in NSG mice injected with TNBC cells. Plasmatic hGM-CSF was analyzed through HS ELISA (#HSGM0, R&D). Mice co-injected with hBC and hWAT progenitors displayed higher hGM-CSF, compared to hBC (n=12, * $p<0.05$, ** $p<0.01$, *** $p<0.001$). No circulating hGM-CSF was detected in mice injected with hWAT progenitors alone (n=5). **A)** MDA-MB-436; **B)** MDA-MB-231.

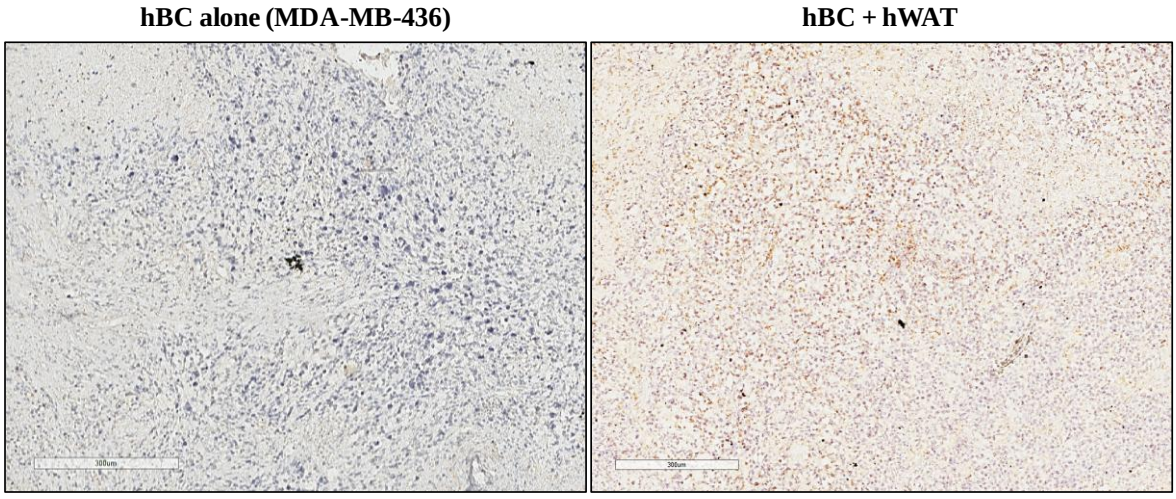

Fig.19 IHC for hMMP9 expression in tumors collected from xenograft BC models. Representative images of MMP9 expression in hBC from MDA-MB-436 injected mice, stained with 1:100 rabbit anti-human MMP9 (#ab76003, Abcam), acquired with APERIO Digital System (scale bars 300µm). NSG mice co-injected with hBC and hWAT progenitors displayed increased MMP9 expression.

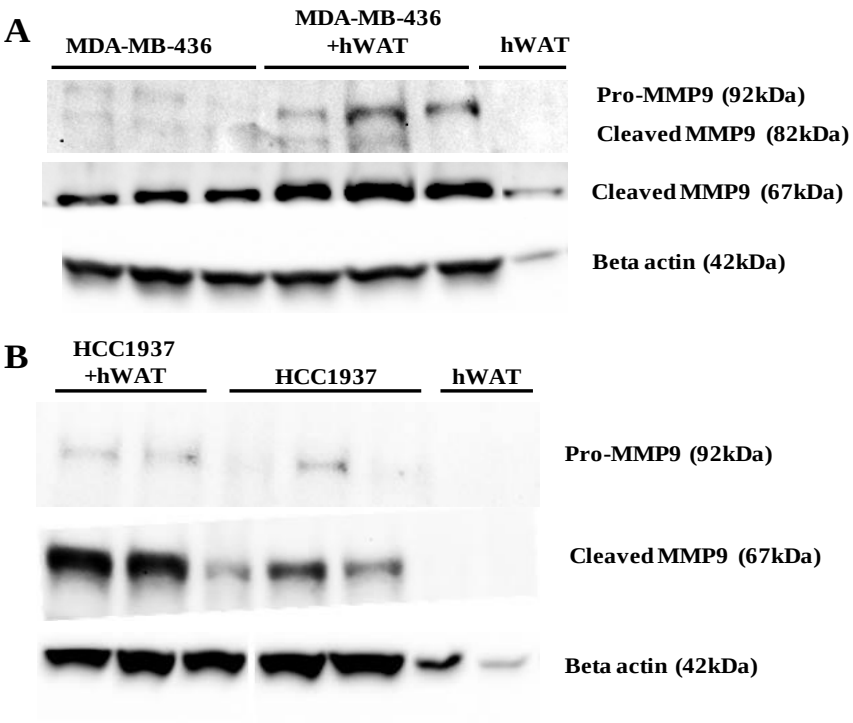

Fig.20 WB for hMMP9 detection in tumor microenvironment from BC xenografts. Representative images of whole tumor lysates (15µg) from NSG mice injected with MDA-MB-436 **(A)** or HCC1937 **(B)** alone or with hWAT $CD45^{-}CD34^{+}$. Co-injected mice displayed increased hMMP9 expression. MMP9 pro-forms (92kDa) and active forms (82kDa and 67kDa) were stained with 1:200 rabbit anti-hMMP9 (#10375-2-AP, Proteintech). Beta actin was used as loading control.

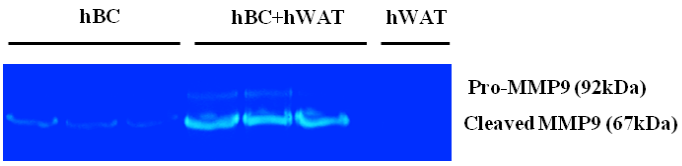

Fig.21 Zymography on tumors from xenograft BC mice. Representative image of zymogram detecting hMMP9 proteolytic activity in whole tumor lysates collected from NSG mice, injected with MDA-MB-436 and/or hWAT $CD45^{-}CD34^{+}$ progenitors. Co-injected mice displayed higher MMP9 activity.

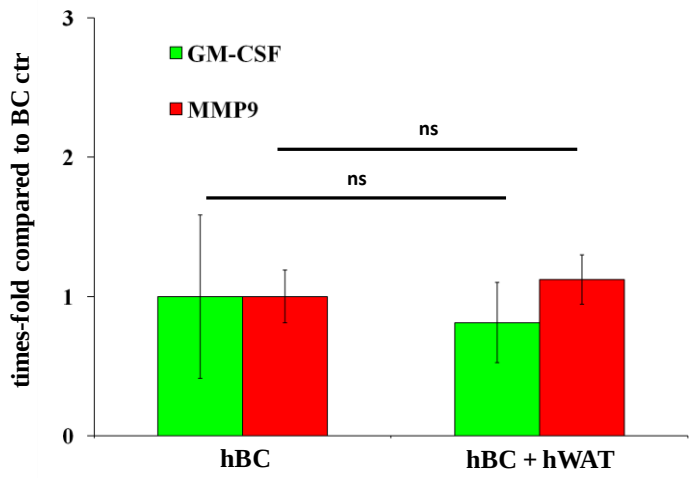

Fig.22 qRT-PCR on tumors collected from NSG mice. GM-CSF and MMP9 transcripts were quantified in BC cells collected from tumors of NSG mice, injected with MDA-MB-436 (BC) alone or in combination with hWAT progenitors. All values were normalized for ABL gene expression and expressed as times-fold compared to mice injected with BC cells alone (n=9, ns: not significant).

3.3 ASCs and EPCs role in GM-CSF and MMP9 release

The $CD45^{-}CD34^{+}$ fraction, isolated from the SVF of WAT, is composed by two sub-populations of progenitors, characterized by distinct biological properties: ASCs ($CD45^{-}CD34^{+}CD31^{-}$) or EPCs ($CD45^{-}CD34^{+}CD31^{+}$). To understand in which cell population occurred the observed GM-CSF and MMP9 up-regulation, primary ASCs and EPCs were co-cultured *in vitro* with TNBC cells (MDA-MB-436).

Secreted GM-CSF was evaluated through ELISA, revealing that both ASCs and EPCs synergically increased the cytokine release in presence of BC (Fig.23). In details, ASCs and EPCs alone did not express detectable levels of GM-CSF, but after being co-cultured with BC, in transwell or direct systems, displayed a significant up-regulation. However, EPCs seemed to be more prone to increase GM-CSF in direct co-cultures, compared to ASCs.

MMP9 release was detected through WB on cellular supernatants (Fig.24). EPCs expressed higher baseline levels of MMP9 compared to ASCs. However, the amount of

MMP9 released was significantly enhanced in co-cultures of ASCs, in both direct and transwell conditions. A minor release was detected in EPCs direct co-cultures.

To confirm the transcriptional up-regulation occurring in ASCs and EPCs after BC exposure, qRT-PCR was used to analyze GM-CSF and MMP9 transcripts (Fig.25). EPCs expressed similar baseline levels of GM-CSF but higher levels of MMP9, although not statistically significant compared to ASCs baseline expression.

GM-CSF was significantly up-regulated in both EPCs and ASCs, when cultured in transwell with MDA-MB-436 (Fig.25). Conversely, MMP9 was significantly up-regulated in ASCs, in a less extent in EPCs (Fig.25). These results suggested that both progenitor populations, ASCs and EPCs, up-regulated GM-CSF and MMP9 after being exposed to BC cells. EPCs seemed to be more effective in GM-CSF release, whereas ASCs may contribute more efficiently to MMP9 secretion.

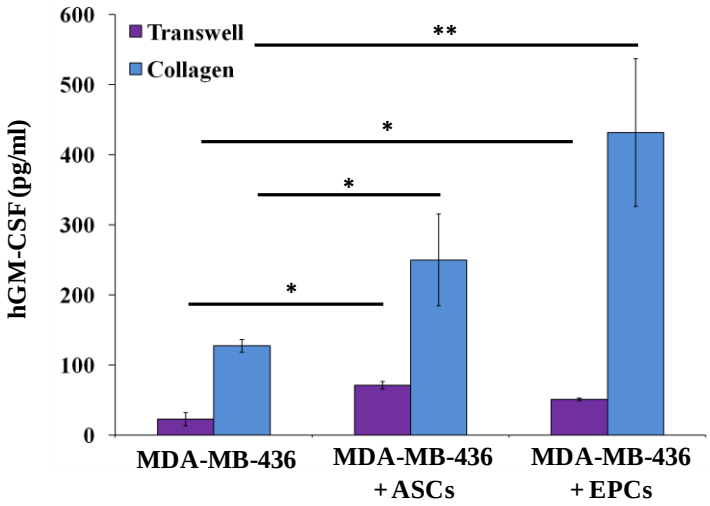

Fig.23 GM-CSF quantitation in ASCs/EPCs co-cultured with BC. MDA-MB-436 (BC) were cultured alone or with ASCs ($CD45^-CD34^+CD31^-$) or EPCs ($CD45^-CD34^+CD31^+$). Co-cultures were performed in transwell or in direct cultures (collagen). GM-CSF, detected through Quantikine ELISA (#DGM00, R&D), was significantly highly released in media of co-cultures, using both ASCs and EPCs (n=3, * $p<0.05$, ** $p<0.01$ vs. BC control).

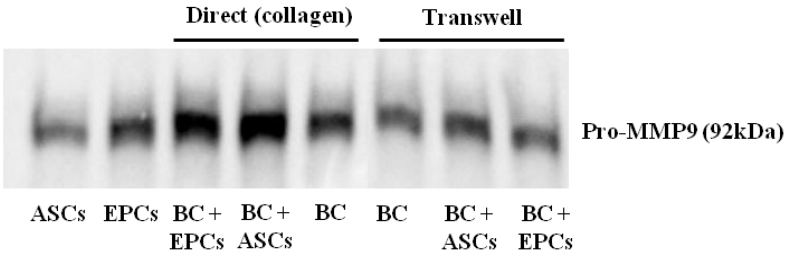

Fig.24 MMP9 evaluation through WB in ASCs/EPCs co-cultured with BC. Representative image of WB staining pro-MMP9 (92kDa) in cellular supernatants, using 1:2000 anti-hMMP9 (#ab76003, Abcam). Image was acquired with ChemiDOC MP System. Both ASCs and EPCs contributed to MMP9 release in co-cultures with MDA-MB-436 (BC).

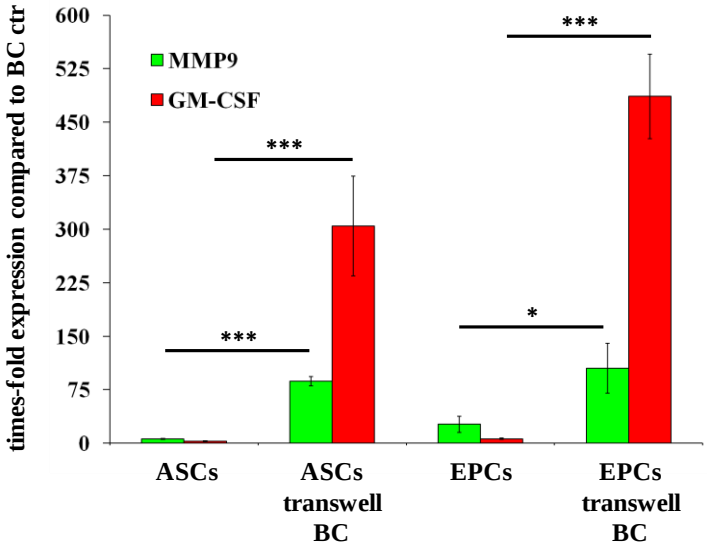

Fig.25 qRT-PCR on ASCs and EPCs co-cultured in transwell with BC. GM-CSF and MMP9 transcripts levels were normalized for ABL gene expression and expressed as times-fold to MDA-MB-436 (BC) control. GM-CSF and MMP9 were significantly up-regulated in both ASCs and EPCs in transwell co-cultures compared to single cultures (n=3, * $p<0.05$, *** $p<0.001$, vs. single cultures).

3.4 Identification of tumor mechanisms regulating GM-CSF and MMP9 release

Different factors were investigated in co-cultures of MDA-MB-436 and WAT $CD45^-$ $CD34^+$ cells, to assess the mechanism by which BC cells induced the release of GM-CSF and MMP9 by WAT progenitors.

NF-κB regulatory pathway was firstly investigated as potential up-stream mechanism. Bortezomib, NF-κB specific inhibitor, was tested at different concentrations to not affect cell viability (data not shown). The selected concentration (3nM) was added to *in vitro* co-cultures. Bortezomib did not affect GM-CSF or MMP9 transcripts level in BC cells or WAT progenitors cultured alone. The drug failed to prevent the up-regulation observed in WAT progenitors following BC exposure (Fig.26). The results were confirmed at protein level (Fig.27-28A).

The inflammatory mediator IL-1β was then analyzed for its ability to regulate GM-CSF and/or MMP9 release. Anti-human IL-1β MoAb was added to culture media. Transcription of both molecules was significantly reduced in treated WAT progenitors cultured alone compared to untreated cells (Fig.26). However, WAT cells in transwell with BC reduced MMP9 release in presence of the MoAb. Conversely, IL-1β neutralization did not affect GM-CSF or MMP9 transcription in BC cells, cultured alone or in transwell system.

The results were confirmed at protein level: GM-CSF was not affected by anti-IL-1β neutralization in co-cultures (Fig.27), whereas MMP9 release was strongly reduced in direct co-cultures, as shown by WB (Fig.28A).

These results suggested that IL-1β may be involved in the observed MMP9 up-regulation, induced in WAT progenitors by BC cells.

The reciprocal regulation of the factors under investigation was also evaluated.

To exclude MMP9 regulation on GM-CSF release, an irreversible inhibitor of MMP9, SB-3CT, was added to co-cultures and analyzed for GM-CSF protein release in cellular

supernatant. SB-3CT did not affect the cytokine release in single or co-cultures, as detected by ELISA (Fig.27).

Anti-human GM-CSF MoAb was then added at two different concentrations (0.5-1µg/ml) to co-culture systems. MMP9 release was found deeply affected by GM-CSF neutralization in a dose-dependent manner, as depicted by WB in transwell and direct co-cultures (Fig.28B). Transcriptional up-regulation was also significantly impaired in WAT progenitors (Fig.26).

GM-CSF release was found itself down-regulated in co-cultures in presence of anti-GM-CSF MoAb (Fig.27). Conversely, anti-GM-CSF MoAb did not significantly affect GM-CSF and MMP9 release by BC cells. These results were further confirmed by qRT-PCR, which detected impaired transcription of GM-CSF and MMP9 in WAT progenitors exposed to BC, and of MMP9 in WAT progenitors cultured alone (Fig.26).

These findings suggested GM-CSF to be an up-stream regulator of MMP9 in WAT progenitors. Moreover, GM-CSF itself further triggered its own expression in the same cells, with a positive feedback regulation.

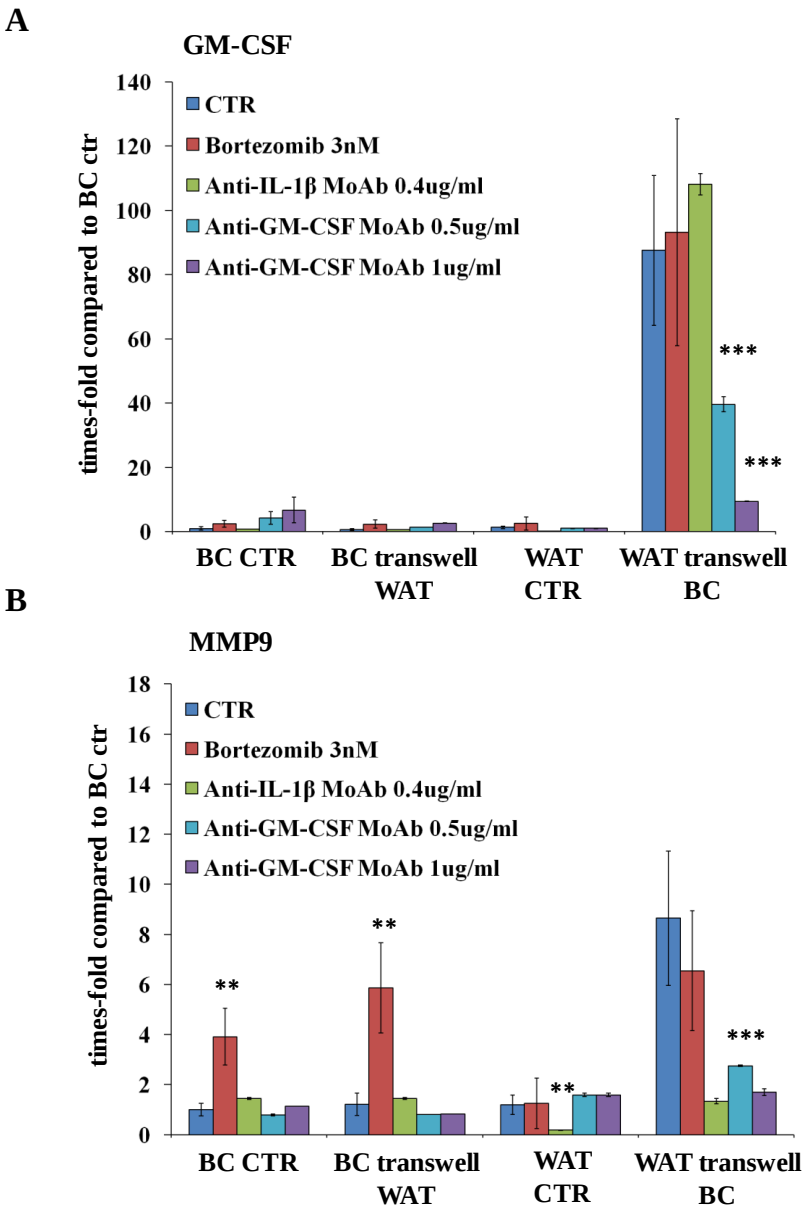

Fig.26 qRT-PCR on co-cultures neutralized for several factors potentially involved in GM-CSF or MMP9 up-regulation. MDA-MB-436 (BC) cells and WAT-derived $CD45^{-}CD34^{+}$ progenitors were cultured alone or in transwell system, in presence of 3nM Bortezomib (Sigma-Aldrich) or 0.4µg/ml MoAb anti-hIL-1β (#MAB201, R&D) or 0.5-1µg/ml MoAb anti-hGM-CSF (#sc-377039, Santa Cruz Biotechnology). All values were normalized for ABL housekeeping gene expression and expressed as times-fold to untreated BC control (n=3, ** $p<0.01$, *** $p<0.001$, ns: not significant, vs. untreated). **A)** GM-CSF (CSF2) up-regulation in WAT progenitors was significantly reduced by GM-CSF neutralization, in a dose-dependent manner; **B)** MMP9 was efficiently down-regulated by anti-IL-1β and anti-GM-CSF MoAbs in WAT cells after BC exposure. Anti-IL-1β MoAb affected MMP9 in WAT progenitors cultured alone. Conversely, Bortezomib significantly increased MMP9 expression in BC.

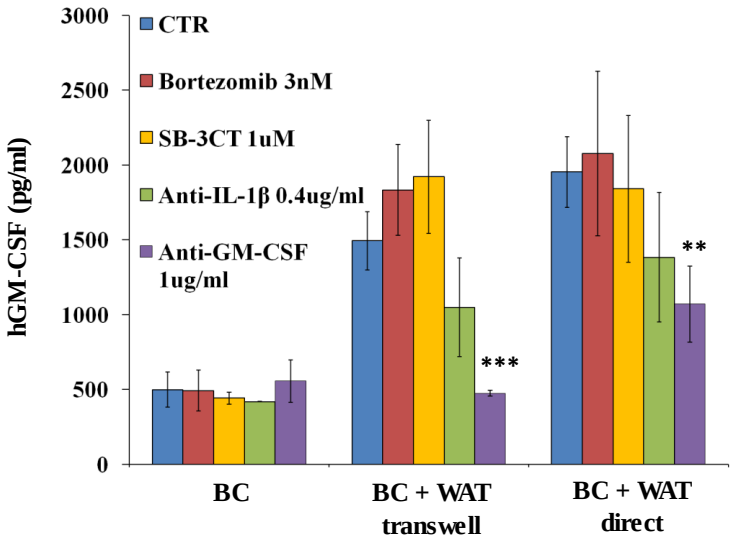

Fig.27 GM-CSF quantitation in co-cultures added with potential inhibitors. ELISA (#DGM00, R&D) detected hGM-CSF in cellular supernatants from MDA-MB-436 (BC) and WAT progenitors $CD45^{-}CD34^{+}$ co-cultures. GM-CSF was efficiently down-regulated when neutralized by its MoAb (1µg/ml) (n=3, ** p<0.01, *** p<0.001, ns: not significant, vs. untreated control).

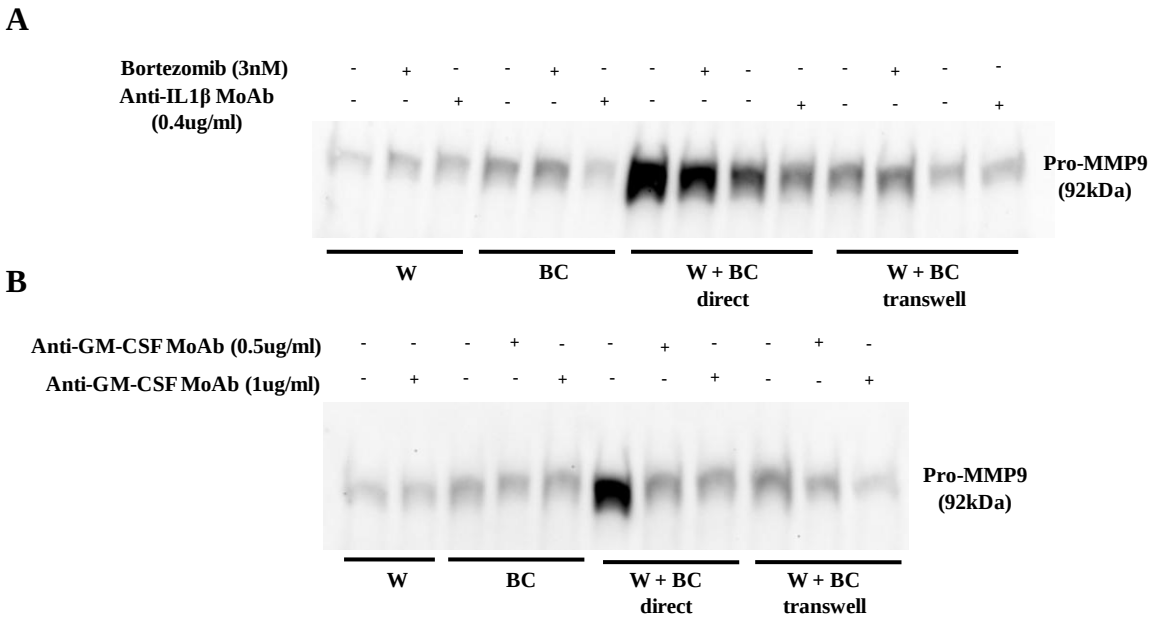

Fig.28 MMP9 release in co-cultures added with potential inhibitors. Representative images of WB staining pro-MMP9 (92kDa) in co-cultures from MDA-MB-436 (BC) and WAT $CD45^{-}CD34^{+}$ progenitors (W), acquired through ChemiDOC MP System. **A)** Medium was added with 3nM Bortezomib or 0.4µg/ml MoAb anti-IL-1β. Bortezomib did not affect MMP9 release, whereas IL-1β neutralization was more effective in preventing MMP9 release in direct co-cultures; **B)** Anti-GM-CSF MoAb (0.5-1µg/ml) added to co-cultures significantly prevented MMP9 release in both direct and transwell co-cultures.

3.5 GM-CSF and MMP9 inhibition in DIO syngeneic model of BC

3.5.1 Tumor growth and metastatic spread

In obesity, the number of $CD45^{-}CD34^{+}$ progenitors is markedly increased in WAT, thus the impact of GM-CSF and MMP9 was investigated in DIO FVB/Hsd or BALB/c mice.

To obtain DIO models, 6-week old FVB/Hsd or BALB/c mice were administered with HFD for 30 days, before BC orthotopic injection. Mice were considered to be obese at that time point (Fig.29).

BALB/c mice displayed an increased body weight and adiposity, although in a less extent compared to FVB/Hsd strain, which weight rapidly increased.

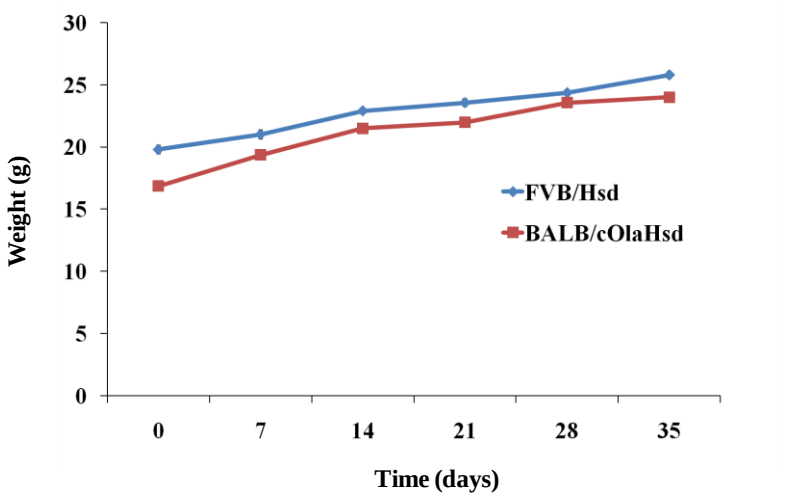

Fig.29 Weekly body weight of DIO mice. Mice were administered with *ad libitum* HFD (60% kcal, Brogaarden) for 30 days before BC injection, until the end of experimental procedures. No statistical difference was observed between the two strains at time points analyzed (n=20, $p>0.05$).

FVB/Hsd mice were orthotopically injected with primary murine MMTV-$ErbB2^{+}$ BC cells and treated with anti-GM-CSF MoAb and/or MMP9 inhibitor (SB-3CT). A first setting of experiments was performed, including distinct controls for each specific treatment (Fig.30). The administration of anti-mGM-CSF MoAb or SB-3CT significantly impaired BC local growth. SB-3CT was effective in reducing BC growth at early phases (Fig.30B),

whereas the anti-tumor effect of anti-GM-CSF MoAb was more stable (Fig.30C). Accordingly, metastatic spread to lungs and axillary lymph nodes was strongly reduced in treated mice, compared to controls (Fig.31).

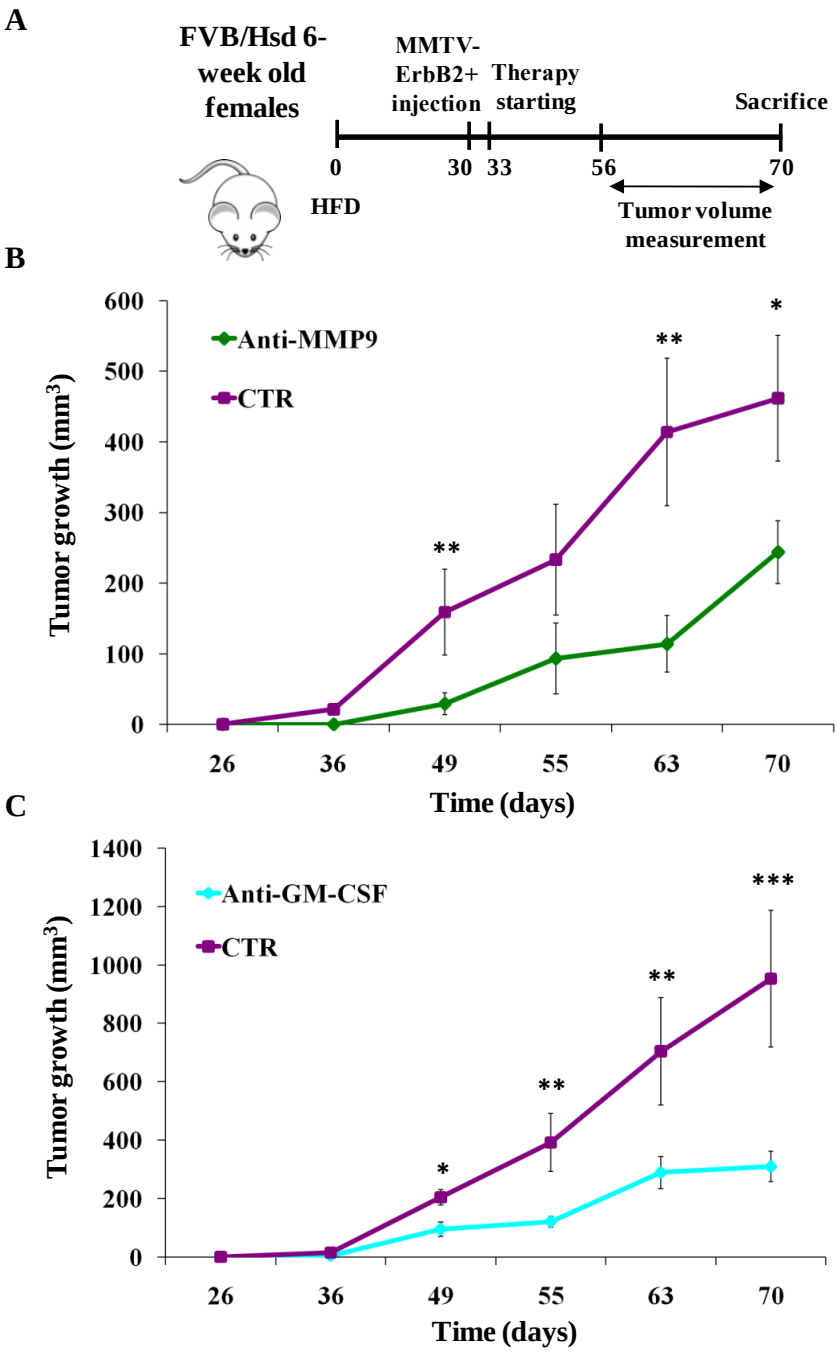

Fig.30 Inhibition of GM-CSF or MMP9 in DIO FVB mice. FVB/Hsd mice, fed with HFD, were injected with $0.5x10^6$ MMTV-ErbB2$^+$ BC cells. **A)** Schematic view of experimental design; **B)** Tumor growth was reduced in anti-MMP9 treated mice (SB-3CT, Sigma-Aldrich) compared to controls administered with vehicle (n=5, * $p<0.05$, ** $p<0.01$); **C)** Tumor growth reduction in anti-mGM-CSF MoAb (#BE0259, BioXcell) mice, compared to IgG2a controls (#BE0089, BioXcell) (n=5, * $p<0.05$, ** $p<0.01$, *** $p<0.001$).

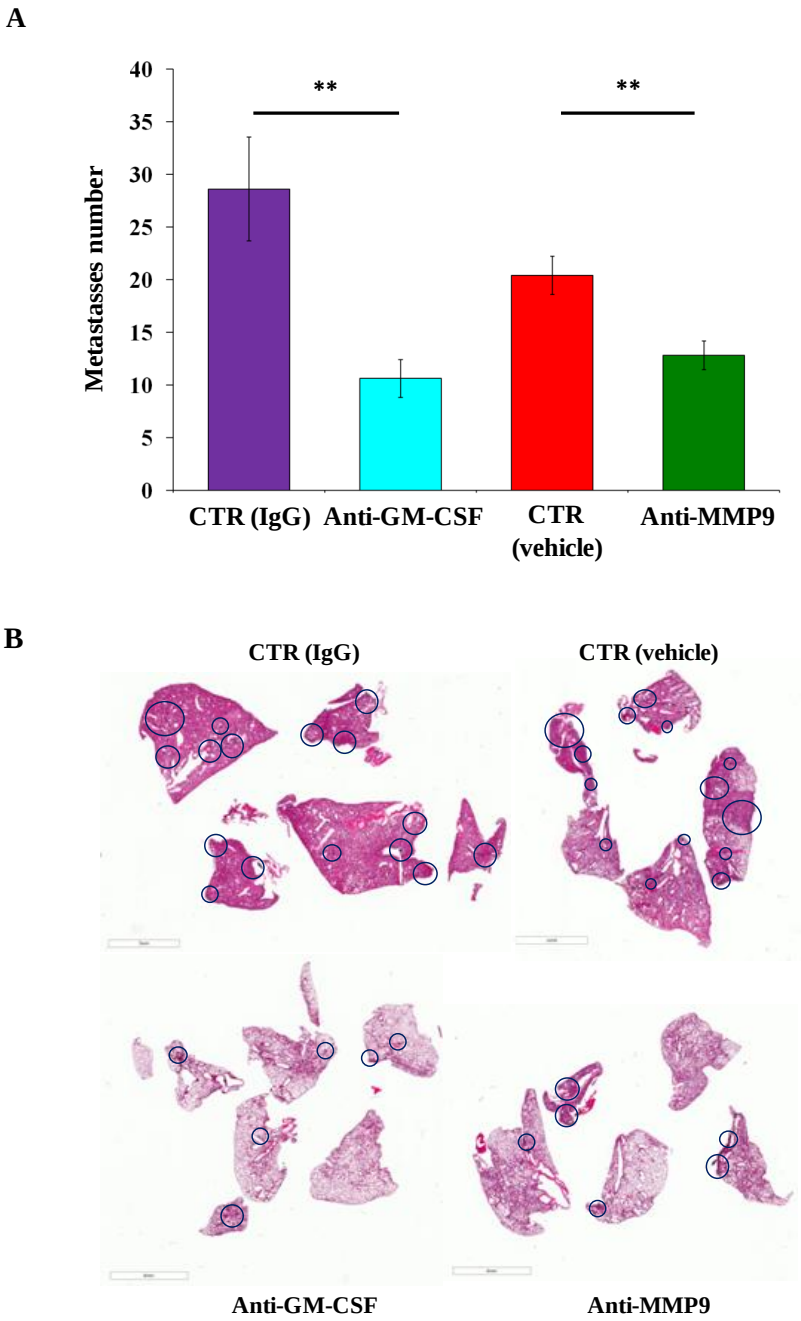

Fig.31 Metastases evaluation in lungs from DIO FVB mice. Lungs were analyzed 70 days after MMTV-ErbB2^{+} injection in DIO FVB/Hsd mice. **A)** Treated mice displayed significant reduction in metastatic spread to lungs compared to respective controls, IgG2a MoAb for anti-GM-CSF or vehicle for SB-3CT (n=5, ** $p<0.01$); **B)** Representative H&E staining of lungs and axillary lymph nodes (scale bars represent 4mm), acquired with APERIO Digital System.

The experiment was repeated to evaluate the combined therapeutic effects and potential synergy of the two inhibitors. The co-administration of anti-GM-CSF MoAb and SB-3CT

displayed a significant synergistic effect in reducing local tumor growth in MMTV-ErbB2^{+} BC injected mice (Fig.32). GM-CSF and MMP9 single inhibitions affected tumor growth in a similar extent, with no significant difference.

To mimic clinical practice, the metastatic evaluation was assessed 30 days after tumor resection (mastectomy). The combined inhibition displayed significant impairment in metastatic spread to lungs and axillary lymph nodes ($p<0.001$), higher than single inhibitions (Fig.33).

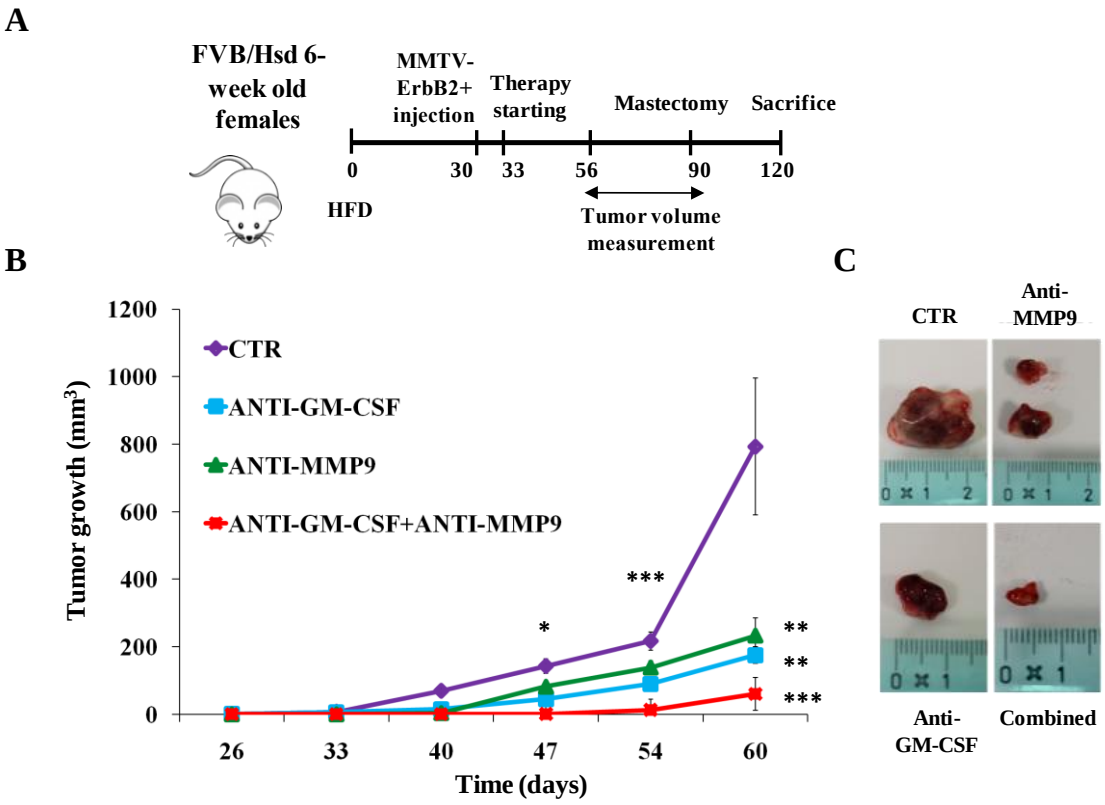

Fig.32 Tumor growth in DIO FVB mice neutralized for GM-CSF and MMP9. FVB/Hsd mice fed with HFD were injected with 0.5x10^{6} MMTV-ErbB2^{+} BC and treated with anti-mGM-CSF MoAb (#BE0259, BioXcell) and/or SB-3CT (Sigma-Aldrich). Control mice were administered with both vehicle and IgG2a MoAb (#BE0089, BioXcell). **A)** Schematic representation of experimental design; **B)** Tumor growth measurement started 26 days after BC injection. Combined inhibition significantly reduced BC growth (n=5, * $p<0.05$, ** $p<0.01$, *** $p<0.001$ vs. IgG2a+vehicle control); **C)** Representative images from tumors collected during mastectomy, 60 days after BC injection.

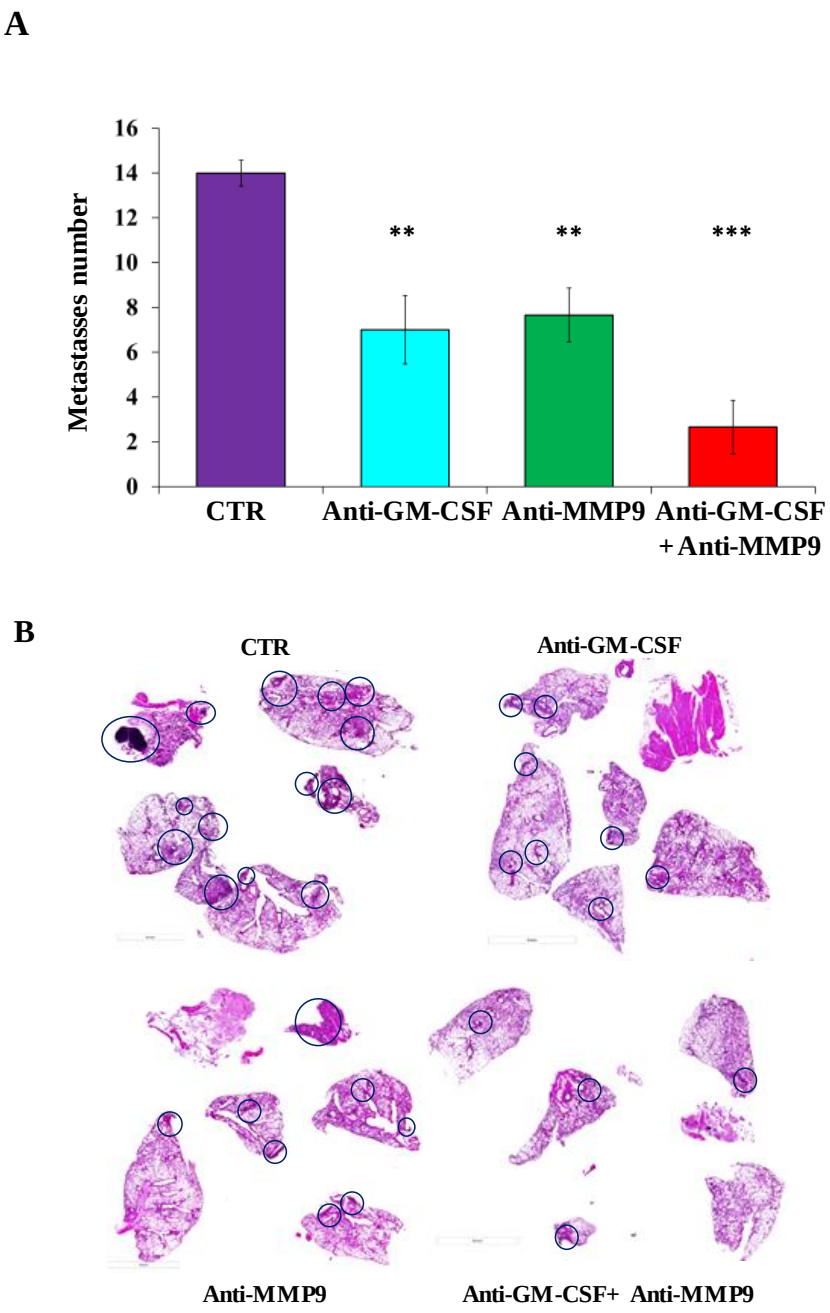

Fig.33 Lungs metastatic spread in DIO FVB mice treated with combined anti-GM-CSF and anti-MMP9. Evaluation of metastatic spread 30 days post mastectomy (120 days from MMTV-ErbB2^{+} BC injection). **A)** Quantitation of lungs metastases revealed a synergic effect of GM-CSF and MMP9 inhibitions in reducing tumor spread (n=5, ** $p<0.01$, *** $p<0.001$, vs. IgG2a+vehicle control); **B)** Representative images of H&E staining of lungs and axillary lymph nodes, acquired with APERIO Digital System (scale bars represent 4mm).

The role of GM-CSF and MMP9 in tumor progression was also investigated in DIO BALB/c injected with TNBC (4T1 cells). The model was characterized by highly aggressive tumor profile, with a fast tumor growth and metastatic spread to multiple sites, including lungs, spleen and liver. Mastectomy was performed 20 days after 4T1 injection (Fig.34A).

BC growth was significantly reduced in all treated groups ($p<0.001$), starting 2 weeks after tumor injection, confirming previously obtained results in FVB/Hsd mice (Fig.34B).

All mice displayed, 15 days after mastectomy, axillary lymph nodes swelling and high metastatic infiltration in lungs, which lost their normal lobular shape and architecture (Fig.35). Nevertheless, treated mice displayed less widespread metastases compared to control mice, especially in case of SB-3CT administration. However, the quantitation of metastases was not possible due to the too extensive tumor infiltration in lungs, which lobules often appeared as a whole tumor mass.

Spleens were deeply infiltrated: spleens collected from tumor-bearing mice appeared enlarged compared to un-injected mice and larger in untreated controls compared to treated mice (Fig.36).

Collectively, these data suggested that GM-CSF and MMP9, produced by WAT, might have a significant role in promoting local and metastatic BC progression in a setting of obesity, both in TNBC and in $ErbB2^{+}$ BC.

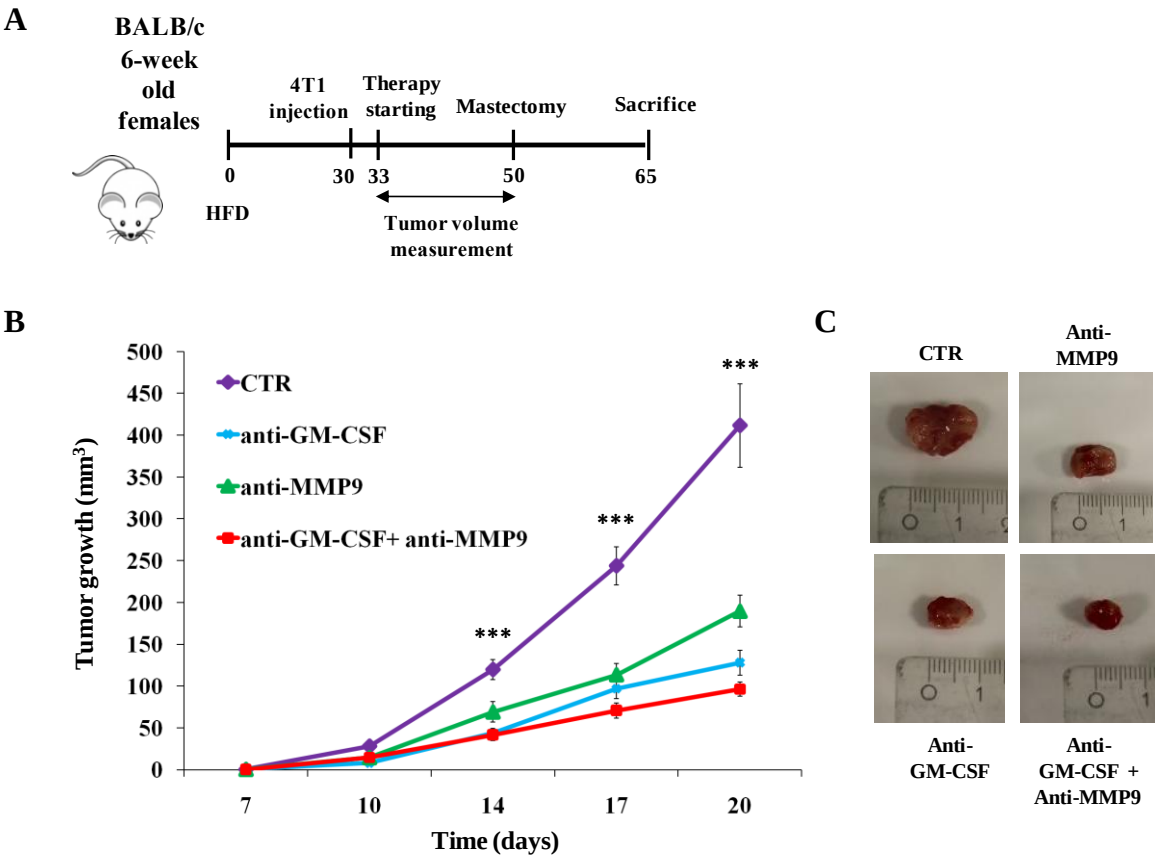

Fig.34 Effect of GM-CSF and/or MMP9 inhibition in DIO BALB/c mice. BALB/c mice were administered with HFD for 30 days and injected with $0.03x10^6$ 4T1 cells. **A)** Schematic view of experimental design; **B)** Tumor growth measured 7 days after BC injection until mastectomy. All treated mice significantly decreased local BC growth compared to controls, administered both with vehicle and IgG2a MoAb (n=10, *** $p<0.001$); **C)** Representative images of tumors collected during mastectomy, 20 days after BC injection.

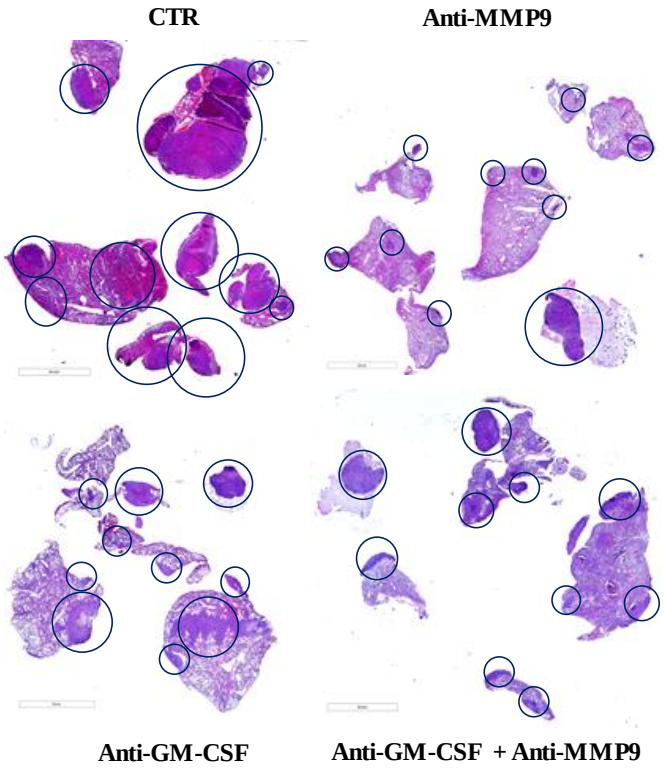

Fig.35 Lungs metastases in DIO BALB/c mice. Representative H&E staining of lungs and axillary lymph nodes, collected 15 days after mastectomy, in HFD BALB/c mice injected with 4T1 cells. Images were acquired with APERIO Digital System (scale bars represent 3mm).

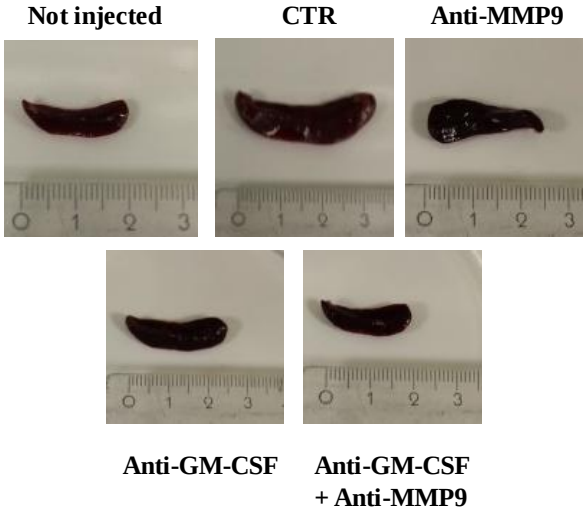

Fig.36 Spleens collected from DIO BALB/c mice injected with 4T1. Representative images of spleens, collected 15 days post mastectomy, from HFD BALB/c mice. Spleen from a not-tumor bearing DIO BALB/c mouse was used as negative control. In tumor-bearing mice, controls displayed higher spleen swelling compared to treated mice.

3.5.2 Immune system regulation

GM-CSF and MMP9 ability to regulate immune system was investigated in syngeneic models of BC, through a multiparametric flow cytometry analysis.

Several immune populations, both lymphoid and myeloid compartments, were analyzed in PB, peritumoral WAT and BC tumors, collected from both DIO FVB/Hsd-MMTV-ErbB2^{+} and BALB/c-4T1 mice.

Circulating levels of classic monocytes and inflammatory monocytes were strongly impaired in anti-GM-CSF treated mice compared to controls, in both syngeneic models (Fig.37). Other myeloid cells were impaired in a less extent, including granulocytes, whereas dendritic cells were unaffected by the treatment.

NK cells and lymphoid populations, such as B lymphocytes, T-helper and cytotoxic T lymphocytes, were also unaffected by GM-CSF neutralization (data not shown). Conversely, circulating T-regs were significantly reduced in both models ($p<0.01$, Fig.37).

Tumors and peritumoral WAT were analyzed for immune cells infiltration (Fig.38-39): T-regs and some myeloid cells were found reduced after anti-GM-CSF treatment, compared to IgG2a control. Cells involved in immunosuppression such as MDSCs were highly reduced: G-MDSCs were impaired in both tumor and WAT and intratumoral Mo-MDSCs were efficiently reduced. Macrophages and TAMs, quantified as CD206^{+}MHCII^{low} macrophages, were also impaired in treated mice.

Furthermore, T-regs were found to be significantly reduced in peritumoral WAT in both BC models, when GM-CSF was neutralized.

Taken together, these data suggested that GM-CSF might promote immune cells recruitment in tumor microenvironment, establishing immunosuppressive mechanisms and fostering tumor escape.

Anti-MMP9 inhibition did not influence PB, WAT or tumor immune populations, compared to vehicle-administered control mice (data not shown).

A

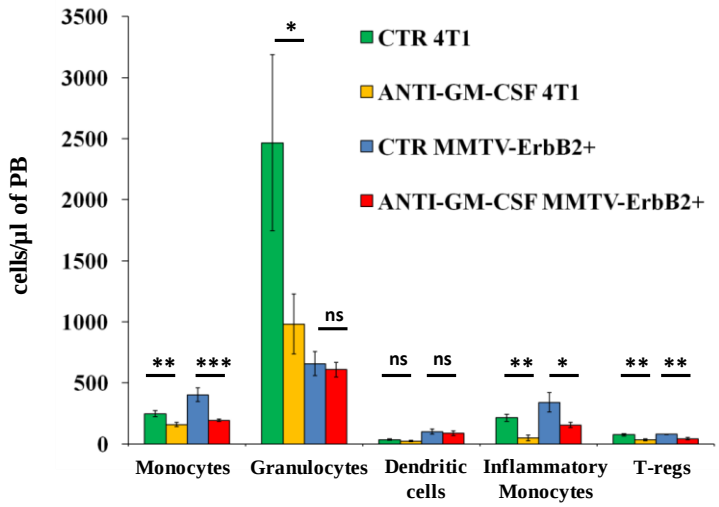

B

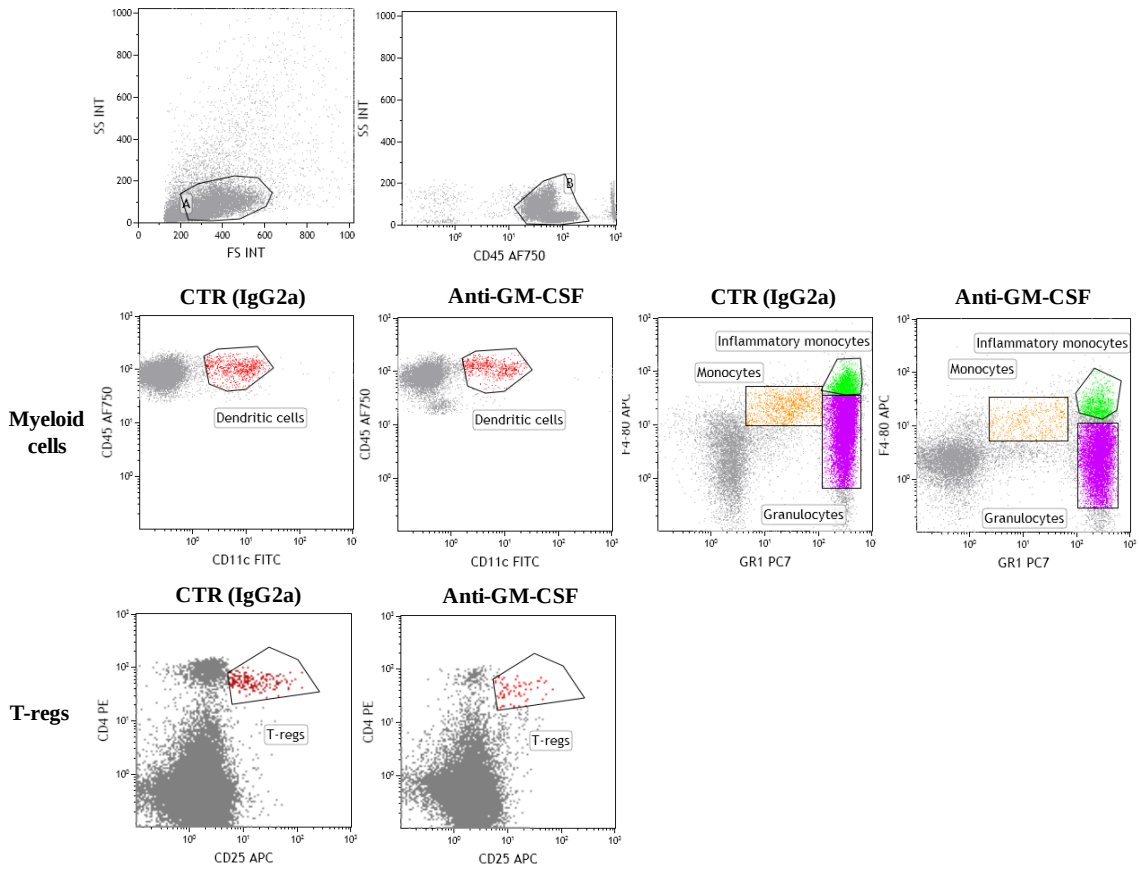

Fig.37 Flow cytometry analysis on circulating immune cells in DIO syngeneic mice neutralized for GM-CSF. A) Absolute quantitation of cells in PB, collected from DIO FVB/Hsd injected with MMTV-ErbB2^{+} BC (30 days post injection) and BALB/c injected with 4T1 (15 days post injection). Anti-GM-CSF treated mice displayed a significant decrease of several immune cells (n=10, * $p<0.05$, ** $p<0.01$, *** $p<0.001$, ns: not significant, vs. IgG2a control); **B)** Gating strategy (top line) and representative images of gated cells in PB collected from BALB/c mice.

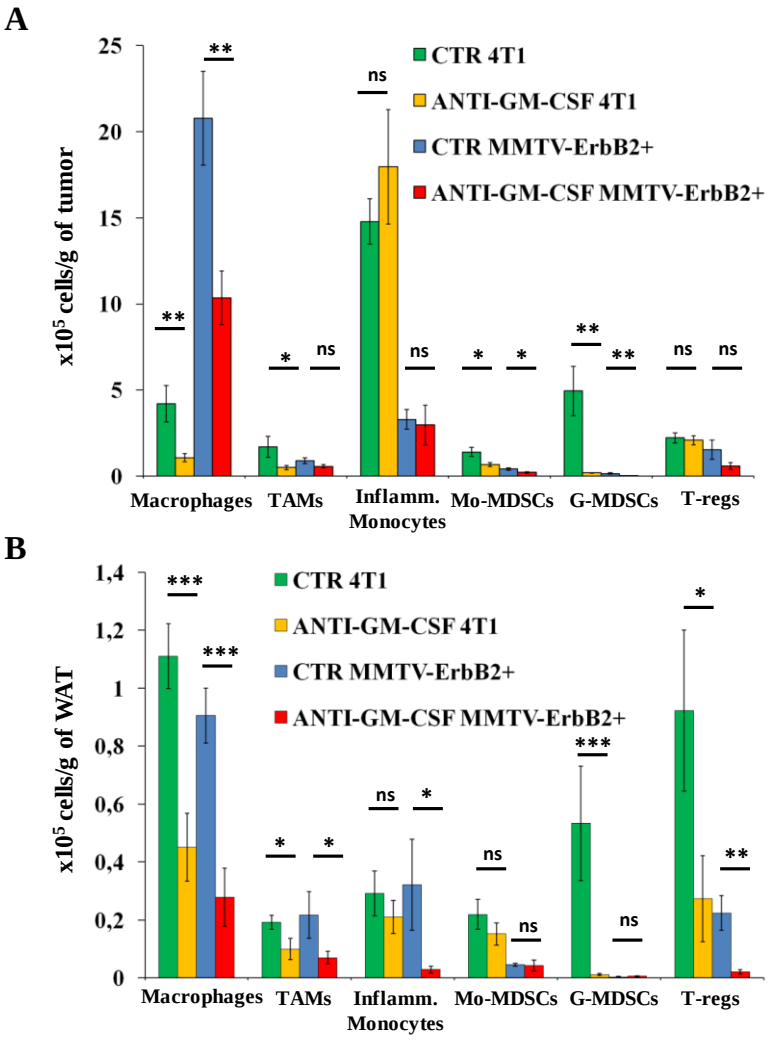

Fig.38 Absolute quantitation of peritumoral and intratumoral immune cells in DIO mice neutralized for GM-CSF. Number of immune cells per gram (g) of tissue in tumors **(A)** or peritumoral WAT **(B)**, collected from DIO syngeneic mice (n=10, * p<0.05, ** p<0.01, *** p<0.001, ns: not significant vs. respective IgG2a control).

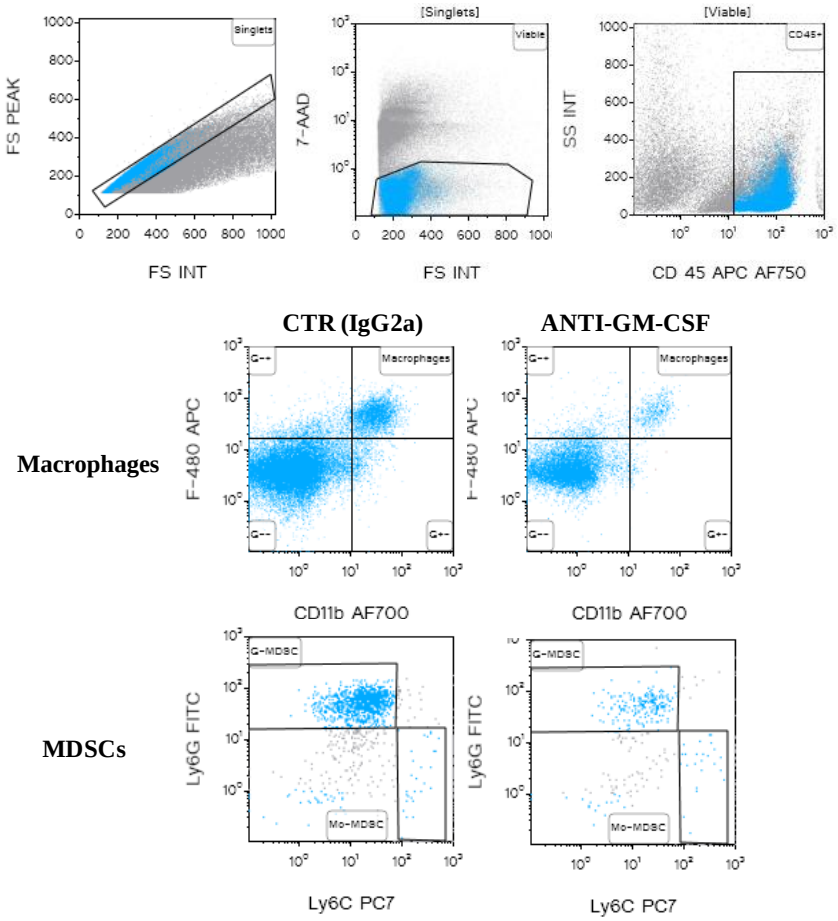

Fig.39 Flow cytometry analysis on intratumoral and peritumoral immune cells. Gating strategy (top line) and representative images of macrophages ($CD45^+CD11b^+F4/80^+$), G-MDSCs ($CD45^+Ly6C^{dim}Ly6G^+$) and Mo-MDSCs ($CD45^+Ly6G^-Ly6C^+$) detected in peritumoral WAT collected from anti-GM-CSF treated mice compared to IgG2a controls.

To further support the hypothesis, WAT and tumor tissue from anti-GM-CSF treated mice were analyzed by qRT-PCR. A PCR array was used to evaluate molecules potentially involved in mouse inflammation and immunity regulation. In anti-GM-CSF treated mice, several factors involved in immunosuppression were down-regulated in both WAT and tumor, compared to IgG2a controls (Fig.40). In general, gene expression was mostly affected in WAT compared to tumor tissue, suggesting a strong reduction of WAT immunosuppressive activity.

Some immunosuppressive factors were detected to be down-regulated, such as IL-10, IL-5, CXCL5 and CD274 (PD-L1). In addition, some molecules and receptors, mainly involved

in TAMs and MDSCs recruitment and functionality, were down-regulated, such as CCL22, CCL4, IL-1β and CXCR5. Of note, GM-CSF (CSF2) itself was found down-regulated in both WAT and tumor tissue, confirming the *in vitro* results that suggested the presence of a feedback regulation.

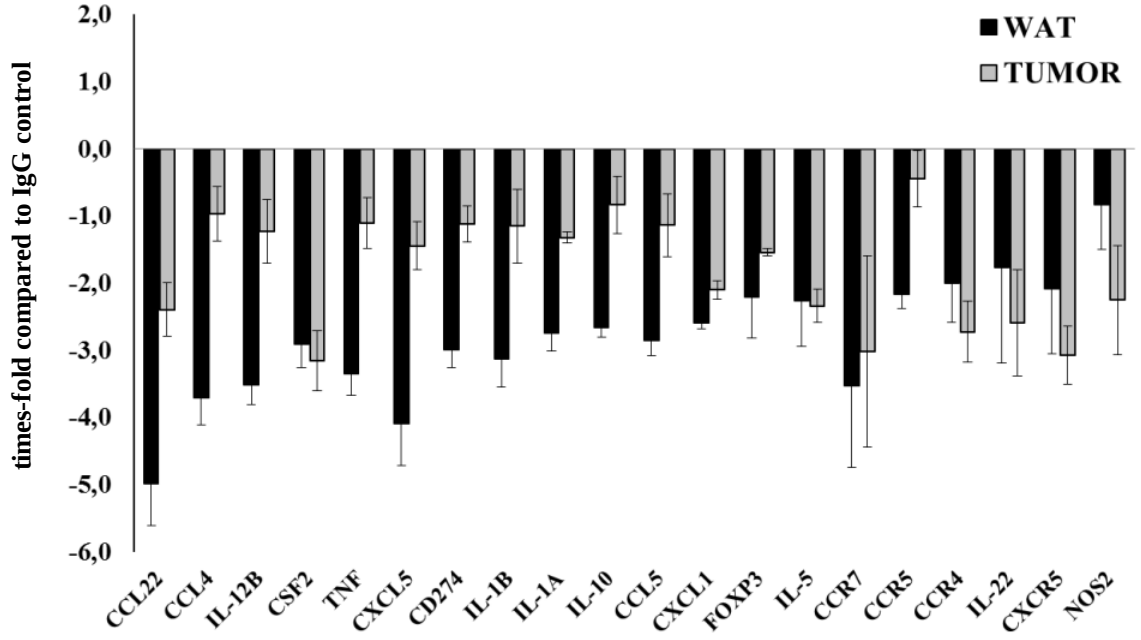

Fig.40 Mouse inflammation and immune system related-genes analysis. Peritumoral WAT and BC tumors were collected from DIO FVB/Hsd mice, injected with MMTV-ErbB2$^+$ BC cells and treated with anti-GM-CSF. Gene expression was analyzed through PCR Array (#PAMM-181Z, Qiagen). Results were calculated with web-based software RT^2 Profiler PCR Array Data Analysis. Values are displayed as times-fold expression compared to IgG2a MoAb controls (n=5).

3.5.3 Inhibition of intratumoral angiogenesis

To investigate if angiogenesis was affected by the inhibition of GM-CSF and/or MMP9, intratumoral microvessel density (MVD) was investigated, through a double immune-fluorescence analysis. IF stained both endothelial cells (CD31$^+$) and pericytes (α-SMA$^+$), in tumor-bearing DIO BALB/c and FVB/Hsd mice.

In both BC models, quantitation of blood vessels indicated a strong inhibition of angiogenesis in treated tumors compared to control group, with a significantly ($p<0.01$) lower MVD (Fig.41). The co-administration of inhibitors further impaired tumor angiogenesis ($p<0.001$), suggesting that both factors might be crucial in promoting BC neovascularization.

The ratio between $CD31^+/\alpha\text{-}SMA^+$ vessels was not significantly affected by any treatment; however, the combined therapy targeted more $\alpha\text{-}SMA^+$ cells than $CD31^+$ endothelial cells (Fig.41D).

A

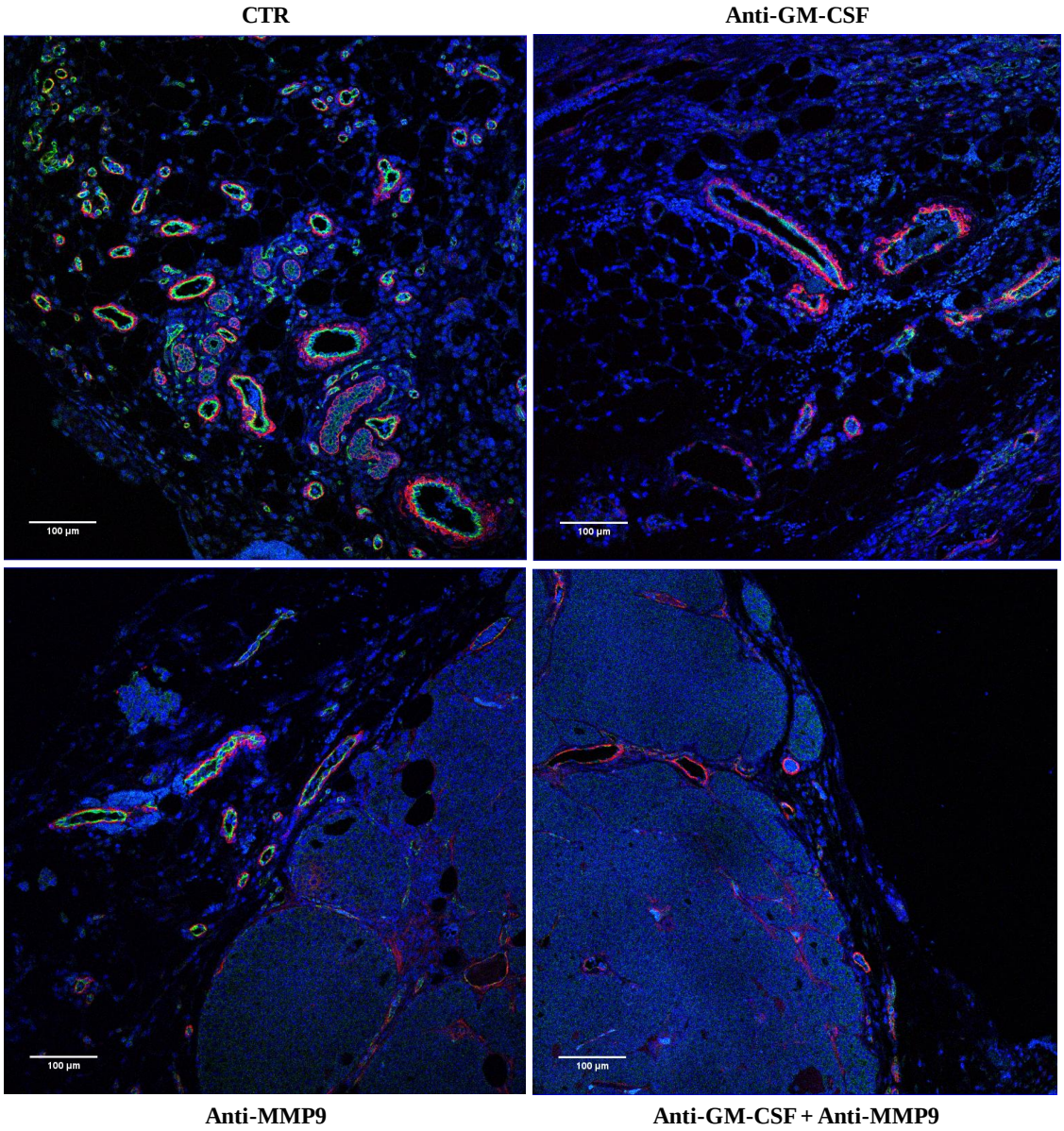

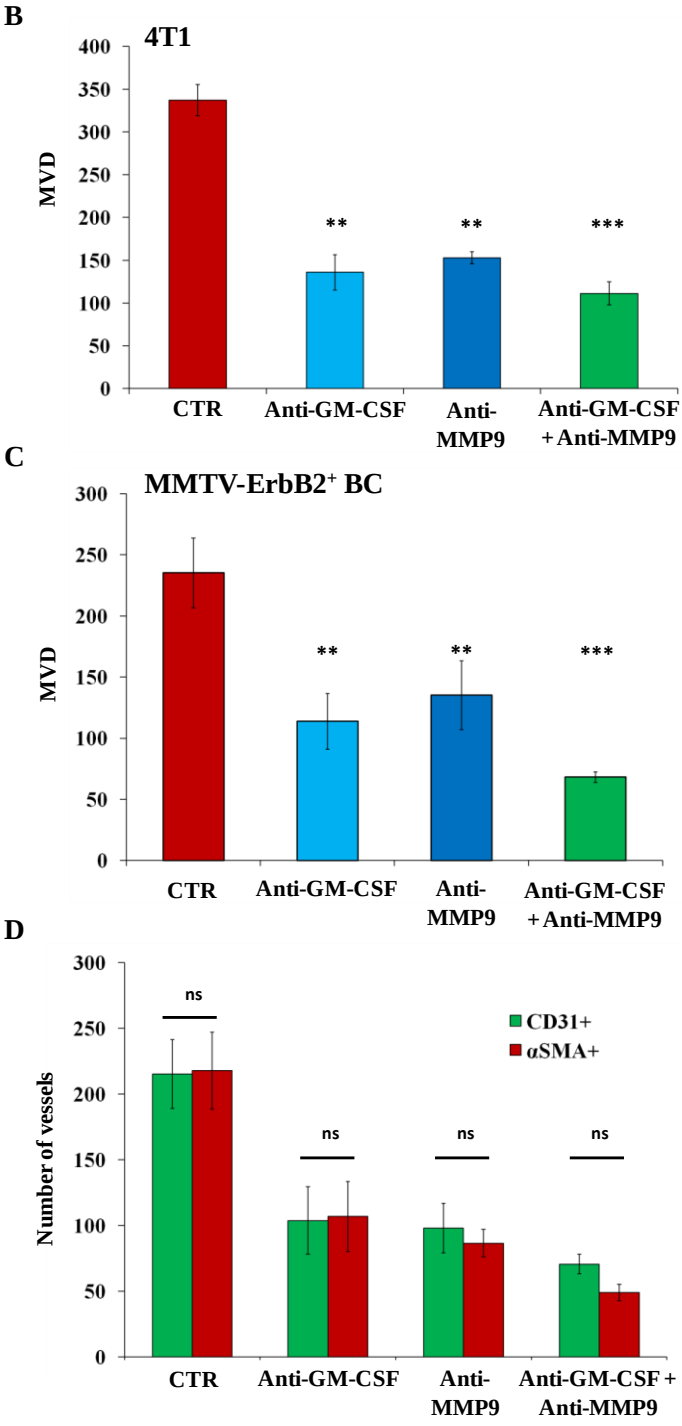

Fig.41 Reduced neoplastic angiogenesis in DIO syngeneic mice. Representative images **(A)** acquired with Leica confocal microscope (20x magnification). Staining was performed with anti-mCD31 (*green*, 1:20 #ab28364, Abcam), anti-αSMA (*red*, 1:3000 #A2547, Sigma-Aldrich) and DAPI nuclear staining (*blue*). Scale bars represent 100µm. Analysis of intratumoral MVD in DIO BALB/c mice injected with 4T1 cells **(B)** or FVB/Hsd mice injected with MMTV-ErbB2$^+$ BC cells **(C)**. Blood vessels quantitation was performed with ImageJ software. In all treated mice the number of vessels was significantly reduced (n=3, ** $p<0.01$, *** $p<0.001$ vs. vehicle+IgG2a control). **D)** Quantitation of relative amount of CD31$^+$ and αSMA$^+$ blood vessels (n=3), normalized for tumor area in MMTV-ErbB2$^+$ injected mice (ns: not significant).

3.6 Metformin regulated GM-CSF and MMP9 release by WAT progenitors

3.6.1 Co-cultures *in vitro*

The antidiabetic drug Metformin has been widely reported to inhibit the onset and metastatic progression of several BC subtypes in diabetic patients (Goodwin *et al*., 2011), especially in presence of concomitant obesity (Ko *et al*., 2015). The drug was reported to target both BC cells and tumor microenvironment, including endothelial cells and WAT-derived progenitors (Dallaglio *et al.*, 2014; Orecchioni *et al.*, 2015).

To assess if Metformin was possibly involved in GM-CSF and/or MMP9 regulation, the drug was added to the *in vitro* co-culture system, between TNBC cells (MDA-MB-436) and hWAT $CD45^{-}CD34^{+}$ progenitors.

Metformin was tested at different concentrations on BC and WAT cells, which were cultured for 72 hours in presence of the drug (Fig.42). Metformin does not require to be metabolized by hepatic enzymes in order to be biologically active. Cells were analyzed to assess apoptosis rate and viability through flow cytometry. The chosen dose (5mM) did not significantly affect cell viability of both BC and WAT progenitor cells.

Cellular supernatant was firstly screened for angiogenesis and inflammatory mediators, through antibody array (Fig.43). Metformin affected the release of several factors in both single and co-cultures: TIMP-4, IGFBP2, IGFBP3, Endostatin and Angiogenin were reduced in BC cells (Fig.43B, top panel); IL-8 and SerpinE1 release was impaired in WAT progenitors (Fig.43B, middle panel).

GM-CSF and MMP9 were strongly inhibited by Metformin in co-cultures, but not in single cells cultures, suggesting that the drug prevented the observed up-regulation in WAT progenitors (Fig.43B bottom panel).

Of note, VEGF was detected to be up-regulated in WAT progenitors cultured alone, but not in co-cultures or in BC cells (Fig.43B, middle panel). This is in accordance with some recent findings suggesting the existence of a paradoxical regulation of angiogenesis

mediated by the drug, that differed according to the cell type analyzed (Dallaglio *et al.*, 2014).

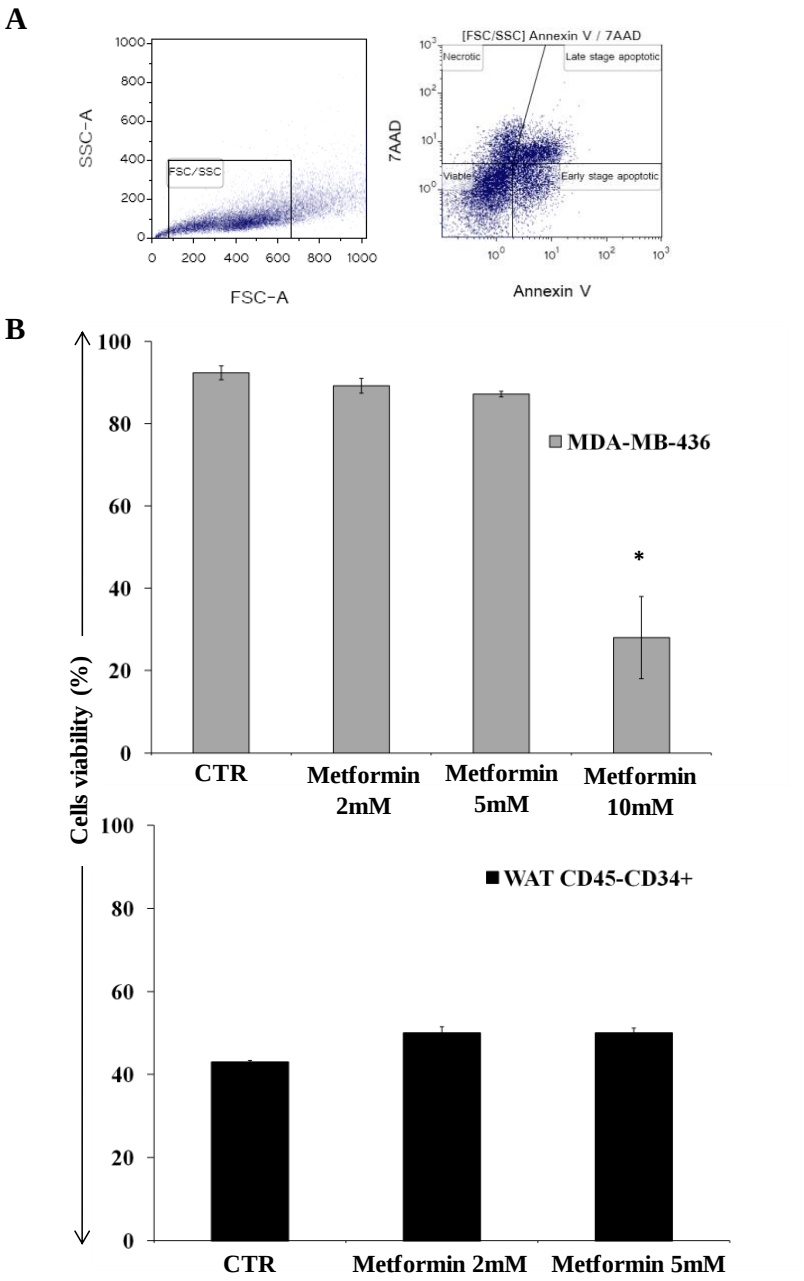

Fig.42 Metformin dose evaluation *in vitro*. Different concentrations (2-10nM) of Metformin (Sigma-Aldrich) were tested to determine the unaffecting dose on cell viability. **A)** Gating strategy of flow cytometry analysis to isolate viable and nucleate cells ($Syto16^{+}7AAD^{-}AnnexinV^{-}$); **B)** Percentages of viable cells after 72 hours: MDA-MB-436 cells (top panel) or hWAT $CD45^{-}CD34^{+}$ progenitors (bottom panel). The chosen dose (5mM) did not alter cells viability (n=3, * $p<0.05$ vs. untreated).

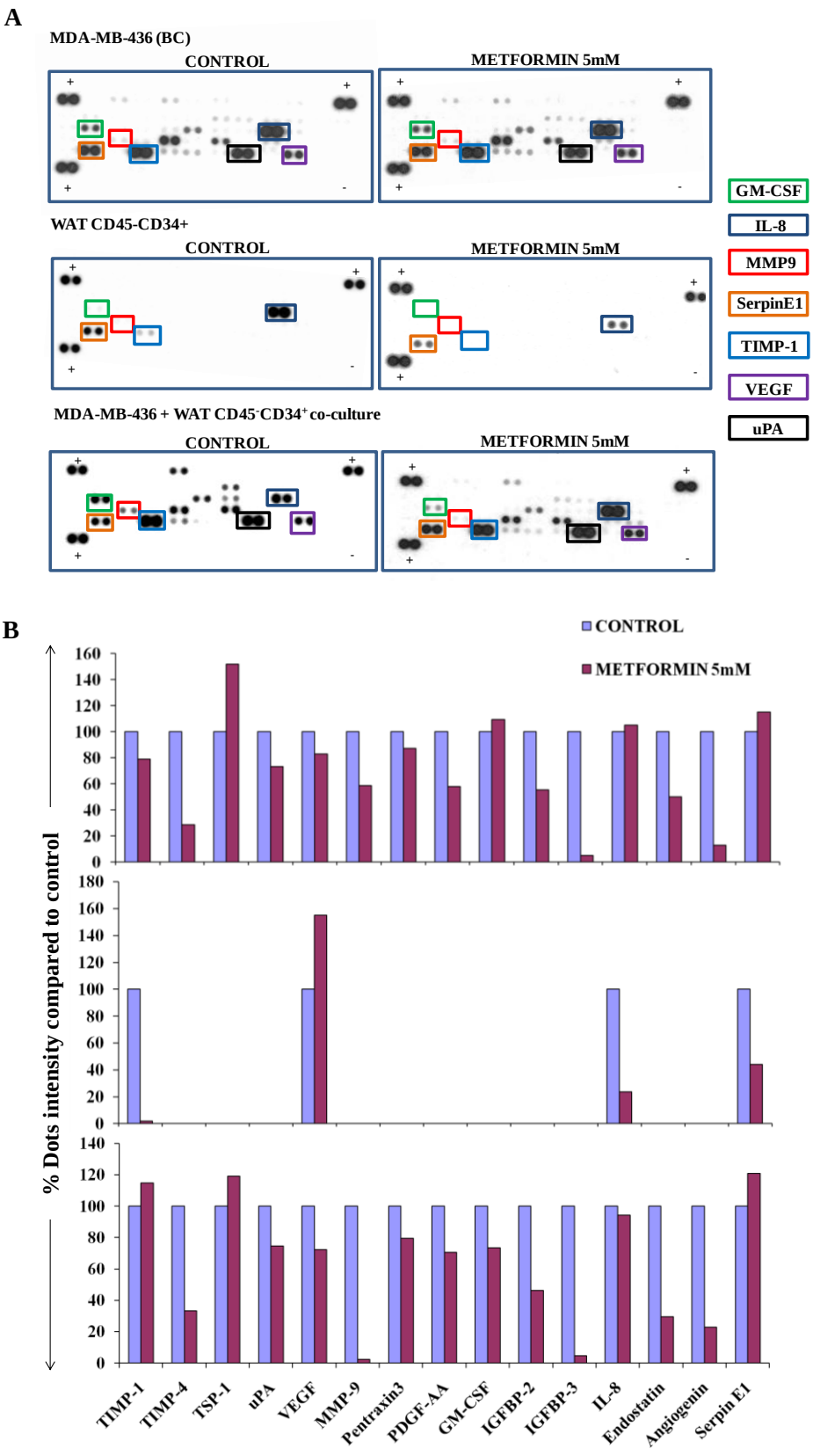

Fig.43 Antibody array on co-cultures added with Metformin. Metformin (5mM) was added to MDA-MB-436 and WAT $CD45^{-}CD34^{+}$ progenitors cultured alone or in transwell system. Cellular supernatant was screened through Proteome Profiler array (#ARY007, R&D). **A)** Representative images acquired with ChemiDOC MP System; **B)** Dots intensity quantitation using ImageJ software: values are displayed as percentages compared to untreated cells (adapted from Orecchioni *et al.*, Int J Cancer, 2015).

Several co-cultures, using WAT $CD45^{-}CD34^{+}$ cells isolated from different subjects (n=5), were analyzed for GM-CSF and MMP9 protein levels in presence of Metformin.

GM-CSF release was significantly inhibited in both transwell and direct co-cultures, as shown by ELISA (Fig.44). Of note, Metformin failed to down-regulate GM-CSF release in BC seeded alone.

MMP9 expression in cellular supernatant was analyzed with WB, confirming the drug ability to prevent protein release in co-cultures, but not in single cells cultures (Fig.45). Accordingly, zymography confirmed the reduced enzymatic activity of MMP9 in direct co-cultures in presence of Metformin (Fig.46).

Unexpectedly, the mRNAs levels of GM-CSF and MMP9 were not down-regulated by Metformin in WAT progenitors, suggesting an alternative mechanism of inhibition of proteins release (Fig.47). Although, GM-CSF transcripts were found up-regulated by Metformin in both BC and WAT progenitors in transwell co-cultures, suggesting a more complex regulation induced by the drug.

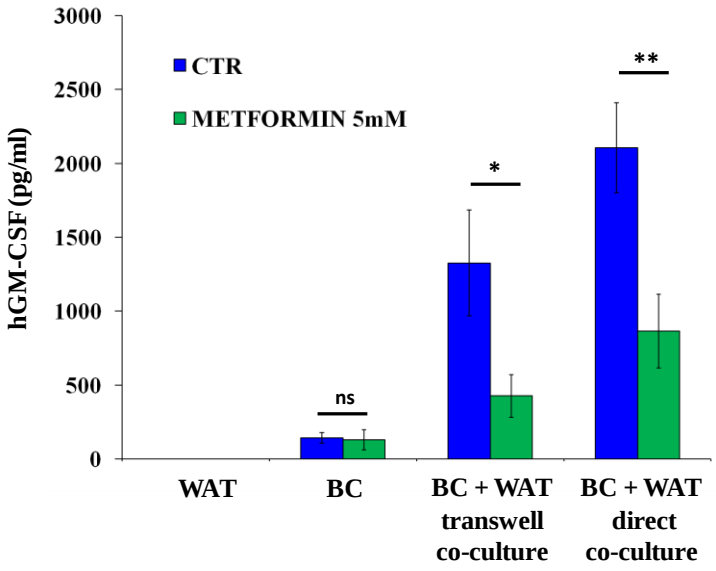

Fig.44 Effect of Metformin on GM-CSF release in co-cultures. Metformin (5mM) was added to *in vitro* co-cultures between MDA-MB-436 and WAT $CD45^{-}CD34^{+}$ progenitors. GM-CSF quantitation was performed through ELISA (#DGM00, R&D). Metformin significantly inhibited GM-CSF release in co-cultures, but not in BC single cultures (n=5, * $p<0.05$, ** $p<0.01$, ns: not significant, vs. untreated).

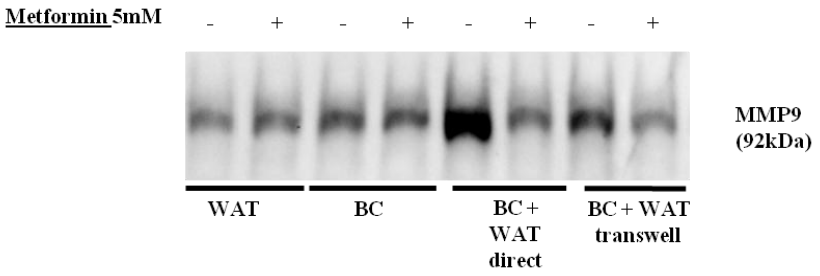

Fig.45 Metformin inhibited MMP9 release in co-cultures. Representative image of WB staining pro-MMP9 (1:2000 #ab76003, Abcam), acquired with ChemiDOC MP System. Metformin (5mM) strongly affected MMP9 release in co-cultures between MDA-MB-436 and WAT $CD45^{-}CD34^{+}$ progenitors.

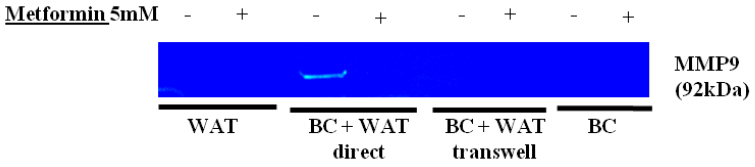

Fig.46 Zymography on culture supernatants added with Metformin. Representative image of zymogram acquired through ChemiDOC MP System. Metformin (5mM) was added to co-cultures of MDA-MB-436 and WAT progenitors, inhibiting MMP9 proteolytic activity in direct co-cultures.

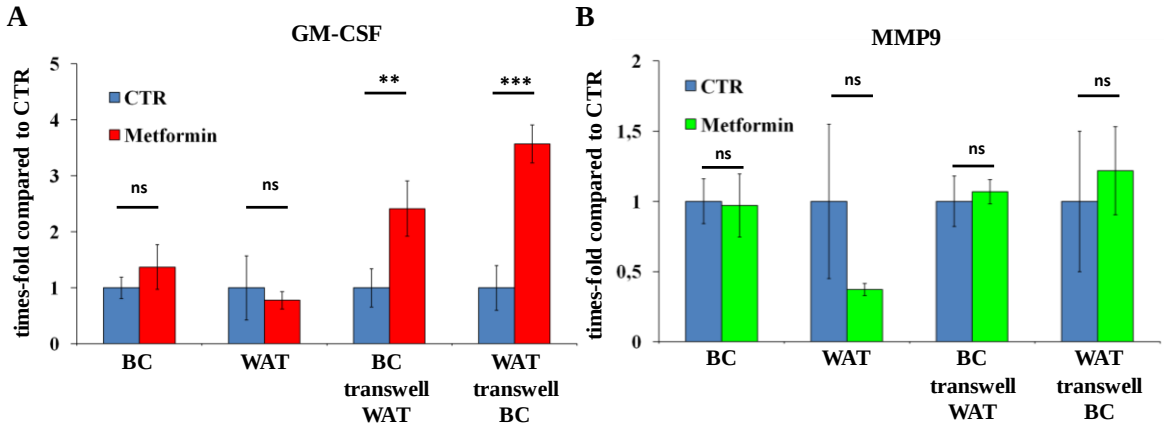

Fig.47 Transcriptional regulation induced by Metformin. qRT-PCR analyzed MDA-MB-436 (BC) and WAT $CD45^{-}CD34^{+}$ progenitors alone or in transwell co-cultured, treated or not with 5mM Metformin. Values of GM-CSF **(A)** or MMP9 **(B)** were normalized for ABL gene expression and expressed as times-fold to corresponding untreated sample (n=5, ** $p<0.01$, *** $p<0.001$, ns: not significant).

3.6.2 Metformin effect in xenograft model of BC

NSG mice, injected with MDA-MB-436 cells alone or in combination with hWAT $CD45^-$ $CD34^+$ progenitors, were administered with Metformin in drinking water (2mg/ml). Mice weight, serum levels of glucose, cholesterol and triglycerides were not significantly affected by the treatment, suggesting that the drug had not adverse effects on mice metabolism (data not shown). Tumor growth was significantly inhibited by Metformin in all treated mice (Fig.48).

Circulating levels of hGM-CSF were analyzed through HS ELISA. In all treated mice a reduction of hGM-CSF was detected, compared to untreated controls. The reduction was highly significant in co-injected mice and the effect was time-dependent (Fig.49).

hMMP9 expression, previously demonstrated to be up-regulated in hBC-hWAT co-injected mice, was reduced in tumors collected from Metformin administered mice (Fig.50). Conversely, Metformin did not reduce hMMP9 expression in mice injected with hBC alone, although pro-MMP9 was even higher in treated compared to untreated ones.

These data confirmed a new possible effect of Metformin *in vivo*, through the modulation of GM-CSF and MMP9.

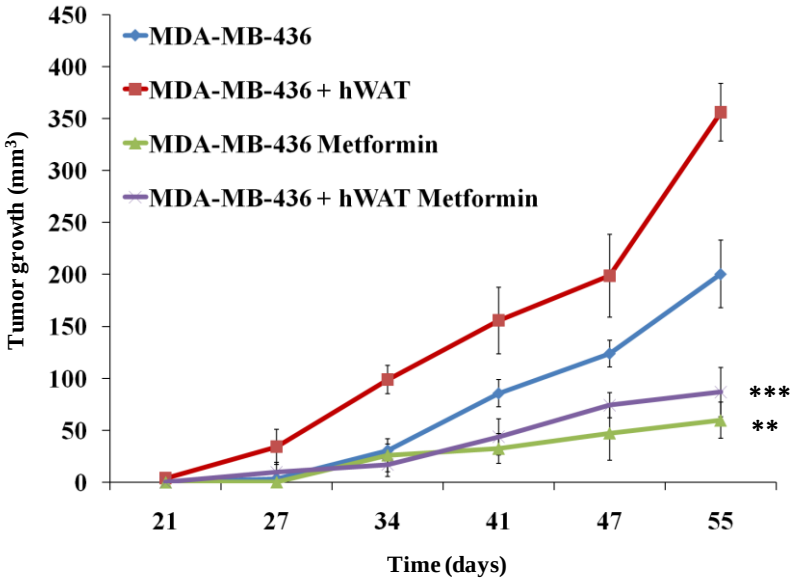

Fig.48 Tumor growth in xenograft mice treated with Metformin. NSG mice were injected with $1x10^6$ MDA-MB-436 cells alone or in combination with $0.2x10^6$ WAT $CD45^-CD34^+$ progenitors (n=12 per study arm). Metformin was administered in drinking water (2mg/ml) starting 3 days after BC injection. Tumor growth was reduced in treated mice compared to respective controls (** p<0.01, *** p<0.001).

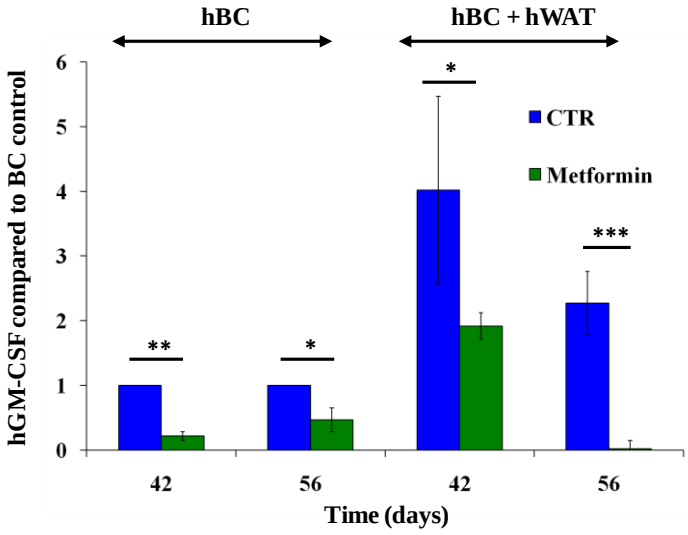

Fig.49 Quantitation of circulating hGM-CSF in xenograft models treated with Metformin. Metformin significantly reduced hGM-CSF in plasma of NSG mice injected with MDA-MB-436 (BC) alone or with hWAT $CD45^-CD34^+$ (n=5, * p<0.05, ** p<0.01, *** p<0.001 vs. respective untreated). The quantitation was done through HS ELISA (#HSGM0, R&D), values expressed as times-fold compared to untreated BC mice.

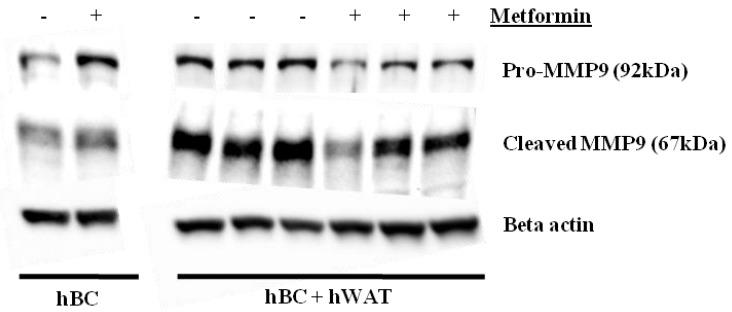

Fig.50 Metformin administration to xenograft mice reduced MMP9 up-regulation in co-injected mice. Representative image of WB detecting pro- and active MMP9 (1:100, #10375-2-AP, Proteintech) in whole tumor lysate, acquired with ChemiDOC MP System. Tumors collected from Metformin-treated co-injected (MDA-MB-436 + WAT progenitors) mice displayed reduced MMP9 expression, in both precursor and active forms, compared to untreated controls. Beta actin was used as loading control.

3.6.3 Metformin administration to DIO syngeneic model

As previously demonstrated, Metformin was able to reduce GM-CSF and MMP9 release *in vitro* and *in vivo*. The efficacy of the drug was then questioned in DIO syngeneic mice, which were administered either with Metformin, anti-GM-CSF MoAb or SB-3CT.

Metformin efficacy in reducing BC volume was confirmed, displaying the same efficiency of anti-GM-CSF or anti-MMP9 specific treatments (Fig.51).

Similarly, the number of metastases in lungs and axillary lymph nodes were significantly reduced in all treated mice compared to controls ($p<0.01$, Fig.52). Of note, none of Metformin treated mice displayed axillary lymph nodes swelling, whereas all control mice displayed deep tumor infiltration and significant lymph nodes swelling.

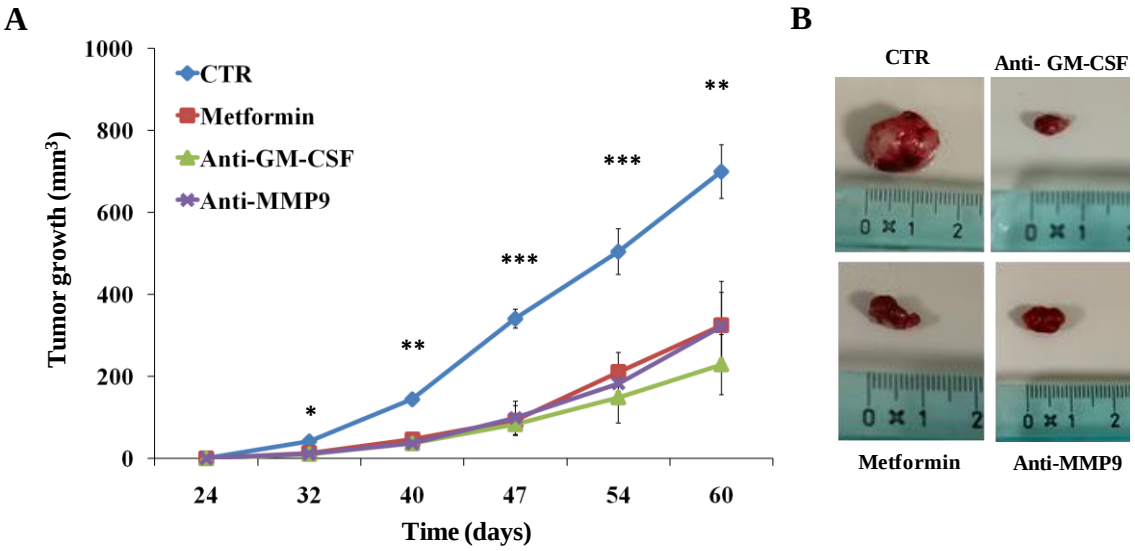

Fig.51 Metformin effect on BC growth in DIO syngeneic models. FVB/Hsd mice, fed with HFD, were injected with $1x10^6$ MMTV-ErbB2$^+$ BC cells. Mice were treated with anti-mGM-CSF MoAb or SB-3CT or Metformin, which was dissolved in drinking water (n=5 per study arm). **A)** Tumor growth was monitored, starting 24 days after BC injection. A significant reduction was detected in all treated mice compared to vehicle+IgG2a controls (* $p<0.05$, ** $p<0.01$, *** $p<0.001$); **B)** Representative images of tumors collected during mastectomy, 60 days after BC injection.

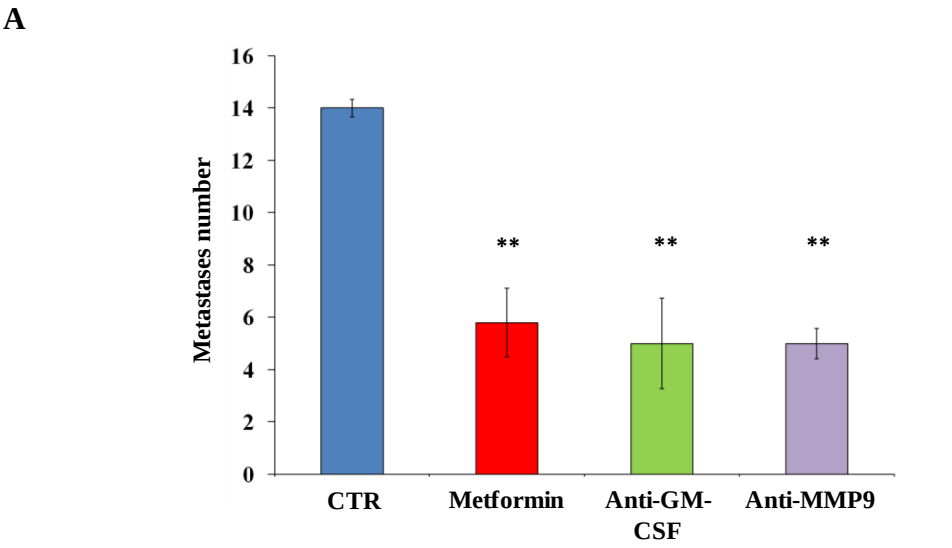

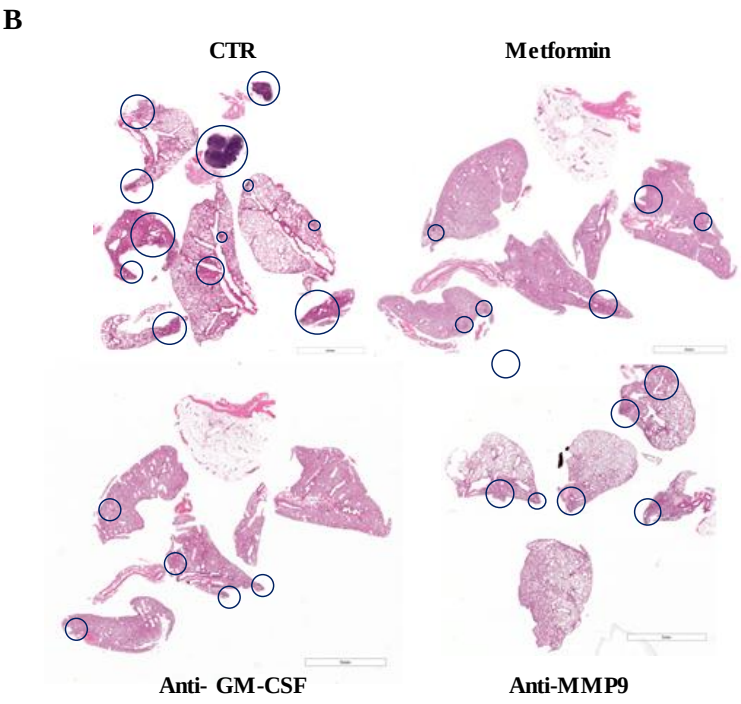

Fig.52 Metastatic evaluation in lungs from DIO mice treated with Metformin. Lungs and axillary lymph nodes were collected from DIO FVB/Hsd mice injected with MMTV-ErbB2^{+} BC. **A)** Quantitation of lungs metastases revealed a significant reduction in metastatic spread in all treated mice (n=5, ** $p<0.01$ vs. vehicle+IgG2a controls); **B)** Representative H&E staining images acquired with APERIO Digital System (scale bars represent 4mm).

The quantitation of intratumoral angiogenesis was evaluated through IF staining of CD31^{+}αSMA^{+} vessels (Fig.53): among different drugs, Metformin was the most effective in reducing angiogenesis ($p<0.001$), compared to anti-GM-CSF or anti-MMP9 specific treatments ($p<0.01$).

Multiparametric flow cytometry analysis of PB and tissues, collected from Metformin-treated mice, revealed that the drug had similar effects displayed by anti-GM-CSF specific neutralization, regarding myeloid cells and immunosuppressive microenvironment modulation (Fig.54-55).

Metformin reduced circulating levels of monocytes, inflammatory monocytes and granulocytes, similarly to GM-CSF neutralization (Fig.54). Conversely, dendritic cells were significantly reduced by Metformin, but not by GM-CSF specific neutralization.

Several populations involved in immunosuppression and tumor immune escape, such as T-regs and TAMs, were down-regulated in peritumoral WAT, whereas G-MDSCs were strongly impaired in tumors of Metformin treated mice (Fig.55). Additionally, Metformin significantly reduced the presence of inflammatory monocytes in both tumors and WAT, supporting the anti-inflammatory activity of the drug.

Collectively these data suggested that GM-CSF and MMP9 inhibition, mediated by Metformin, might explain some of its anti-tumor effects already reported in BC preclinical models.

A

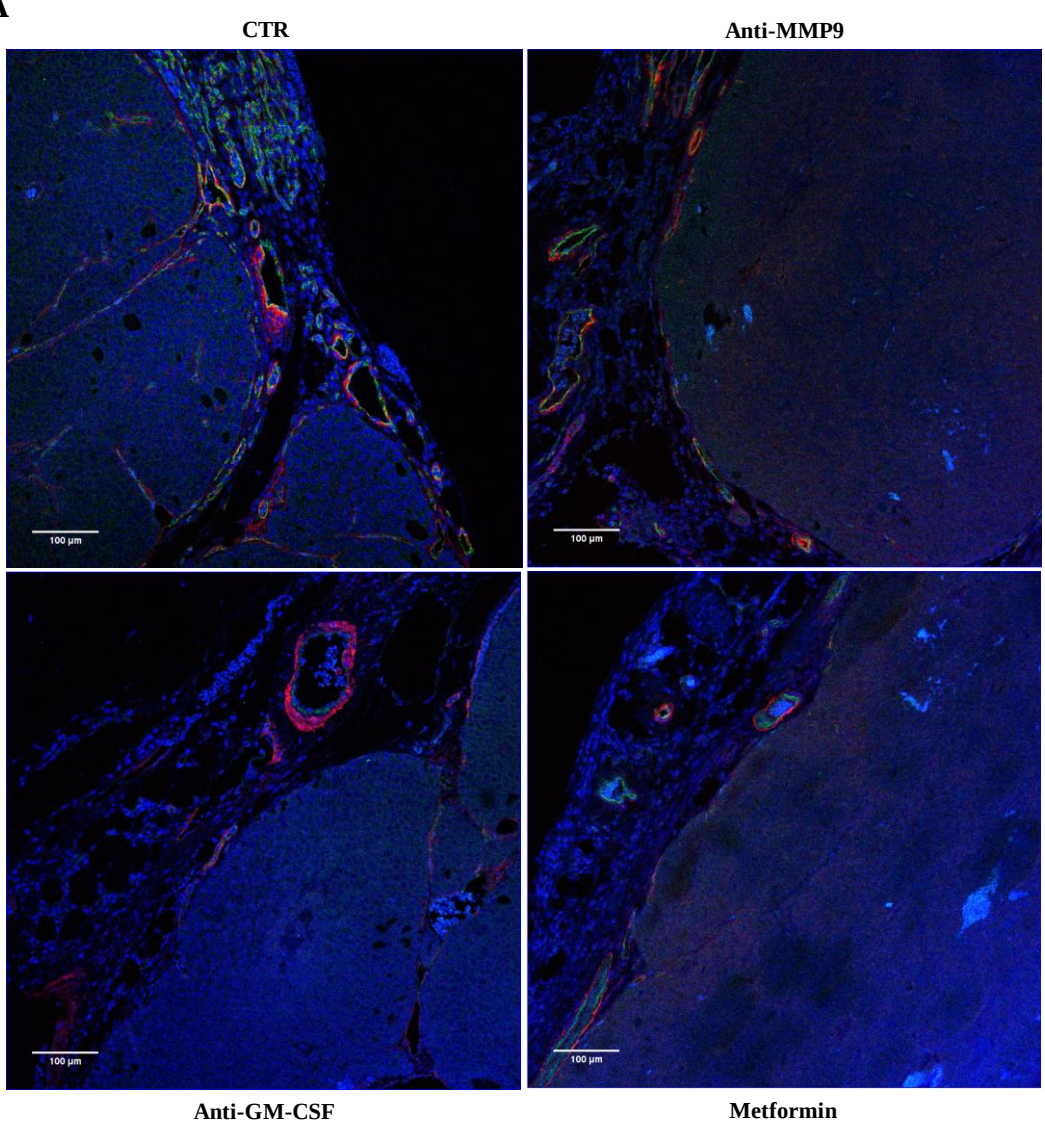

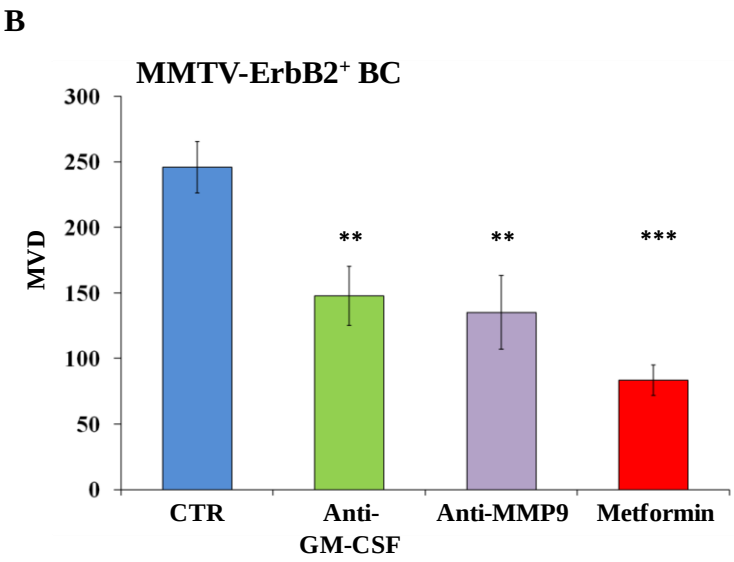

Fig.53 Intratumoral angiogenesis regulated by Metformin. DIO FVB/Hsd mice injected with MMTV-ErbB2^{+} BC were treated either with Metformin, anti-GM-CSF MoAb or SB-3CT. **A)** Representative images acquired with Leica Confocal microscope (20x magnification). Staining was performed with anti-mCD31 (*green*, 1:20 #ab28364, Abcam), anti-αSMA (*red*, 1:3000 #A2547, Sigma-Aldrich) and DAPI nuclear staining (*blue*). Scale bars represent 100µm; **B)** MVD evaluation in BC through IF (n=3, ** p<0.01, *** p<0.001 vs. vehicle+IgG2a control).

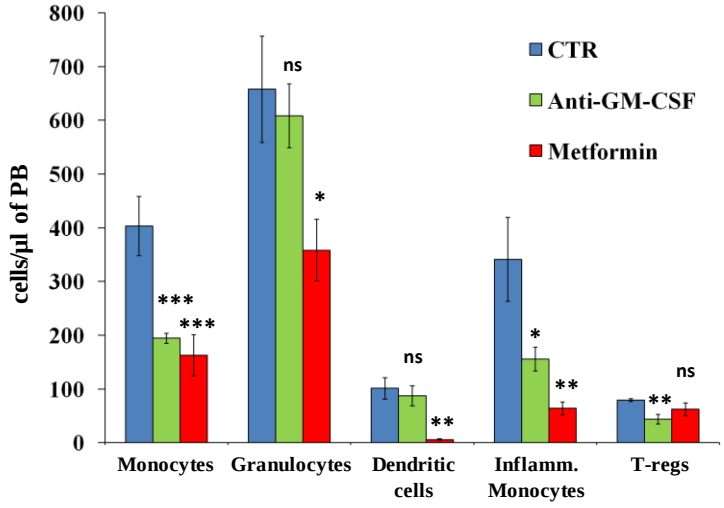

Fig.54 Circulating immune cells in Metformin treated mice. Multiparametric flow cytometry analysis on PB from DIO FVB/Hsd mice, injected with MMTV-ErbB2^{+} BC. Metformin and GM-CSF inhibition had similar effects (n=5, * p<0.05, ** p<0.01, *** p<0.001, ns: not significant, vs. IgG2a control).

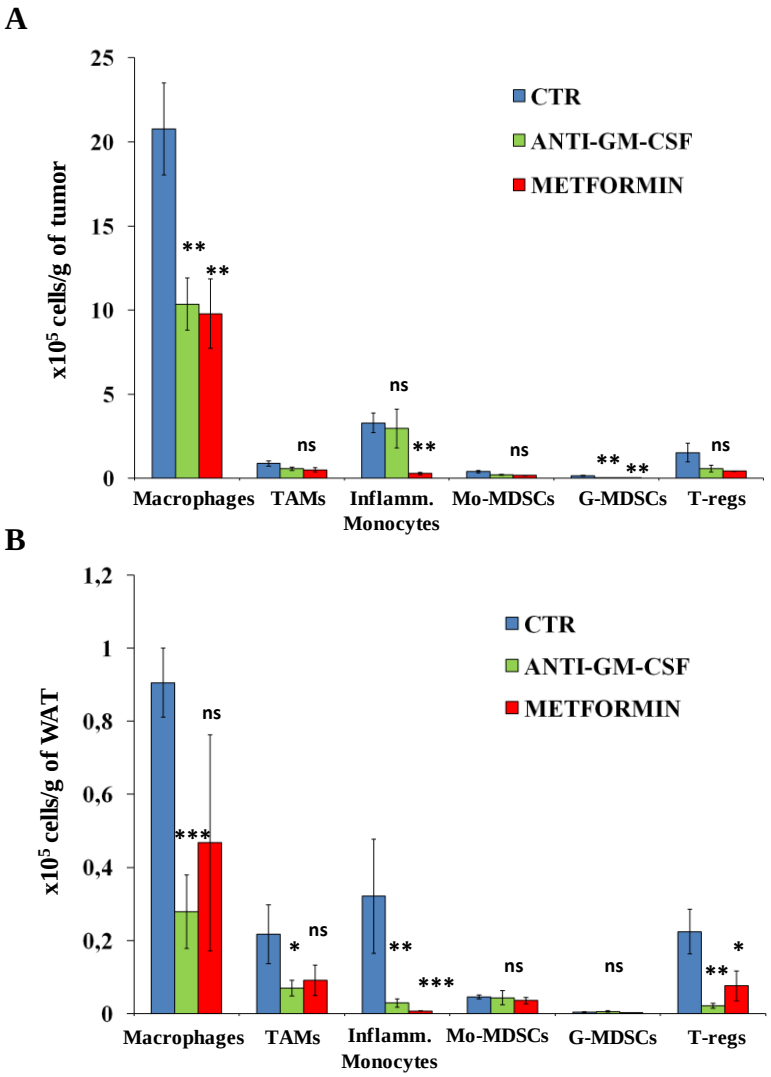

Fig.55 Metformin regulation of immunity in tumor microenvironment in DIO syngeneic mice. Multiparametric flow cytometry analysis of BC **(A)** and peritumoral WAT **(B)** isolated from DIO FVB/Hsd mice injected with MMTV-ErbB2^{+} BC cells: direct comparison of Metformin and GM-CSF neutralization. The two treatments displayed similar effects in modulating immune cells (n=5, * $p<0.05$, ** $p<0.01$, *** $p<0.001$, ns: not significant, vs. IgG2a control).

4. Discussion

Recent and abundant epidemiology and clinical literature have reported a relationship between WAT and BC progression (van den Brandt *et al.*, 2000; Cleary P and Grossmann, 2009). In particular, dysfunctional WAT in obesity has been associated with an increased risk of developing BC and a poorer prognosis.

WAT is composed by several populations, which might cooperate to promote the establishment of a permissive microenvironment (Muller C *et al*., 2013; Bertolini *et al*., 2014; Orecchioni *et al*., 2015).

A complex network of interactions exists between different WAT stroma cells and BC. Among them, the interaction with the progenitor-like population, contained in the $CD45^-$ $CD34^+$ fraction, seemed particularly relevant. This resident population of progenitors has recently been characterized in the SVF from lipofilling samples, displaying some unique features compared to BM-derived progenitors (Martin-Padura *et al*., 2012; Orecchioni *et al*., 2013). The fraction is composed by two distinct sub-populations of progenitors, ASCs and EPCs, displaying different surface markers and biological properties. The role of these progenitors in BC progression was extensively investigated in preclinical models (Martin-Padura *et al.*, 2012; Zhang Y *et al*., 2012; Orecchioni *et al*., 2013). WAT progenitors increased local tumor growth and metastatic spread to lungs and axillary lymph nodes. In addition, they promoted BC vascularization, differentiating to mature endothelial cells (EPCs) or pericytes (ASCs) and being recruited into blood vessels (Zhang Y *et al*., 2012; Orecchioni *et al*., 2013). ASCs were also able to generate CAAs and fibroblast-like cells, which might contribute to BC progression (Chandler *et al*., 2012; Zhang Y *et al*., 2012). ASCs and EPCs synergistically contributed to EMT in ductal carcinoma (Orecchioni *et al*., 2013).

The molecular mechanism underlying the interaction between WAT progenitors and BC has not completely been clarified yet. The involved molecular signaling was investigated in the present study.

4.1 Identification of GM-CSF and MMP9 in WAT progenitors-BC interaction

Several studies suggested that distinct molecules, produced either by BC or ASCs, might promote a permissive tumor microenvironment. Among them, IL-6, TGFβ and IL-10 were the most studied (Walter *et al.,* 2009; Razmkhah *et al*., 2011; Kucerova *et al*., 2013), frequently associated with the obesity-related chronic inflammation (Subbaramaiah *et al.*, 2011; Iyengar *et al.*, 2016).

A general overview of BC-WAT progenitors interplay was obtained through a screening of multiple factors through a proteomic antibody array. It analyzed 55 soluble factors involved in human angiogenesis, inflammation and ECM remodeling. A preliminary evaluation was performed using a TNBC human cell line (MDA-MB-436), that has already been used in cell assays and in xenograft models in combination with primary human WAT progenitors (Orecchioni *et al.*, 2013; Martin-Padura *et al.*, 2012).

Paracrine signaling was predominantly proposed in defining the interaction between WAT progenitors and BC (Kucerova *et al*., 2013). However, some cell-to-cell mechanisms were also suggested, such as exosome-related interactions (Lin *et al*., 2013). Therefore, cellular supernatant was screened in single cell cultures, in transwell co-cultures (allowing only paracrine interactions) and in direct co-cultures (allowing also adhesion-mediated cell-to-cell mechanisms).

BC produced a large amount of pro-angiogenic and inflammatory mediators, whereas WAT progenitors expressed a limited variety of these factors, such as IL-8 and SerpinE1. However, secreted levels of these highly secreted molecules were not affected in co-cultures, suggesting to not be involved in the interaction.

Two soluble molecules were found significantly up-regulated in both transwell and direct co-cultures: GM-CSF and MMP9.

The observed results needed to be further validated with quantitative assays, using different BC cell lines and WAT progenitors isolated from different subjects. Therefore, protein up-regulation was confirmed through ELISA, whereas MMP9 release and activity were detected, respectively, by WB and zymography.

GM-CSF and MMP9 were detected to be up-regulated in co-culture supernatants in all three available TNBC cell lines (MDA-MB-436, MDA-MB-231, HCC1937), whereas in ductal ER^+ carcinoma (ZR-75-1) were poorly detectable.

qRT-PCR analysis revealed that WAT progenitors significantly up-regulated transcription of both transcripts, after TNBC exposure. BC cells did not modify their baseline expression after being exposed to WAT progenitors. Of note, ductal carcinoma displayed a reduced production of GM-CSF and MMP9, compared to other TNBC cell lines. This is in accordance to the more aggressive phenotype observed in TNBC compared to ductal ER^+ carcinoma.

WAT progenitors cultured alone expressed poor levels of both factors and secreted proteins were usually undetectable in culture media. However, after being exposed to BC, the secreting profile of these cells dramatically changed, with a significant release of GM-CSF and MMP9. The up-regulation occurred even when murine WAT progenitors were co-cultured with human BC cell line, suggesting that the mechanism might be highly conserved.

The up-regulation occurred in both transwell and direct co-cultures, suggesting being dependent on paracrine interactions. Although, an adhesion-mediated release cannot be exclude for MMP9, due to the higher release detected in direct co-cultures.

The hypothesis might be that BC induces a cancer-associated phenotype in WAT progenitors, which normally do not express significant levels of GM-CSF or MMP9. Upon

BC exposure, WAT progenitors displayed a dramatic up-regulation of GM-CSF/MMP9 transcripts and protein release.

Since WAT $CD45^{-}CD34^{+}$ fraction is composed by distinct progenitor sub-populations, co-culture experiments were set up with purified ASCs and EPCs.

Results showed that the highly release occurred in both progenitors after BC exposure, in a complementary manner: MMP9 was higher released by ASCs, whereas GM-CSF was preferentially up-regulated by EPCs. This is in accordance with the previously published data obtained in preclinical models, where ASCs and EPCs cooperated to support BC growth, angiogenesis and metastatic spread (Orecchioni *et al*., 2013). However, distinct up-stream regulatory mechanisms cannot be excluded for the two populations.

ASCs have already been reported to produce higher levels of GM-CSF compared to BM-derived mesenchymal stem cells or fibroblasts (Banas *et al*., 2008). The release of GM-CSF by ASCs was enhanced in hypoxia conditions (Rehman *et al*., 2004), suggesting that hypoxia-related factors released by BC cells might be involved in the observed protein release. According to our findings, GM-CSF up-release was detected in direct co-cultures media between SKBR3 BC cell line and ASCs (Kucerova *et al*., 2013), although the authors did not investigate its specific source, attributing the increased expression to BC altered profile. Another study reported that ASCs expressed high levels of MMP9, which secretion was not altered in co-cultures with inflammatory cells (Hattori and Ishihara, 2015). MMP9 was also produced by BM-derived EPCs and its secretion was significantly enhanced in co-cultures with BC cells (Suriano *et al.*, 2008).

To our knowledge, this is the first work that specifically investigates the role of GM-CSF and MMP9 release in BC-associated WAT progenitors.

4.2 Up-regulation of GM-CSF and MMP9 in xenograft models

To assess if the observed *in vitro* interaction occurred in preclinical models, WAT progenitors were co-injected with TNBC cells in immunodeficient NSG mice. This model

was previously used to validate the pro-tumorigenic effects of WAT progenitors in BC xenografts (Martin-Padura *et al*., 2012; Orecchioni *et al*., 2013).

GM-CSF is a known hematopoietic and growth cytokine, able to mobilize stem cells to PB and to induce the differentiation of macrophages and granulocytes (Bhattacharya *et al.*, 2015). Therefore, circulating levels of hGM-CSF were investigated in PB through HS ELISA. This assay did not cross-react with the murine counterpart, confirming its specificity. Mice injected with WAT progenitors alone, as negative controls, did not display any detectable levels of the cytokine.

On the contrary, MMP9 expression was evaluated in tumor microenvironment, since its activity is essential in promoting tumor invasion into surrounding tissues (Duffy *et al*., 2000). In addition to the inactive pro-MMP9, active forms were also detected in whole tumor lysate, due to the presence in tumor microenvironment of other MMPs and enzymes, mostly absent *in vitro* conditions.

Both human GM-CSF and MMP9, including its biologically active forms, were found significantly higher released in co-injected mice, compared to mice injected with BC alone. However, transcriptional up-regulation was not observed in BC cells collected from co-injected mice, suggesting WAT progenitors as putative secreting cells.

The presence of WAT progenitors was associated with a more aggressive BC phenotype, directly linking GM-CSF and MMP9 release to the previously observed increased tumor invasion and metastatic spread in these xenograft models (Martin-Padura *et al*., 2012; Zhang Y *et al.*, 2012; Orecchioni *et al.*, 2013).

4.3 Investigation of up-stream mechanisms leading to GM-CSF/MMP9 release

The mechanism underneath GM-CSF and MMP9 up-regulation needed to be unveiled. In the present work, several BC cell lines differentially stimulated GM-CSF and MMP9 release by WAT progenitors. This suggests that distinct tumor cells produce different

amount of soluble mediator(s), which may regulate GM-CSF/MMP9 transcription in WAT progenitors.

Both GM-CSF and MMP9 were induced by several pathways, including NF-κB, which was often found de-regulated in obesity (Morris *et al*., 2011). However, this hypothesis was excluded since Bortezomib, a specific NF-κB inhibitor, was unable to prevent GM-CSF and MMP9 up-regulation *in vitro* co-cultures.

IL-1β was reported to induce the expression of GM-CSF in WAT (Kim *et al.*, 2008) and MMP9 in mature endothelial cells (Qin *et al*., 2012). The neutralization of IL-1β in single cell cultures was able to reduce GM-CSF/MMP9 transcription in WAT progenitors, but not in BC cells. In co-cultures, the neutralization of the factor reduced MMP9 transcriptional up-regulation in cancer-associated WAT progenitors, but failed to prevent GM-CSF release.

One hypothesis might be that BC produces high levels of IL-1β that, in turn, induces the observed MMP9 transcriptional up-regulation in WAT progenitors, independently from NF-κB pathway activation. This is supported by the finding that IL-1β release is significantly altered in obesity, contributing to chronic low grade inflammation and cancerogenesis (Subbaramaiah *et al*., 2011; Arendt *et al*., 2013).

GM-CSF was reported to up-regulate MMP9 in squamous carcinoma, increasing invasiveness and malignancy of tumor cells (Gutschalk *et al*., 2013). Accordingly, our results demonstrated that GM-CSF neutralization significantly reduced MMP9 transcription and protein release in co-cultures, targeting WAT progenitors, but not BC.

Of note, in the present work GM-CSF neutralization significantly affected its own release *in vitro* co-cultures and *in vivo* syngeneic models. The neutralization of GM-CSF resulted in its impaired transcription and protein release, in WAT progenitors both cultured alone or after BC exposure. From these findings, GM-CSF might affect the dysfunctional profile of WAT progenitors through two mechanisms: a) Induction of a positive feedback regulation on its own release; b) Transcriptional up-regulation of MMP9.

The existence of a positive GM-CSF feedback regulation has already been reported in myeloid cells (Seydel *et al.*, 2008), where GM-CSF induced STAT5 epigenetic regulation of its own promoter.

The last question is whether the amount of GM-CSF produced by BC is sufficient alone to trigger GM-CSF/MMP9 production by WAT progenitors or, more likely, other tumor-related factors are involved in this complex regulatory network. Moreover, IL-1β role needed to be clarified. IL-1β might be induced by GM-CSF and, consequently, implicated into MMP9 regulation, or might independently affect MMP9 expression. In support of the first option, GM-CSF was reported to significantly induce IL-1β expression in inflammatory microenvironment (Kim *et al.*, 2008).

4.4 Role of GM-CSF and MMP9 in BC progression

GM-CSF displays a pleiotropic activity on a multitude of cells, including both precursors and mature cells (Bhattacharya *et al.*, 2015). However, its main role involves immune system regulation, through the modulation of granulocytes, macrophages and dendritic cells (DC) in inflammation and autoimmunity.

The increased expression of type IV collagenase, MMP9, was instead correlated to higher tumor grade, metastasis and angiogenesis in several types of cancer (Duffy *et al.*, 2000; van't Veer *et al.*, 2002; La Rocca *et al.*, 2004; Hattori and Ishihara, 2015), including TNBC (Mehner *et al.*, 2014).

In the present study the impact of GM-CSF and MMP9 on tumor progression was evaluated in DIO FVB/Hsd and Balb/c mice injected, respectively, with primary MMTV-ErbB2$^+$ BC cells or 4T1 TNBC cell line. The DIO models were chosen because in obesity the number of WAT CD45$^-$CD34$^+$ progenitors is dramatically increased (Martin-Padura *et al.*, 2012; Dallaglio *et al.*, 2014). Furthermore, the possible regulatory effect of GM-CSF over immune system can be assessed only in immunocompetent syngeneic models.

Both GM-CSF and MMP9 inhibitions significantly impaired local tumor growth and metastatic spread to lungs, confirming the relevance of these molecules in promoting a permissive tumor microenvironment, independently from BC hormone receptors status. The combined inhibition synergically impaired BC progression and angiogenesis, strengthened the relevance of these factors in tumor progression.

The observed outcome may not involve a direct effect on tumor cells, but, more likely, a modulation of tumor microenvironment and ECM properties. In particular, in GM-CSF neutralization there was a reduction of tumor angiogenesis and immunosuppressive microenvironment. Conversely, MMP9 inhibition impaired tumor angiogenesis affecting ECM properties, reducing tumor invasion and metastasis. At variance with some studies reporting a possible modulation of T-cells induced by MMP9 (Benson *et al.*, 2011), in the present study MMP9 inhibition did not affect immune cells in PB, tumors or peritumoral WAT. Both factors have already been reported to promote angiogenesis, through ECM remodeling induced by MMP9 (Duffy *et al*., 2000) or VEGF induced-release caused by GM-CSF (Wang *et al*., 2014).

Regarding immune regulation, myeloid cells appeared to be the main target of GM-CSF in peritumoral WAT. GM-CSF has been reported to regulate the homing of myeloid cells to WAT (Kim *et al*., 2008). In our models, the neutralization of GM-CSF was associated with a reduced number of PB monocytes and WAT/tumor macrophages. In particular, TAMs (M2 macrophages) were impaired in WAT, supporting the findings of Su *et al*. (2014), who suggested GM-CSF to be a crucial TAMs inducer. Macrophages accumulation was previously shown to promote tumor growth in obesity, by increasing chronic inflammation, tumor immune escape and angiogenesis (Arendt *et al.*, 2003; Su *et al*., 2014). Therefore, some of the observed effects in anti-GM-CSF treated mice were possibly due to the lower macrophages activation. According to TAMs reduction, MDSCs were strongly impaired in tumors and WAT collected from anti-GM-CSF mice. In particular, G-MDSCs were strongly reduced in both tumor and WAT, whereas Mo-MDSCs were found impaired only

in tumors. This is supported by the reported GM-CSF ability to expand MDSCs in BC (Morales *et al.*, 2010), further triggering immune tolerant microenvironment.

In contrast, lymphoid cells seemed to be not affected by GM-CSF neutralization. This was expected, as GM-CSF receptors are usually not expressed by T-cells, B-cells and NK-cells (Rosas *et al*., 2007). Of note, T-regs were down-regulated in both WAT and PB from anti-GM-CSF treated mice. This finding suggests a possible regulatory role of GM-CSF over T-regs differentiation, supported by the related impaired FOXP3 expression. This is in accordance with the proposed role of GM-CSF in T-regs expansion (Gangi *et al.*, 2005; Kared *et al*., 2008).

Several interleukins and cytokines, involved in immunosuppression, were found strongly down-regulated in WAT of GM-CSF neutralized mice: IL-10 is produced by MDSCs and TAMs and is involved in immune tolerance and T-regs expansion (Razmkhah *et al*., 2011); CCL2 recruits TAMs and inflammatory monocytes (Arendt et al., 2013; Movahedi *et al.*, 2010); PD-L1 expression was also down-regulated, suggesting an involvement of GM-CSF in the promising PD-1/PD-L1 pathway. These data are in accordance with some recent evidence, collected from pancreatic cancer patients, in which *in vitro* GM-CSF ablation helped defeating immune escape mechanisms (Takeuchi *et al*., 2015). Furthermore, GM-CSF was reported to induce tolerogenic dendritic cells in BC, activating a regulatory Th2 immune response and increasing BC malignancy (Ghirelli *et al*., 2015).

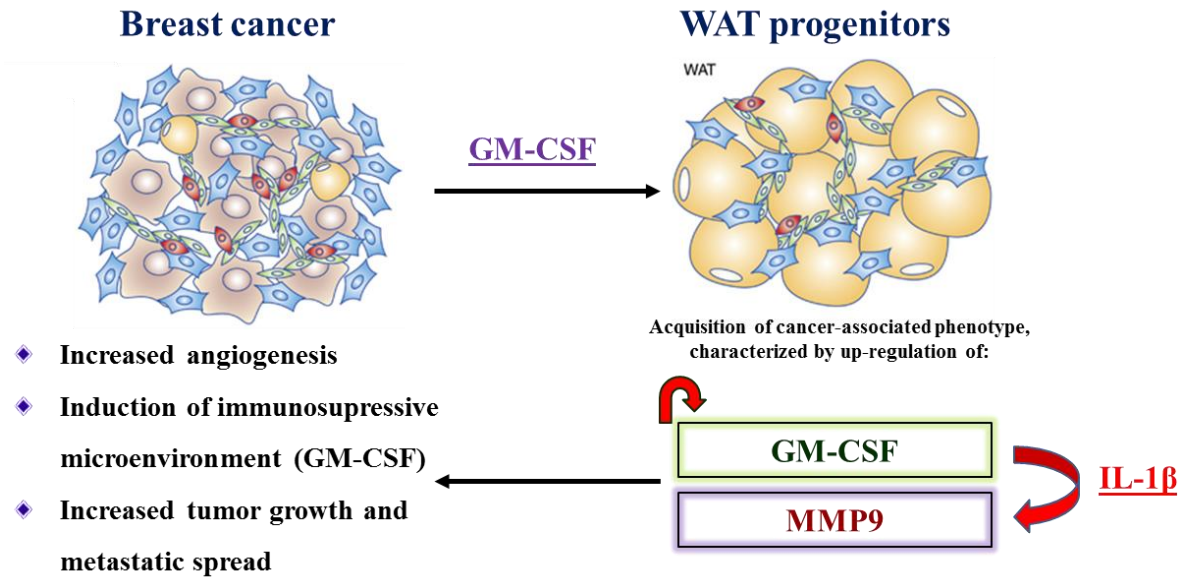

Fig.56 Schematic view of the proposed molecular interaction between BC and WAT-derived progenitors.

4.5 Therapeutic intervention targeting GM-CSF and MMP9 and the role of Metformin

GM-CSF over-expression in WAT progenitors might be relevant in the observed pro-tumorigenic activity of these cells. To our knowledge, this is the first study underlines GM-CSF over-expression by WAT-derived progenitors in response to BC and its neutralization in obese preclinical models.

The role of GM-CSF in tumor progression has recently been investigated (Gutschalk *et al.*, 2013; Su *et al.*, 2014; Wang *et al.*, 2014; Ghirelli *et al.*, 2015). However, in many of those studies GM-CSF was analyzed when expressed by tumor cells. The knockout of GM-CSF in TNBC or its neutralization through specific MoAb in lean xenograft models did not affect local tumor growth, but inhibited metastatic spread (Park *et al.*, 2007; Su *et al.*, 2014). These results strengthen our data collected in orthotopic models with concomitant obesity, suggesting that GM-CSF neutralization might be more effective in WAT-enriched tumors.

The total amount of GM-CSF released in tumor microenvironment might be essential in defining its biological effect, which was reported to be dose- and context-dependent (Li *et al.*, 2004; Parmiani *et al.*, 2007). A positive correlation was observed between high production of GM-CSF, increased metastasis and reduced survival in BC patients (Su *et al*., 2014). Conversely, low levels of GM-CSF were associated with enhanced innate immunity response. GM-CSF might enhance vaccine-induced immune response, if administered at low doses, whereas an opposite effect was detected at higher dosages (Parmiani *et al.*, 2007). This might explain why in some studies GM-CSF was reported to have anti-tumor activity (Eubank *et al*., 2009).

Our and other findings challenge the therapeutic applications of GM-CSF, which is widely used for PB mobilization/collection of hematopoietic stem cells and, more recently, for immunotherapy protocols (Arellano *et al*., 2008). The use of GM-CSF should be critically evaluated in BC patients, especially with concomitant obesity.

To our knowledge, no clinical trial involving GM-CSF inhibition in BC patients was ever approved.

MMP9 was selected as the other putative factor potentially involved in the pro-tumorigenic role of WAT-derived progenitors. MMP9 neutralization has already been investigated in several preclinical models of BC, including orthotopic TNBC (Mehner *et al*., 2014). The silencing of the molecule in BC cells was associated with an impaired BC growth, angiogenesis and invasion in surrounding tissues. However, in those studies MMP9 production by microenvironment cells, such as WAT-derived progenitors, has never been investigated. Conversely, our data suggest that MMP9 neutralization might be more effective in obese models of BC compared to their lean counterparts.

In spite of the encouraging preclinical results, early clinical trials with MMPs inhibitors had failed, showing no beneficial effect in cancer patients (Fingleton, 2007). This may be explained by the poor efficiency of MMPs inhibitors at that time and/or by the enrolment of patients with late-stage, advanced metastatic cancer (Fingleton, 2007). Our data, instead,

suggested that MMPs inhibition could be more efficient in the early stages of tumor progression and, in particular, in obese patients and/or in WAT-embedded cancers.

Recently, Metformin administration was reported to significantly reduce BC incidence in diabetic patients (Goodwin *et al*., 2011; Zhang P *et al*., 2013), especially with concomitant obesity, as demonstrated by a recent clinical trial (Ko *et al*., 2015). Furthermore, hyperglycemia and hyperinsulinemia were frequently associated with breast WAT inflammation and BC progression with a poor prognosis (Iyengar *et al.*, 2016), suggesting Metformin as a safe and cheap therapeutic option.

In preclinical models, Metformin significantly affected tumor progression and neoplastic angiogenesis, targeting both BC and WAT cells (Liu B *et al.*, 2009; Brown *et al*., 2010; Dallaglio *et al*., 2014; Orecchioni *et al.*, 2015). However, the mechanism by which the drug inhibits tumor progression has been so far elusive. In this context, our study is one of the first to report GM-CSF and MMP9 as potential Metformin targets.

In the present work, Metformin significantly reduced factors release *in vitro* co-cultures and in BC xenograft mice. The drug failed in regulating GM-CSF/MMP9 release by single BC and WAT progenitors, suggesting to preferentially target proteins higher release in co-cultures.

Previous studies confirmed the putative role of Metformin in reducing MMP9 in mature endothelial cells (Esfahanian *et al*., 2012) or in BC (Dallaglio *et al*., 2014).

However, in the present study the inhibition did not involve transcriptional regulation, but, more likely, post-transcriptional mechanisms and/or protein synthesis and exocytosis. This hypothesis might be supported by the finding that Metformin dephosphorylates the eukaryotic initiation factor 4E-binding protein (4E-BP) and ribosomal protein S6 kinase (S6K) through mTOR inhibition, leading to protein synthesis inhibition (Dowling *et al*., 2007).

Conversely, paradoxical effects induced by Metformin in BC and endothelial cells were reported *in vitro* (Dallaglio *et al*., 2014): the drug displayed opposite effects over

angiogenesis-related genes, with a short-term induction of transcription of pro-angiogenesis mediators, including VEGF, and long-term anti-angiogenic regulation. This might explain some of our contradictory results, which displayed increased VEGF release by WAT progenitors and a paradoxical up-regulation of GM-CSF transcripts in co-cultures in presence of Metformin.

Metformin administration to DIO syngeneic models confirmed the anti-diabetic drug ability to reduce BC local growth, metastasis and angiogenesis. The effect was comparable to anti-GM-CSF or anti-MMP9 specific treatments. Metformin was even more effective in reducing intratumoral angiogenesis and in modulating immune system, suggesting that more complex regulation of the drug might occur, additionally to the proposed GM-CSF/MMP9 inhibition.

Collectively, these data proposed Metformin as inhibitor of GM-CSF and MMP9, which might be key targets of its anti-neoplastic activity.

Even though further investigations are required to clarify the mechanism used by Metformin to reduce GM-CSF and MMP9 levels, the present study supports Metformin clinical studies in BC, particularly in a setting of obesity and/or insulin resistance.

4.6 Conclusions and future perspectives

Obesity is often associated with a poor BC prognosis and higher grade. This might be partially mediated by the significant expansion of WAT-derived progenitors. WAT progenitors displayed increased pro-tumorigenic activity in preclinical model of BC, promoting the establishment of a permissive microenvironment. In this context, the inhibition of mechanisms involved in BC progression acquires a tremendous relevance in the choice of the proper therapeutic strategy.

In the present study, MMP9 and GM-CSF are suggested as therapeutic targets to disrupt the interaction between WAT progenitors and BC cells. These cytokines are poorly expressed by WAT progenitors, but face a dramatic up-regulation in the presence of BC

cells. The effect was pronounced in TNBC, characterized by high tumor grade and poor prognosis.

To our knowledge, this is the first work specifically investigating the interaction between BC and both ASCs and EPCs, isolated from primary human WAT. Present findings unveil a dramatic alteration occurring in both ASCs and EPCs, after being exposed to tumor cells. WAT progenitors acquire a cancer-associated phenotype, characterized by unique secretion profile and higher pro-tumorigenic activity.

The role of GM-CSF and MMP9 in tumor biology has already been investigated, but, within the present work, their inhibition is suggested as potential adjuvant therapy to standard chemotherapeutic agents, especially in obesity setting. Of note, both proteins appeared to be suitable targets of Metformin, which has widely been investigated as repurposed drug in BC clinical trials. The mechanism by which Metformin reduces GM-CSF/MMP9 protein release needs to be further elucidated.

The complex network of regulation, leading to GM-CSF/MMP9 up-regulation in WAT progenitors, is currently under investigation. However, soluble mediators (GM-CSF, IL-1β or others) produced by tumor cells are likely to be involved in this regulation.

One possible debatable argument might be the validity of this up-regulation in other WAT-embedded tumors, such as in prostate, colon or even in hematological malignancies. It would be of interest to investigate how WAT- or BM-derived progenitors interact with different tumors and if the observed GM-CSF/MMP9 up-regulation still occurs. Furthermore, GM-CSF and/or MMP9 up-regulation needs to be clarified: it might be not restricted to WAT progenitors, but be induced in other tumor microenvironment cells, such as CAAs, CAFs, pericytes or mature endothelial cells.

References

- Agresti R, Meneghini E, Baili P, Minicozzi P, Turco A, Cavallo I, Funaro F, Amash H, Berrino F, Tagliabue E, Sant M. Association of adiposity, dysmetabolisms, and inflammation with aggressive breast cancer subtypes: a cross-sectional study. Breast Cancer Res Treat, 2016; 157(1):179-89.
- AIOM. Guidelines for mammary neoplasia, 2015. www.aiom.it (visited August 2016).
- Al-Hamodi Z, AL-Habori M, Al-Meeri A, Saif-Ali R. Association of adipokines, leptin/adiponectin ratio and C-reactive protein with obesity and type 2 diabetes mellitus. Diabetol Metabol Syndr, 2014; 6(1):99.
- American Cancer Society. Breast Cancer Facts & Figures 2015-2016. 2015, Atlanta: American Cancer Society Inc.
- Arellano M, Lonial S. Clinical uses of GM-CSF, a critical appraisal and update. Biologics, 2008; 2(1):13-27.
- Arendt LM, McCready J, Keller PJ, Baker DD, Naber SP, Seewaldt V, Kuperwasser C. Obesity promotes breast cancer by CCL2-mediated macrophage recruitment and angiogenesis. Cancer Res, 2013; 73(19):6080-93.
- Armani A, Mammi C, Marzolla V, Calanchini M, Antelmi A, Rosano GMC, Fabbri A, Caprio M. Cellular models for understanding adipogenesis, adipose dysfunction, and obesity. J Cell Biochem, 2010; 110:564-72.
- Banas A, Teratani T, Yamamoto Y, Tokuhara M, Takeshita F, Osaki M, Kawamata M, Kato T, Okochi H, Ochiya T. IFATS collection: in vivo therapeutic potential of human adipose tissue mesenchymal stem cells after transplantation into mice with liver injury. Stem cells, 2008; 26(10):2705-12.

- Benson HL, Mobashery S, Chang M, Kheradmand F, Hong JS, Smith GN, Shilling RA, WilkesDS. Endogenous Matrix Metalloproteinases 2 and 9 Regulate Activation of $CD4^+$ and $CD8^+$ T cells. Am J Respir Cell Mol Biol 2011; 44(5):700-8.
- Bergström A, Pisani P, Tenet V, Wolk A, Adami HO. Overweight as an avoidable cause of cancer in Europe. Int J Cancer, 2001; 91(3):421-30.
- Bertolini F, Orecchioni S, Petit JY, Kolonin MG. Obesity, pro-inflammatory mediators, adipose tissue progenitors, and breast cancer. Curr Opin Oncol, 2014; 26(6):545-50.
- Bhattacharya P, Budnick I, Singh M, Thiruppathi M, Alharshawi K, Elshabrawy H, Holterman MJ, Prabhakar BS. Dual role of GM-CSF as a pro-inflammatory and a regulatory cytokine: implications for immune therapy. Cytokine, 2015; 75(2):261-71.
- Bowers LW, Maximo IX, Brenner AJ, Beeram M, Hursting SD, Price RS, Tekmal RR, Jolly CA, deGraffenried LA. NSAID use reduces breast cancer recurrence in overweight and obese women: role of prostaglandin-aromatase interactions. Cancer Res, 2014; 74(16):4446-47.
- Brown KA, Hunger NI, Docanto M, Simpson ER. Metformin inhibits aromatase expression in human breast adipose stromal cells via stimulation of AMP-activated protein kinase. Breast Cancer Res Treat, 2010; 123(2):591-6.
- Burcelin R, Kamohara S, Li J, Tannenbaum GS, Charron MJ, Friedman JM. Acute intravenous leptin infusion increases glucose turnover but not skeletal muscle uptake in ob/ob mice. Diabetes, 1999; 48(6):1264-69.
- Carboni JM, Lee AV, Hadsell DL, Rowley BR, Lee FY, Bol DK, Camuso AE, Gottardis M, Greer AF, Ho CP, Hurlburt W, Li A, Saulnier M, Velaparthi U, Wang C, Wen ML, Westhouse RA, Wittman M, Zimmermann K, Rupnow BA, Wong TW. Tumor development by transgenic expression of a constitutively active insulin-like growth factor I receptor. Cancer Res, 2005; 65(9):3781-7.

- Chandler EM, Seo BR, Califano JP, Andresen Eguiluz RC, Lee JS, Yoon CJ, Tims DT, Wang JX, Cheng L, Mohanan S, Buckley MR, Cohen I, Nikitin AY, Williams RM, Gourdon D, Reinhart-King CA, Fischbach C. Implanted adipose progenitor cells as physicochemical regulators of breast cancer. Proc Natl Acad Sci USA, 2012; 109(25):9786-91.
- Choi BH, Chakraborty G, Baek K, Yoon HS. Aspirin-induced Bcl-2 translocation and its phosphorylation in the nucleus trigger apoptosis in breast cancer cells. Exp Mol Med, 2013; 45:e47.
- Cicalese A, Bonizzi G, Pasi CE, Faretta M, Ronzoni S, Giulini B, Brisken C, Minucci S, Di Fiore PP, Pelicci PG. The tumor suppressor p53 regulates polarity of self-renewing divisions in mammary stem cells. Cell 2009;138(6):1083-95.
- Cleary MP, Phillips FC, Getzin SC, Jacobson TL, Jacobson MK, Christensen TA, Juneja SC, Grande JP, Maihle NJ. Genetically obese MMTV-TGF-alpha/Lep(ob)Lep(ob) female mice do not develop mammary tumors. Breast Cancer Res Treat, 2003; 77(3):205-15.
- Cleary MP, Grande JP, Maihle NJ. Effect of a high fat diet on body weight and mammary tumor latency in MMTV-TGF-α mice. Int J Obes Relat Metab Disord, 2004; 28(8):956-62.
- Cleary P, Grossmann ME. Obesity and Breast Cancer: The Estrogen Connection. Endocrinology, 2009; 150(6):2537-42.
- Cui J, Chen S, Zhang C, Meng F, Wu E, Hu R, Hadass O, Lehmidi T, Blair GJ, Lee M, Chang M, Mobashery S, Sun GY, Gu Z. Inhibition of MMP9 by a selective gelatinase inhibitor protects neurovasculature from embolic focal cerebral ischemia. Molecular Neurodegener, 2012; 7:21.
- Dallaglio K, Bruno A, Cantelmo AR, Esposito AI, Ruggiero L, Orecchioni S, Calleri A, Bertolini F, Pfeffer U, Noonan DM, Albini A. Paradoxic effects of metformin on endothelial cells and angiogenesis. Carcinogenesis, 2014; 35(5): 1055-66.

- Dignam JJ, Wieand K, Johnson KA, Fisher B, Xu L, Mamounas EP. Obesity, tamoxifen use, and outcomes in women with estrogen receptor-positive early-stage breast cancer. J Natl Cancer Inst, 2003; 95(19):1467-76.
- Dirat B, Bochet L, Dabek M, Daviaud D, Dauvillier S, Majed B, Wang YY, Meulle A, Salles B, Le Gonidec S, Garrido I, Escourrou G, Valet P, Muller C. Cancer-associated adipocytes exhibit an activated phenotype and contribute to breast cancer invasion. Cancer Res, 2011; 71(7):2455-65.
- Dowling RJ, Zakikhani M, Fantus IG, Pollak M, Sonenberg N. Metformin inhibits mammalian target of rapamycin-dependent translation initiation in breast cancer cells. Cancer Res 2007; 67(22):10804-12.
- Duffy MJ, Maguire TM, Hill A, McDermott E, O'Higgins N. Metalloproteinases: role in breast carcinogenesis, invasion and metastasis. Breast Cancer Res, 2000; 2(4):252-7.
- Esfahanian N, Shakiba Y, Nikbin B, Soraya H, Maleki-Dizaji N, Ghazi-Khansari M, Garjani A. Effect of metformin on the proliferation, migration, and MMP-2 and -9 expression of human umbilical vein endothelial cells. Mol Med Rep, 2012; 5(4):1068-74.
- Eubank TD, Roberts RD, Khan M, Curry JM, Nuovo GJ, Kuppusamy P, Marsh CB. Granulocyte macrophage colony-stimulating factor inhibits breast cancer growth and metastasis by invoking an anti-angiogenic program in tumor-educated macrophages. Cancer Res, 2009; 69(5):2133-40.
- Faruk Aykan N, Yildiz I, Sen F, Kilic L, Keskin S, Ciftci R, Karabulut S, Sakar B, Disci R. Effect of increased body mass index (BMI) on time to tumour progression (TTP) in unresectable metastatic colorectal cancer (mCRC) patients treated with bevacizumab-based therapy. Med Oncol, 2013; 30(3):679.
- Fingleton B. Matrix metalloproteinases as valid clinical targets. Curr Pharm Des 2007; 13(3):333-46.

- Freese KE, Kokai L, Edwards RP, Philips BJ, Sheikh MA, Kelley J, Comerci J, Marra KG, Rubin JP, Linkov F. Adipose-derived stems cells and their role in human cancer development, growth, progression, and metastasis: a systematic review. Cancer Res, 2015;75(7):1161-8.
- Gabrilovich DI, Ostrand-Rosenberg S, Bronte V. Coordinated regulation of myeloid cells by tumors. Nat Rev Immunol, 2012; 12(4):253-68.
- Gangi E, Vasu C, Cheatem D, Prabhakar BS. IL-10-producing $CD4^{+}CD25^{+}$ regulatory T cells play a critical role in granulocyte-macrophage colony-stimulating factor-induced suppression of experimental autoimmune thyroiditis. J Immunol, 2005; 174(11):7006-13.
- Gehmert S, Gehmert S, Prantl L, Vykoukal J, Alt E, Song YH. Breast cancer cells attract the migration of adipose tissue-derived stem cells via the PDGF-BB/PDGFR-beta signaling pathway. Biochem Biophys Res Commun, 2010;398(3):601-5.
- Ghirelli C, Reyal F, Jeanmougin M, Zollinger R, Sirven P, Michea P, Caux C, Bendriss-Vermare N, Donnadieu MH, Caly M, Fourchotte V, Vincent-Salomon A, Sigal-Zafrani B, Sastre-Garau X, Soumelis V. Breast cancer cells-derived GM-CSF licenses regulatory Th2 induction by plasmacitoid predendritic cells in aggressive disease subtypes. Cancer Res, 2015; 75(14):2775-87.
- Goodwin PJ, Stambolic V, Lemieux J, Chen BE, Parulekar WR, Gelmon KA, Hershman DL, Hobday TJ, Ligibel JA, Mayer IA, Pritchard KI, Whelan TJ, Rastogi P, Sheperd LE. Evaluation of metformin in early breast cancer: a modification of the traditional paradigm for clinical testing of anti-cancer agents. Breast Cancer Res Treat, 2011; 126(1):215-20.
- Gutschalk CM, Yanamandra AK, Linde N, Meides A, Depner S, Mueller MM. GM-CSF enhances tumor invasion by elevated MMP-2, -9 and -26 expression. Cancer Med, 2013; 2(2):117-29.

- Hadass O, Tomlinson BN, Gooyit M, Chen S, Purdy JJ, Walker JM, Zhang C, Giritharan AB, Purnell W, Robinson CR, Shin D, Schroeder VA, Suckow MA, Simonyi A, Sun GY, Mobashery S, Cui J, Chang M, Gu Z. Selective inhibition of matrix metalloproteinase-9 attenuates secondary damage resulting from severe traumatic brain injury. PLoS One 2013; 8(10):e76904.
- Hattori H, Ishihara M. Altered protein secretions during interactions between adipose tissue- or bone marrow-derived stromal cells and inflammatory cells. Stem Cell Res Ther, 2015; 6(1):70.
- Hu X, Breeton C. Detection of functional matrix metalloproteases by zimography. J Vis Exp, 2010; (45):2445.
- Iyengar NM, Zhou XK, Gucalp A, Morris PG, Howe LR, Giri DD, Morrow M, Wang H, Pollak M, Jones LW, Hudis CA, Dannenberg AJ. Systemic correlates of white adipose tissue inflammation in early-stage breast cancer. Clin Cancer Res, 2016; 22(9):2283-89.
- Kared H, Leforban B, Montandon R, Renand A, Layseca Espinosa E, Chatenoud L, Rosenstein Y, Schneider E, Dy M, Zavala F. Role of GM-CSF in tolerance induction by mobilized hematopoietic progenitors. Blood, 2008; 112(6):2575-8.
- Khandekar MJ, Cohen P, Spiegelman BM. Molecular mechanisms of cancer development in obesity. Nat Rev Cancer, 2011; 11(12):886-95.
- Kim DH, Sandoval D, Reed JA, Matter EK, Tolod EG, Woods SC, Seeley RJ. The role of GM-CSF in adipose tissue inflammation. Am J Physiol Endocrinol Metab, 2008; 295(5):E1038-46.
- Kim JB, O'Hare MJ, Stein R. Models of breast cancer: is merging human and animal models the future? Breast Cancer Res, 2004; 6(1):22-30.
- Ko KP, Ma SH, Yang JJ, Hwang Y, Ahn C, Cho YM, Noh DY, Park BJ, Han W, Park SK. Metformin intervention in obese non-diabetic patients with breast cancer: phase II

randomized, double-blind, placebo-controlled trial. Breast Cancer Res Treat, 2015; 153(2): 361-70.

- Kowanetz M, Wu X, Lee J, Tan M, Hagenbeek T, Qu X, Yu L, Ross J, Korsisaari N, Cao T, Bou-Reslan H, Kallop D, Weimer R, Ludlam MJ, Kaminker JS, Modrusan Z, van Bruggen N, Peale FV, Carano RM Meng YG, Ferrara N. Granulocytes-colony stimulating factor promotes lung metastasis through the mobilization of $Ly6G^{+}Ly6C^{+}$ granulocytes. Proc Natl Acad Sci USA, 2010; 107(50):21248-55.
- Kruger A, Arlt MJE, Georg M, Kopitz C, Bernardo MM, Chang M, Mobashery S, Fridman R. Antimetastatic activity of a novel mechanism-based gelatinase inhibitor. Cancer Res, 2005; 65(9):3523-6.
- Kucerova L, Skolekova S, Matuskova M, Bohac M, Kozovska Z. Altered features and increased chemosensitivity of human breast cancer cells mediated by adipose tissue-derived mesenchymal stromal cells. BMC Cancer, 2013; 13:535.
- La Rocca G, Pucci-Minafra I, Marrazzo A, Taormina P, Minafra F. Zymographic detection and clinical correlations of MMP-2 and MMP-9 in breast cancer sera. Br J Cancer, 2004; 90(7):1414-21.
- Lakhani S, Ellis I, Schnitt S, Tan PH, van der Vijver MJ. WHO Classification of Tumors of the Breast. 2012; 4th. Lyon: IARC Press.
- Lai L, Alaverdi N, Maltais L, Morse HC. Mouse cell surface antigens: nomenclature and immunophenotyping. J Immunol, 1998; 160(8):3861-68.
- Lew EA, Garfinkel L. Variations in mortality by weight among 750 000 men and women. J Chronic Dis, 1979; 32(8):563-76.
- Li J, Bouton-Verville H, Holmes LM, Burgin KE, Jakubchak S, Yu X, Wagner TE, Wei Y. Inhibition or promotion of tumor growth by granulocyte-macrophage colony stimulating factor derived from engineered tumor cells is dose-dependent. Anticancer Res, 2004; 24(5A):2717-21.

- Lin R, Wang S, Zhao RC. Exosomes from human adipose-derived mesenchymal stem cells promote migration through Wnt signaling pathway in a breast cancer cell model. Mol Cell Biochem, 2013; 383(1-2):13-20.
- Liu B, Fan Z, Edgerton SM, Deng XS, Alimova IN, Lind SE, Thor AD. Metformin induces unique biological and molecular responses in triple negative breast cancer cells. Cell Cycle, 2009; 8(13):2031-40.
- Liu Y, Tamimi RM, Collins LC, Schnitt SJ, Gilmore HL, Connolly JL, Colditz GA. The association between vascular endothelial growth factor expression in invasive breast cancer and survival varies with intrinsic subtypes and use of adjuvant systemic therapy: results from the Nurses' Health Study. Breast Cancer Res Treat, 2011; 129(1):175-84.
- Lumeng CN, Bodzin JL, Saltiel AR. Obesity induces a phenotypic switch in adipose tissue macrophage polarization. J Clin Invest, 2007; 117(1):175-84.
- Martin MD, Carter KJ, Jean-Philippe SR, Chang M, Mobashery S, Thiolloy S, Lynch CC, Matrisian LM, Fingleton B. Effect of ablation or inhibition of stromal matrix metalloproteinase-9 on lung metastasis in a breast cancer model is dependent on genetic background. Cancer Res, 2008; 68(15):6251-9.
- Martin-Padura I, Gregato G, Marighetti P, Mancuso P, Calleri A, Corsini C, Pruneri G, Manzotti M, Lohsiriwat v, Rietjens M, Petit JY, Bertolini F. The white adipose tissue used in lipotransfer procedures is a rich reservoir of CD34+ progenitors able to promote cancer progression. Cancer Res, 2012; 72(1):325-34.
- Mehner C, Hockla A, Miller E, Ran S, Radisky DC, Radisky ES. Tumor cell-produced matrix metalloproteinase 9 (MMP-9) drives malignant progression and metastasis of basal-like triple negative breast cancer. Oncotarget, 2014; 5(9):2736-49.
- Montero AJ, Escobar M, Lopes G, Gluck S, Vogel C. Bevacizumab in the treatment of metastatic breast cancer: friend or foe? Curr Oncol Rep, 2012; 14(1):1-11.

- Montgomery MK, Hallahan NL, Brown SH, Liu M, Mitchell TW, Cooney GJ, Turner N. Mouse strain-dependent variation in obesity and glucose homeostasis in response to high-fat feeding. Diabetologia, 2013; 56(5):1129-39.
- Morales JK, Kmieciak M, Knutson KL, Bear HD, Manjili MH. GM-CSF is one of the main breast tumor-derived soluble factors involved in the differentiation of CD11b-Gr1- bone marrow progenitor cells into myeloid-derived suppressor cells. Breast Cancer Res Treat, 2010; 123(1):39-49.
- Morris PG, Hudis CA, Giri D, Marrow M, Falcone DJ, Zhou XK, Du B, Brogi E, Crawford CB, Kopelovich L, Subbaramaiah K, Dannenberg AJ. Inflammation and increased aromatase expression occur in the breast tissue of obese women with breast cancer. Cancer Prev Res (Phila), 2011; 4(7):1021-9.
- Movahedi K, Laoui D, Gysemans C, Baeten M, Stangé G, Van den Bossche J, Mack M, Pipeleers D, In't Veld P, De Baetselier P, Van Ginderachter JA. Different tumor microenvironments contain functionally distinct subsets of macrophages derived from Ly6C(high) monocytes. Cancer Res, 2010; 70(14):5728-39.
- Muehlberg FL, Song YH, Krohn A, Pinilla SP, Droll LH, Leng X, Seidensticker M, Ricke J, Altman AM, Devarajan E, Liu W, Arlinghaus RB, Alt EU. Tissue-resident stem cells promote breast cancer growth and metastasis. Carcinogenesis, 2009; 30(4):589-97.
- Muller C, Nieto L, Valet P. Unraveling the local influence of tumor-surrounding adipose tissue on tumor progression: cellular and molecular actors involved. In: Kolonin MG, 2013. Adipose tissue and cancer. New York NY: Springer Science and Business Media, pp 121-46.
- Muller WJ, Sinn E, Pattengale PK, Wallace R, Leder P. Single-step induction of mammary adenocarcinoma in transgenic mice bearing the activated c-neu oncogene. Cell, 1988; 54(1):105-15.

- Nilsson C, Raun K, Yan F, O Larsen M, Tang-Christensen. Laboratory animals as surrogate models for human obesity. Acta Pharmacol Sin, 2012; 33(2):173-81.
- Orecchioni S, Gregato G, Martin-Padura I, Reggiani F, Braidotti P, Mancuso P, Calleri A, Quarna J, Marighetti P, Aldeni C, Pruneri G, Martella S, Manconi A, Petit JY, Rietjens M, Bertolini F. Complementary populations of human adipose $CD34^+$ progenitor cells promote growth, angiogenesis and metastasis of breast cancer. Cancer Res, 2013; 73(9):5880-91.
- Orecchioni S, Reggiani F, Talarico G, Bertolini F. Mechanisms of obesity in the development of breast cancer. Discov Med, 2015; 109(20):121-8.
- Park BK, Zhang H, Zeng Q, Dai J, Keller ET, Giordano T, Gu K, Shah V, Pei L, Zarbo RJ, McCauley L, Shi S, Chen S, Wang CY. NF-kappaB in breast cancer cells promotes osteolytic bone metastasis by inducing osteoclastogenesis via GM-CSF. Nat Med, 2007; 13(1):62-9.
- Parmiani G, Castelli C, Pilla L, Santinami M, Colombo MP, Rivoltini L. Opposite immune functions of GM-CSF administered as vaccine adjuvant in cancer patients. Ann Oncol, 2007; 18(2):226-32.
- Paz-Filho G, Mishra AK, Licinio J. Adipokines: soluble factors from adipose tissue implicated in cancer. In: Kolonin MG, 2013. Adipose tissue and cancer. New York NY: Springer Science and Business Media, pp 71-97.
- Pellikainen JM, Ropponen KM, Kataja WW, Kellokoski JK, Eskelinen MJ, Kosma VM. Expression of matrix metalloproteinase (MMP)-2 and MMP9 in breast cancer with a special reference to activation protein-2, HER2 and prognosis. Clin Cancer Res, 2004; 10(22):7621-8.
- Petit JY, Rietjens M, Botteri E, Rotmensz N, Bertolini F, Curigliano G, Rey P, Garusi C, De Lorenzi F, Martella S, Manconi A, Barbieri B, Veronesi P, Intra M, Brambullo T, Gottardi A, Sommario M, Lomeo G, Iera M, Giovinazzo V, Lohsiriwat V. Evaluation of

fat grafting safety in patients with intraepithelial neoplasia: a matched-cohort study. Ann Oncol, 2013; 24(6):1479-84.

- Pinilla S, Alt E, Abdul Khalek FJ, Jotzu C, Muehlberg F, Beckmann C, Song YH. Tissue resident stem cells produce CCL5 under the influence of cancer cells and thereby promote breast cancer cell invasion. Cancer Lett, 2009; 284(1):80-5.
- Qin W, Lu W, Li H, Yuan X, Li B, Zhang Q, Xiu R. Melatonin inhibits IL1β-induced MMP9 expression and activity in human umbilical vein endothelial cells by suppressing NF-κB activation. J Endocrinol, 2012; 214(2):143-53.
- Razmkhah M, Jaberipour M, Erfani N, Habibagahi M, Talei AR, Ghaderi A. Adipose derived stem cells (ASCs) isolated from breast cancer tissue express IL-4, IL-10 and TGF-β1 and upregulate expression of regulatory molecules on T cells: do they protect breast cancer cells from the immune response? Cell Immunol, 2011; 266(2):116-22.
- Rehman J, Traktuev D, Li J, Merfeld-Clauss S, Temm-Grove CJ, Bovenkerk JE, Pell CL, Johnstone BH, Considine RV, March KL. Secretion of angiogenic and antiapoptotic factors by human adipose stromal cells. Circulation, 2004; 109(10):1292-8.
- Rene Gonzalez R, Watters A, Xu Y, Singh UP, Mann DR, Rueda BR, Penichet ML. Leptin-signaling inhibition results in efficient anti-tumor activity in estrogen receptor positive or negative breast cancer. Breast Cancer Res, 2009; 11(3):R36.
- Renehan AG, Roberts DL, Dive C. Obesity and cancer: pathophysiological and biological mechanisms. Arch Physiol Biochem, 2008; 114(1):71-83.
- Rodeheffer MS, Birsoy K, Friedman JM. Identification of white adipose progenitor cells in vivo. Cell, 2008; 135(2):240-9.
- Rosas M, Gordon S, Taylor PR. Characterization of the expression and function of the GM-CSF receptor alpha-chain in mice. Eur J Immunol 2007; 37(9):2518-28.

- Sabatier R, Finetti P, Guille A, Adelaide J, Chaffanet M, Viens P, Birnbaum D, Bertucci F. Claudin-low breast cancers: clinical, pathological, molecular and prognosis characterization. Mol Cancer, 2014; 13:228.
- Santander AM, Lopez-Ocejo O, Casas O, Agostini T, Sanchez L, Lamas-Basulto E, Carrio R, Cleary MP, Gonzalez-Perez RR, Torroella-Kouri M. Paracrine interactions between adipocytes and tumor cells recruit and modify macrophages to the mammary tumor microenvironment: the role of obesity and inflammation in breast adipose tissue. Cancers, 2015; 7(1):143-78.
- Seo BR, Bhardwaj P, Choi S, Gonzalez J, Andresen Eguiluz RC, Wang K, Mohanan S, Morris PG, Du B, Zhou XK, Vahdat LT, Verma A, Elemento O, Hudis CA, Williams RM, Gourdon D, Dannenberg AJ, Fischbach C. Obesity-dependent changes in interstitial ECM mechanics promote breast tumorigenesis. Sci Transl Med, 2015; 7(301):301ra130.
- Sestak I, Distler W, Forbes JF, Dowsett M, Howell A, Cuzick J. Effect of body mass index on recurrences in tamoxifen and anastrozole treated women: an exploratory analysis from the ATAC trial. J Clin Oncol, 2010; 28(21):3411-5.
- Seydel F, Garrigan E, Stutevoss B, Belkin N, Makadia B, Carter J, Shi JD, Davoodi-Semiromi A, McDuffie M, Litherland SA. GM-CSF induces STAT5 binding at epigenetic regulatory sites within the Csf2 promoter of non-obese diabetic (NOD) mouse myeloid cells. J Autoimmun, 2008; 31(4):377-84.
- Sorlie T, Perou CM, Tibshirani R, Aas T, Geisler S, Johnsen H, Hastie T, Eisen MB, van de Rijn M, Jeffrey SS, Thorsen T, Quist H, Matese JC, Brown PO, Botstein D, Lønning PE, Borresen-Dale AL. Gene expression patterns of breast carcinomas distinguish tumor subclasses with clinical implications. Proc Natl Acad Sci USA, 2001; 98(19):10869-74.
- Strong AL, Strong TA, Rhodes LV, Semon JA, Zhang X, Shi Z, Zhang S, Gimble JM, Burow ME, Bunnell BA. Obesity associated alterations in the biology of adipose stem

cells mediate enhanced tumorigenesis by estrogen dependent pathways. Breast Cancer Res, 2013; 15(5):R102.

- Su S, Liu Q, Chen J, Chen J, Chen F, He C, Huang D, Wu W, Lin L, Huang W, Zhang J, Cui X, Zheng F, Li H, Yao H, Su F, Song E. A positive feedback loop between mesenchymal-like cancer cells and macrophages is essential to breast cancer metastasis. Cancer Cell, 2014; 25(5):605-20.
- Subbaramaiah K, Howe LR, Bhardway P, Du B, Gravaghi C, Yantiss RK, Zhou XK, Blaho VA, Hla T, Yang P, Kopelovich L, Hudis CA, Dannenberg AJ. Obesity is associated with inflammation and elevated aromatase expression in the mouse mammary gland. Cancer Prev Res, 2011; 4(3):329-46.
- Suriano R, Chaudhuri D, Johnson RS, Lambers E, Ashok BT, Kishore R, Tiwari RK. 17Beta-estradiol mobilizes bone marrow-derived endothelial progenitor cells to tumors. Cancer Res, 2008; 68(15):6038-42.
- Talarico G, Orecchioni S, Dallaglio K, Reggiani F, Mancuso P, Calleri A, Gregato G, Labanca V, Rossi T, Noonan DM, Albini A, Bertolini F. Aspirin and atenolol enhance metformin activity against breast cancer by targeting both neoplastic and microenvironment cells. Sci Rep, 2016; 6:18673.
- Takeuchi S, Baghdadi M, Tsuchikawa T, Wada H, Nakamura T, Abe H, Nakanishi S, Usui Y, Higuchi K, Takahashi M, Inoko K, Sato S, Takano H, Shichinohe T, Seino K, Hirano S. Chemotherapy-Derived Inflammatory Responses Accelerate the Formation of Immunosuppressive Myeloid Cells in the Tissue Microenvironment of Human Pancreatic Cancer. Cancer Res, 2015; 75(13):2629-40.
- Tworoger SS, Eliassen AH, Kelesidis T, Colditz GA, Willett WC, Mantzoros CS, Hankinson SE. Plasma adiponectin concentrations and risk of incident breast cancer. J Clin Endocrinol Metab, 2007; 92(4):1510-6.

- Ueno T, Toi M, Saji H, Muta M, Bando H, Kuroi K, Koike M, Inadera H, Matsushima K. Significance of macrophage chemoattractant protein-1 in macrophage recruitment, angiogenesis, and survival in human breast cancer. Clin Cancer Res, 2000; 6(8):3282-9.
- van den Brandt PA, Spiegelman D, Yaun SS, Adami HO, Beeson L, Folsom AR, Fraser G, Goldbohm RA, Graham S, Kushi L, Marshall JR, Miller AB, Rohan T, Smith-Warner SA, Speizer FE, Willett WC, Wolk A, Hunter DJ. Pooled analysis of prospective cohort studies on height, weight, and breast cancer risk. Am J Epidemiol, 2000; 152(6):514-27.
- van't Veer LJ, Dai H, van de Vijver MJ, He YD, Hart AA, Mao M, Peterse HL, van der Kooy K, Marton MJ, Witteveen AT, Schreiber GJ, Kerkhoven RM, Roberts C, Linsley PS, Bernards R, Friend SH. Gene expression profiling predicts clinical outcome of breast cancer. Nature, 2002; 415(6871):530-6.
- Viale G. The current state of breast cancer classification. Ann Oncol, 2012; 23(Suppl.10):x207-10.
- Walter M, Liang S, Ghosh S, Hornsby PJ, Li R. Interleukin 6 secreted from adipose stromal cells promotes migration and invasion of breast cancer cells. Oncogene, 2009; 28(30):2745-55.
- Walzer T, Bléry M, Chaix J, Fuseri N, Chasson L, Robbins SH, Jaeger S, André P, Gauthier L, Daniel L, Chemin K, Morel Y, Dalod M, Imbert J, Pierres M, Moretta A, Romagné F, Vivier E. Identification, activation, and selective in vivo ablation of mouse NK cells via NKp46. Proc Natl Acad Sci USA, 2007; 104(9):3384-89.
- Wang Y, Han G, Wang K, Liu G, Wang R, Xiao H, Li X, Hou C, Shen B, Guo R, Li Y, Chen G. Tumor-derived GM-CSF promotes inflammatory colon carcinogenesis via stimulating epithelial release of VEGF. Cancer Res, 2014: 74(3):716-26.
- Weisberg SP, McCann D, Desai M, Rosenbaum M, Leibel RL, Ferrante AW Jr. Obesity is associated with macrophage accumulation in adipose tissue. J Clin Invest, 2003; 112(12): 1796-808.

- West DB, Boozer CN, Moody DL, Atkinson RL. Dietary obesity in nine inbred mouse strains. Am J Physiol, 1992; 262(6 Pt 2):R1025-32.
- World Health Organization (WHO). Obesity and overweight. 2016; Fact Sheet No. 311.
- Yang Y, Smith DL, Keating KD, Allison DB, Nagy TR. Variations in body weight, food intake and body composition after long-term high-fat diet feeding in C57BL/6J mice. Obesity, 2014; 22(10):2147-55.
- Youn JI, Nagaraj S, Collazo M, Gabrilovich DI. Subsets of myeloid-derived suppressor cells in tumor-bearing mice. J Immunol, 2008; 181(8):5791-802.
- Yu Q, Stamenkovich I. Cell surface-localized matrix metalloproteinase-9 proteolytically activates TGF-β and promotes tumor invasion and angiogenesis. Genes Dev, 2000; 14(2):163-76.
- Zhang P, Li H, Tan X, Chen L, Wang S. Association of metformin use with cancer incidence and mortality: a meta-analysis. Cancer Epidemiol, 2013; 37(3):207-218.
- Zhang Y, Daquinag A, Traktuev DO, Amaya-Manzanares F, Simmons PJ, March KL, Pasqualini R, Arap W, Kolonin MG. White adipose tissue cells are recruited by experimental tumors and promote cancer progression in mouse models. Cancer Res, 2009; 69(12):5259-66.
- Zhang Y, Bellows CF, Kolonin MG. Adipose tissue-derived progenitor cells and cancer. World J Stem Cells, 2010; 2(5):103-13.
- Zhang Y, Daquinag AC, Amaya-Manzanares F, Sirin O, Tseng C, Kolonin MG. Stromal progenitor cells from endogenous adipose tissue contribute to pericytes and adipocytes that populate the tumor microenvironment. Cancer Res, 2012; 72(20):5198-208.
- Zhang Y, Cheng S, Zhang M, Zhen L, Pang D, Zhang Q, Li Z. High-infiltration of tumor-associated macrophages predicts unfavorable clinical outcome for node-negative breast cancer. Plos One, 2013; 8(9):e76147.

- Zhang T, Tseng C, Zhang Y, Sirin O, Corn PG, Li-Ning-Tapia EM, Troncoso P, Davis J, Pettaway C, Ward J, Frazier ML, Logothetis C, Kolonin MG. CXCL1 mediates obesity-associated adipose stromal cell trafficking and function in the tumour microenvironment. Nat Commun, 2016; 7:11674.

Appendix

Relevant publications:

1. Complementary populations of human adipose CD34+ progenitor cells promote growth, angiogenesis, and metastasis of breast cancer

Orecchioni S, Gregato G, Martin-Padura I, Reggiani F, Braidotti P, Mancuso P, Calleri A, Quarna J, Marighetti P, Aldeni C, Pruneri G, Martella S, Manconi A, Petit JY, Rietjens M, Bertolini F.

Cancer Res. 2013 Oct 1;73(19):5880-91. doi: 10.1158/0008-5472.CAN-13-0821.

Abstract

Obesity is associated with an increased frequency, morbidity, and mortality of several types of neoplastic diseases, including postmenopausal breast cancer. We found that human adipose tissue contains two populations of progenitors with cooperative roles in breast cancer. CD45($^-$)CD34($^+$)CD31($^+$)CD13($^-$)CCRL2($^+$) endothelial cells can generate mature endothelial cells and capillaries. Their cancer-promoting effect in the breast was limited in the absence of CD45($^-$)CD34($^+$)CD31($^-$)CD13($^+$)CD140b($^+$) mesenchymal progenitors/adipose stromal cells (ASC), which generated pericytes and were more efficient than endothelial cells in promoting local tumor growth. Both endothelial cells and ASCs induced epithelial-to-mesenchymal transition (EMT) gene expression in luminal breast cancer cells. Endothelial cells (but not ASCs) migrated to lymph nodes and to contralateral nascent breast cancer lesions where they generated new vessels. In vitro and in vivo, endothelial cells were more efficient than ASCs in promoting tumor migration and in inducing metastases. Granulocyte colony-stimulating factor (G-CSF) effectively mobilized endothelial cells (but not ASCs), and the addition of chemotherapy and/or of CXCR4 inhibitors did not increase endothelial cell or ASC blood mobilization. Our findings suggest that adipose tissue progenitor cells cooperate in driving progression and metastatic spread of breast cancer.

2. The biguanides metformin and phenformin inhibit angiogenesis, local and metastatic growth of breast cancer by targeting both neoplastic and microenvironment cells

Orecchioni S*, Reggiani F*, Talarico G*, Mancuso P, Calleri A, Gregato G, Labanca V, Noonan DM, Dallaglio K, Albini A, Bertolini F.

* equally contributed

Int J Cancer. 2015 Mar 15;136(6):E534-44. doi: 10.1002/ijc.29193.

Abstract

The human white adipose tissue (WAT) contains progenitors with cooperative roles in breast cancer (BC) angiogenesis, local and metastatic progression. The biguanide Metformin (Met), commonly used for Type 2 diabetes, might have activity against BC and was found to inhibit angiogenesis in vivo. We studied Met and another biguanide, phenformin (Phe), in vitro and in vivo in BC models. In vitro, biguanides activated AMPK, inhibited Complex 1 of the respiratory chain and induced apoptosis of BC and WAT endothelial cells. In coculture, biguanides inhibited the production of several angiogenic proteins. In vivo, biguanides inhibited local and metastatic growth of triple negative and $HER2^+$ BC in immune-competent and immune-deficient mice orthotopically injected with BC. Biguanides inhibited local and metastatic BC growth in a genetically engineered murine model model of $HER2^+$ BC. In vivo, biguanides increased pimonidazole binding (but not HIF-1 expression) of WAT progenitors, reduced tumor microvessel density and altered the vascular pericyte/endothelial cell ratio, so that cancer vessels displayed a dysplastic phenotype. Phe was significantly more active than Met both in vitro and in vivo. Considering their safety profile, biguanides deserve to be further investigated for BC prevention in high-risk subjects, in combination with chemo and/or targeted therapy and/or as post-therapy consolidation or maintenance therapy for the prevention of BC recurrence.

3. The presence of wild type p53 in hematological cancers improves the efficacy of combinational therapy targeting metabolism

Allende-Vega N, Krzywinska E, Orecchioni S, Lopez-Royuela N, Reggiani F, Talarico G, Rossi JF, Rossignol R, Hicheri Y, Cartron G, Bertolini F, Villalba M.

Oncotarget. 2015 Aug 7;6(22):19228-45.

Abstract

Manipulation of metabolic pathways in hematological cancers has therapeutic potential. Here, we determined the molecular mechanism of action of the metabolic modulator dichloroacetate (DCA) in leukemic cells. We found that DCA induces the AMP-activated protein kinase (AMPK)/p53 pathway with increased efficacy in tumors expressing wild type (wt p53). Clinically relevant, low concentrations of doxorubicin synergize in vitro and in vivo with DCA to further enhance p53 activation and to block tumor progression. Leukemia cell lines and primary leukemic cells containing mutant p53 are resistant to the above-described combination approach. However, DCA synergized with the Hsp90 inhibitor 17-AAG to specifically eliminate these cells. Our studies strongly indicate that depending on the p53 status, different combination therapies would provide better treatment with decreased side effects in hematological cancers.

4. Mechanisms of obesity in the development of breast cancer

Orecchioni S*, Reggiani F*, Talarico G*, Bertolini F.

* equally contributed

Discov Med. 2015 Sep;20(109):121-8.

Abstract

Preclinical models and clinical retrospective data indicate that obesity is associated with a significant increase in the incidence, severity, and mortality from different types of cancer, including postmenopausal breast cancer. As discussed in the present review, both soluble factors and cellular players are involved in the mechanisms promoting local and metastatic breast cancer progression by adipose tissue. As the incidence of obesity is increasing worldwide, there is an urgent need for adequate preclinical models and preclinical and clinical studies designed to investigate how to inhibit the tumor-promoting activity of the adipose tissue.

5. The pan-class I phosphatidyl-inositol-3 kinase inhibitor NVP-BKM120 demonstrates anti-leukemic activity in acute myeloid leukemia

Allegretti M, Ricciardi MR, Licchetta R, Mirabilii S, Orecchioni S, Reggiani F, Talarico G, Foà R, Bertolini F, Amadori S, Torrisi MR, Tafuri A.

Sci Rep. 2015 Dec 17;5:18137. doi: 10.1038/srep18137.

Abstract

Aberrant activation of the PI3K/Akt/mTOR pathway is a common feature of acute myeloid leukemia (AML) patients contributing to chemoresistance, disease progression and unfavourable outcome. Therefore, inhibition of this pathway may represent a potential therapeutic approach in AML. The aim of this study was to evaluate the pre-clinical activity of NVP-BKM120 (BKM120), a selective pan-class I PI3K inhibitor, on AML cell lines and primary samples. Our results demonstrate that BKM120 abrogates the activity of the PI3K/Akt/mTOR signaling, promoting cell growth arrest and significant apoptosis in a dose- and time-dependent manner in AML cells but not in the normal counterpart. BKM120-induced cytotoxicity is associated with a profound modulation of metabolic behaviour in both cell lines and primary samples. In addition, BKM120 synergizes with the glycolitic inhibitor dichloroacetate enhancing apoptosis induction at lower doses. Finally, in vivo administration of BKM120 to a xenotransplant mouse model of AML significantly inhibited leukemia progression and improved the overall survival of treated mice. Taken together, our findings indicate that BKM120, alone or in combination with other drugs, has a significant anti-leukemic activity supporting its clinical development as a novel therapeutic agent in AML.

6. Aspirin and atenolol enhance metformin activity against breast cancer by targeting both neoplastic and microenvironment cells

Talarico G, Orecchioni S, Dallaglio K, Reggiani F, Mancuso P, Calleri A, Gregato G, Labanca V, Rossi T, Noonan DM, Albini A, Bertolini F.

Sci Rep. 2016 Jan 5;6:18673. doi: 10.1038/srep18673.

Abstract

Metformin can induce breast cancer (BC) cell apoptosis and reduce BC local and metastatic growth in preclinical models. Since Metformin is frequently used along with Aspirin or beta-blockers, we investigated the effect of Metformin, Aspirin and the beta-blocker Atenolol in several BC models. In vitro, Aspirin synergized with Metformin in inducing apoptosis of triple negative and endocrine-sensitive BC cells, and in activating AMPK in BC and in white adipose tissue (WAT) progenitors known to cooperate to BC progression. Both Aspirin and Atenolol added to the inhibitory effect of Metformin against complex I of the respiratory chain. In both immune-deficient and immune-competent preclinical models, Atenolol increased Metformin activity against angiogenesis, local and metastatic growth of $HER2^+$ and triple negative BC. Aspirin increased the activity of Metformin only in immune-competent $HER2^+$ BC models. Both Aspirin and Atenolol, when added to Metformin, significantly reduced the endothelial cell component of tumor vessels, whereas pericytes were reduced by the addition of Atenolol but not by the addition of Aspirin. Our data indicate that the addition of Aspirin or of Atenolol to Metformin might be beneficial for BC control, and that this activity is likely due to effects on both BC and microenvironment cells.

7. Extracellular ATP induces apoptosis through P2X7R activation in Acute Myeloid Leukemia cells but not in normal hematopoietic stem cells

Salvestrini V, Orecchioni S, Talarico G, Reggiani F, Mazzetti C, Bertolini F, Orioli E, Adinolfi E, Pezzi A, Cavo M, Lemoli RM, Curti A.

Oncotarget. 2016 Dec 13. doi: 10.18632/oncotarget.13927.

Abstract

Recent studies have shown that high ATP levels exhibit direct cytotoxic effects on several cancer cells types. Among the receptors engaged by ATP, P2X7R is the most consistently expressed by tumors. P2X7R is an ATP-gated ion channel that could drive the opening of a non-selective pore, triggering cell-death signal. We previously demonstrated that acute myeloid leukemia (AML) cells express high level of P2X7R. Here, we show that P2X7R activation with high dose ATP induces AML blast cells apoptosis. Moreover, P2X7R is also expressed on leukemic stem/progenitor cells (LSCs) which are sensitive to ATP-mediated cytotoxicity. Conversely, this cytotoxic effect was not observed on normal hematopoietic stem cell (HSC) progenitors. Notably, the antileukemic activity of ATP was also observed in presence of bone marrow stromal cells and its addition to the culture medium enhanced cytosine arabinoside cytotoxicity despite stroma-induced chemoresistance. Xenotransplant experiments confirmed ATP antineoplastic activity in vivo.

Overall, our results demonstrate that P2X7R stimulation by ATP induced a therapeutic response in AML at the LSC level while the normal stem cell compartment was not affected. These results provide evidence that ATP would be promising for developing innovative therapy for AML.

8. GM-CSF and MMP9 are key regulators of the effect of adipose progenitor cells over breast cancer onset and metastatic progression (Submitted)

Reggiani F, Labanca V, Mancuso P, Rabascio C, Talarico G, Orecchioni S, Manconi A, Bertolini F.

Abstract

We recently described a human cell population with progenitor-like phenotype ($CD45^{-}CD34^{+}$), resident in the white adipose tissue (WAT) and able to promote local and metastatic breast cancer (BC) progression and angiogenesis. However, the molecular mechanism involved in this interaction has been so far elusive. An extensive screening of candidate molecules revealed that two proteins were significantly up-regulated in WAT-derived progenitors following culture with BC cells: Granulocyte-macrophage colony-stimulating factor (GM-CSF) and Matrix metallopeptidase 9 (MMP9). In vivo, both proteins were overexpressed in orthotopic models of human BC co-injected with human WAT progenitors. The inhibition of GM-CSF in diet-induced obese BC mice led to a reduced intratumor vascularization and to a strong impairment of immunosuppressive microenvironment, targeting mainly myeloid cells such as macrophages and myeloid derived suppressor cells. This resulted in a significantly reduced local BC growth and lower metastatic progression. MMP9 inhibition reduced neoplastic angiogenesis and significantly decreased local and metastatic tumor growth. The combination of GM-CSF and MMP9 inhibition was synergic in impairing angiogenesis, local and metastatic tumor growth. As we recently reported that Metformin targets both BC cells and the neoplastic WAT environment, we investigated Metformin effect over GM-CSF and MMP9 expression. Metformin inhibited GM-CSF and MMP9 up-release from WAT progenitors in vitro. Circulating GM-CSF and MMP9 were significantly reduced in BC xenografts administered with Metformin and in obese mice Metformin had similar effects of GM-CSF/MMP9 specific inhibitions. Collectively, these results indicate GM-CSF and MMP9 as candidate targets to prevent the pro-tumorigenic effect of WAT progenitors on BC local and metastatic progression.